ISTANBUL TECHNICAL UNIVERSITY ★ GRADUATE SCHOOL OF INFORMATICS

DIRECTIONAL WIDE BAND PRINTED MONOPOLE ANTENNA FOR USE IN MICROWAVE BREAST CANCER IMAGING

M.Sc. THESIS

JAVAD JANGI GOLEZANI

Department of Communication Systems

Satellite Communication & Remote Sensing Programme

JUNE 2012

ISTANBUL TECHNICAL UNIVERSITY ★ GRADUATE SCHOOL OF INFORMATICS

DIRECTIONAL WIDE BAND PRINTED MONOPOLE ANTENNA FOR USE IN MICROWAVE BREAST CANCER IMAGING

M.Sc. THESIS

Javad JANGI GOLEZANI
(705101004)

Department of Communication Systems

Satellite Communication & Remote Sensing Programme

Thesis Advisor: Prof. Dr. Ibrahim AKDUMAN

JUNE 2012

İSTANBUL TEKNİK ÜNİVERSİTESİ ★ BİLİŞİM ENSTİTÜSÜ

MİKRODALGA MEME KANSERİ GÖRÜNTÜLEME KULLANIMI İÇİN GENİŞ BANTLI YÖNLÜ MİKROŞERİT ANTEN

YÜKSEK LİSANS TEZİ

Javad JANGI GOLEZANI
(705101004)

Haberleşme Sistemleri Anabilim Dalı

Uydu Haberleşme ve Uzaktan Algılama Programı

Tez Danışmanı: Prof. Dr. Ibrahim AKDUMAN

HAZİRAN 2012

Javad-Jangi Golezani, a **M.Sc.** student of ITU **Institute of Informatics** student ID **705101004,** successfully defended the **thesis** entitled "**DIRECTIONAL WIDE BAND PRINTED MONOPOLE ANTENNA FOR USE IN MICROWAVE BREAST CANCER IMAGING**", which he prepared after fulfilling the requirements specified in the associated legislations, before the jury whose signatures are below.

Thesis Advisor :   **Prof. Dr. Ibrahim AKDUMAN**   ....
İstanbul Technical University

Jury Members :   **Prof. Dr. Ali YAPAR**   ....
İstanbul Technical University

        Assoc. Prof. Dr. Hülya ŞAHİNTÜRK   ....
Yıldız Technical University

Date of Submission : 4 May 2012
Date of Defense :   **7 June 2012**

To my parents,

FOREWORD

I would like to gratefully acknowledge the enthusiastic supervision of Prof. Dr. Ibrahim Akduman during this work. This research project would not have been possible without your support. Thank you for offering different ideas and perspectives that have enriched the study. Despite lack of time, you have been so caring and supportive, providing guidance and critical insight when I needed.

I also appreciate the aid of Assis. Prof. Dr. Ender Mete eksioglu, Prof. Dr. Ahmet Hamdi Kayran, Assoc. Prof. Dr. Selcuk Paker, Prof. Dr. Ali Yapar, Dr. Mehmet Cayoren, Mehmet Abbak, Tolga Ulas Gurbuz and many others at Istanbul Technical University.

Foremost, I would like to thank to my beloved Parents for their blessings. I am forever indebted to my parents for their understanding, endless patience and encouragement when it was most required and my sister and brother for their boundless love, giving me all the support I needed. You are my life's angels, encouraging and supporting me both physically and morally in difficulties. I dedicate this project to you as you are my invaluable precious persons in the world.

My friends have provided much encouragement, support, and laughter over the years. I would like to express my heartfelt thanks to my friends for their help and wishes for the successful completion of this project. My best friends, Shahin Shakibaei, Mahsa Safaei, Sareh Naji, Gunash Rostami, Meysam Behnam, Sasan Ahdi and many others for their understandings and morally supports on me in Istanbul.

June 2012   Javad JANGI GOLEZANI

x

TABLE OF CONTENTS

ABBREVIATIONS

CMI	**:** Confocal Microwave Imaging
HPBW	**:** Half Power Beam Width
WBAN	**:** Wireless Body Area Network
UWB	**:** Ultra Wide Band
MWA	**:** Microwave Application
VSWR	**:** Voltage Standing Wave Ratio
FNBW	**:** First-Null Beamwidth
MIC	**:** Microwave Integrated Circuit
MSA	**:** Microstrip antenna
BW	**:** Band Width
St	**:** Station
GSM	**:** Global system for mobile communication
GPS	**:** Global positioning system
CP	**:** Circulary Polarization
ITU	**:** Istanbul Technical University

LIST OF TABLES

LIST OF FIGURES

DIRECTIONAL WIDEBAND PRINTED MONOPOLE ANTENNA FOR USE IN MICROWAVE BREAST CANCER IMAGING

SUMMARY

Breast cancer is the most common cancer in women. Detection of small breast lesions by mammography screening facilitates the cancer treatment by noninvasive techniques. Recently, new therapies than traditional surgery have been explored to satisfy these demands. The physical basis for breast cancer detection with microwave imaging is the difference in dielectric properties of normal and malignant breast tissues. Microwave imaging involves illuminating the breast with an ultra-wideband pulse from a number of antenna locations, then synthetically focusing reflections from the breast. The detection of malignant tumors is achieved by the coherent addition of returns from these strongly scattering objects.

Radar-based microwave imaging techniques have been proposed for early stage breast cancer detection. Radar-based microwave breast imaging approaches involve illuminating the breast with an ultra-wideband pulse of microwaves and detecting reflections. The reflections are then processed to create images that indicate the presence and location of tumors in the breast. A key component of these systems is the antenna that is used to radiate and receive the ultra-wideband pulses. So the antenna design requirements for use in near field near surface measurement applications, such as radar-based microwave breast cancer imaging are as follows: radiation of ultra-wideband signal to transmit short pulses, size of the antenna on the order of a few centimeters to selectively illuminate and permit scanning, an optimum half power near-field beam width(HPBW) to avoid smearing of the scatterers that occurs if the field of view of each antenna is too broad, and finally a good impedance matching across the entire band, This ensures that most of the energy is transmitted. In order to decrease the HPBW of an antenna we have to increase the directivity of the antenna in a desired direction. Nevertheless, most of the wide band and UWB antennas like planar monopoles, which are in use, have almost Omni-Directional radiation pattern.

Directivity can be achieved if the antenna is large in a desired direction, such as Horn or Vivaldi antennas. Printed disc monopole antennas with an L-shaped or parabolic-shaped ground plane are introduced as another type of directional antennas. In these antennas it has been shown how partial ground optimization influences the antenna's performance, in maximizing the directivity and gain of the antenna. These kinds of directional antennas are similar to the UWB type Omni-Directional monopole antennas, where it is shown the effect of ground plane on obtaining the desired directional characteristics of the antenna.

This Thesis presents a new design of directional wide band monopole antenna with parabolic-shaped ground plane. Ground plane of the antenna consists of a symmetrical parabolic curve, which its axis extended along the direction of the substrate's diagonal. In order to accomplish high gain and directivity, axis of

parabola in the ground plane is extended throughout the direction of square substrate's diagonal that maximizes the capability of symmetrical ground plane as a reflector. The directivity of the antenna is further improved by inserting parabolic-shaped slots at the corners of ground plane. The second edge of the ground plane which is created by inserting the slots, behaves as an additional reflector which cause to increase in the gain and directivity.

Then, the presented planar antenna is composed of a disc-monopole fed by a 50Ω microstrip line printed on a FR4 substrate. Simulation and measurements show that the proposed antenna has stable directional radiation pattern and higher gain compared to the previous directional monopole antennas. Impedance bandwidth of the antenna covers the frequency range of 4-9 GHz. Measured HPBW is among the degrees 54-22 in the same range of frequencies. In comparison with conventional antennas with a similar structure, gain of the antenna is improved between 1.1 and 3.1 dBi among 4-9 GHz. HPBW of the antenna is also between 5 and 15 degrees through the bandwidth .Results confirm the good characteristics for use in radar and microwave Breast cancer imaging applications where high resolution is required. For example, at 8.5 GHz, measured HPBW of the antenna is decreased from 38 degrees to 23 degrees (mentioned in the result section), which confirms a 40 % decrease in HPBW of the antenna (simulated HPBW is 26 = 33 % improvement). That is very important in order to increase the resolution of a radar system.

As an additional attempt, another novel compact directional monopole antenna in microstrip technology is also presented. Dimensions of this antenna are considerably miniaturized in comparison with conventional directional antennas. The main effort is to convert an Omni-directional radiation pattern of a compact monopole antenna to the desired directional radiation pattern, by using a novel ground plane, and a parasitic element. The ground plane and parasitic element are accurately designed in a way that make the surface currents of radiating elements to move toward the desired direction, which increase the radiation density in the preferred direction and also decrease the radiation intensity in the opposite sides. Simulations confirm a good directional characteristic of the antenna at the frequencies between 5 and 9 GHz. Gain of the antenna is increased over 5 dBi at the desired frequencies. Reflection coefficient bandwidth of the antenna covers the frequencies among 5-9 GHz. Miniaturized size and an acceptable directional characteristic of the antenna make it possible to use it in the microwave imaging systems and radar applications.

MİKRODALGA MEME KANSERİ GÖRÜNTÜLEME KULLANIMI İÇİN GENİŞ BANTLI YÖNLÜ MİKROŞERİT ANTEN

ÖZET

Meme kanseri kadınlarda en yaygın görülen kanser türüdür. Mamografi küçük meme lezyonlarının noninvaziv tekniklerle kanser tedavisini kolaylaştırır. Son zamanlarda, geleneksel cerrahiden daha yeni tedaviler bu talepleri karşılamak için araştırılmıştır. Meme kanseri tespiti için Mikrodalga görüntüleme teknolojisi günümüzde çok ilgi çekmiş. Mikrodalga görüntüleme ile meme kanseri tespiti için fiziksel temel, normal ve malign meme dokuların dielektrik özellikleri arasındaki farktır. Mikrodalga frekanslarında normal ve malign memenin dielektrik özelliklerin arasında önemli fark neden ile cevapsız-tespitler ve yanlış-pozitiflerin sayısı çok düşük sayılardır ve bu neden meme kanseri tespitinde bir mikrodalga görüntüleme tekniğinin geliştirilmesi için en önemi motivasyon sayılır. Tahmini malign-to-normal meme dokusu arasındaki kontrast normal doku yoğunluğuna bağlı olarak 2: 1 ve 10: 1 arasında. Başka bir avantaj olarak, mikrodalga görüntüleme tekniği sonucunda ilgili doku özellikleri bir üç boyutlu (3-D) hacimsel haritasında gosteriliyor. Ayrıca Mikrodalga meme kanseri görüntüleme noninvaziv ve hatta potansiyel olarak düşük maliyetli bir alternatiftir. Bahsedilen tüm nedenlerden dolayı, mikrodalga meme görüntüleme geleneksel meme kanseri tarama sistemleri kısıtlamaların bazılarının üstesinden gelmek için bir potansiyele sahiptir.

Mikrodalga görüntüleme, tıbbi uygulamalara ilişkin literatürde çok geniş araştırmalara sahiptir. Topografik yöntemleri ve backscatter yöntemleri dielektrik özellikleri karşıtlıklarından faydalanarak aktif mikrodalga görüntüleme tekniklerinin iki farklı yöntem sayılır. Mikrodalga tomografi yönteminde amaç cismin tarafından yansıyan mikrodalga enerjinin ölçümleri ile bir cismin dielektrik-özellikleri profilin toplamaktır. Ancak, diğer tarafta, yer radarı durumunda olduğu gibi, backscatter yöntemlerde amaç ölçülen geri yansıyan sinyallerin kullanımı ile önemli mikrodalga dağıtıcıların yerlerini çıkarmaktır. Normal meme dokusu ve malign lezyonlar arasında, dielektrik özelliklerin önemli kontrast nedeni ile Saçılma yükselir.

Son zamanlarda meme kanseri tespiti için başka bir yol önerilmiştir. Bu yöntem konfokal mikrodalga görüntüleme ve ingilizce olarak confocal microwave imaging (CMI) olarak adlandırılır. CMI meme tümörü saptama prosedürün yöntemi memeni bir fiziksel anten dizisi sistemi ile gönderilen ultra-geniş bant darbe ile aydınlatmak ve yansimaktir. Saçılan yerini belirlemek için kullanılan bilgi sağlamak amacıyla, saçılan sinyalinin nispi varış süreleri ve amplitüdleri, ilgili algoritmalar ile analiz edilir. Mikrodalga tomografi ile karşılaştırıldığında, CMI yöntemi dielektrik özellikleri profilini tamamen yeniden yapmak yerine yalnızca memede güçlü sikliklerin yerini tanımlamak istiyor.

Kısaca Radar tabanlı mikrodalga meme görüntülemesinde, metodun prosedürü memeni ultra-geniş bantlı mikrodalga darbe ile aydınlatmak ve dolayısıyla yansımaları tespit etmektir. Daha sonra dokudan geri yansıyan dalgalar memede

tümörün yerini tespit eden ve gösteren görüntüler e oluşturmak için kullanır. Bu sistemlerin önemli bir bölümü ultra-geniş bant sinyal yaymak ve almak için kullanılan antendir. Hem giriş empedans uydurma açısından ve hem radyasyon desen istenen bant genişliği üzerinde, antenin bu uygulamalarda kullanmak için, iyi performans göstermesi gerekir.

Antenin yüksek çözünürlükte elde etmek için antenin direktivitesi en önemli özelliklerinden biridir. Antenin Yarı Güç Işın Genişliği, ingilizce Half Power Beam Width (HPBW) küçük ayrıntıları tespit etmek için yeterince küçük olmalıdır. Diğer yandan, antenin fiziksel montaj karmaşıklığını azaltmak için ve aynı zamanda vücut ile iyi derecede konformluğunu elde etmek için kompakt bir anten tasarımı arzu edilir. Bu yüzden bu tür radar tabanlı mikrodalga göğüs kanseri görüntüleme gibi yüzey yakınındaki yakın alanda ölçüm uygulamalarında kullanım için antenin tasarım gereksinimleri aşağıdaki gibidir:

- Kısa darbeleri iletmek için ultra-geniş bant yayılan sinyal.
- Seçici aydınlatmak ve taramak için birkaç santimetre anten büyüklüğü.
- Antenlerin görüş alanının çok geniş olma nedeni ile ortaya çıkan dağıtıcıların arasındaki bulaşmani önlemek için optimum bir yakın alanda yarım güç ışın genişliği (HPBW).
- Ve nihayet tüm bant boyunca iyi bir empedans eşleştirmesi, bu mesele enerjinin böyük kısmının iletılmesini sağlar.

Bir antenin HPBW ini azaltmak için antenin direktivitesini bir istenen yönde arttırmak şarttır. Darbeli radar teknikleri kullanılarak doku algılama uygulamalarında çeşitli farklı antenler araştırma grupları tarafından kabul edilmiştir. Bu tür antenlerin tipik örnekleri vivaldi, bowtie, slotline bowtie, horn ve mikroşerit antenler içerir. Günümüzde Ultra Wide band (UWB) uygulamalarında kullanmak için yönlü antenlere artan talepler vardır. Yönlü antenler ışımanı yakınsamak ile ışınım şiddetini istenilen yönde artırmak için, daha net, Yarı Güç Işın Genişliği (HPBW) optimize etmek için kullanılır. Radar sistemlerinde antenin HPBW i radar çözünürlüğünü belirleyen temel parametrelerden biridir, diğer bir deyişle, daha ince ayrıntıları daha dar bir ışın kullanılarak çözülebilir. Yönerge antenin diğer avantajları olarak, uzun bir mesafe örtmek amacıyla HPBW oldukça azaltmak gereklidir. Bir yönlü antenin ışını Body-Worn Cihazlarında, Wireless Body Area Network (WBAN) kullanmak için elektromanyetik radyasyonun etkilerini insan vücuduna azaltmak için arzu edilir. Bu halde, kullanımda olan geniş bantlı Planar Monopole gibi UWB antenlerin çoğu Omni Directional radyasyon deseni var.

İlgi uygulama sağlıklı ve malign doku arasındaki dielektrik özelliklerinin farkını açıklayarak mikrodalga meme kanseri tespit edilmesidir. Farklı Yönlü Anten türleri vardır. Horn ya Vivaldi gibi antenlerde, antenin boyutu istenen bir doğrultuda büyük olması durumunda direktivite elde edilebilir. Mikrodalga meme görüntüleme için fiziksel ve radyasyon özelliklerine göre sınıflandırılabilen genellikle üç tip (dipol, slot ve monopole) Kompakt geniş bant yönlü antenler sunulmuştur. Diğer tipleri de, direktivite elde etmek amacıyla antende kavite ya da arkasında koruyucu ve ya emici malzeme kullanılır. Ancak bu gibi yaklaşımlar kullanılarak anten boyutu veya antenin verim azalması gibi üretim sürecinde bir komplikasyon ya arttırma neden olur. Ancak bu gibi yaklaşımlar kullanılarak antenin boyutu arttırma veya verim azalması gibi sorunlar ve üretim sürecinde bir komplikasyona neden olur. Radar tabanlı meme kanseri tespiti için 2-4 GHz frekansında çalışan kompakt bowtie anten veya 3.4-9.6 GHz frekansında çalışan geniş bantlı tek kutuplu anten yakın alanda

mikrodalga görüntüleme için sunulmuştur. Geleneksel slot anten gibi bazı diğer yönlü antenler de sunulmuş, ancak bir dezavantaj olarak sınırlı bir çalışma frekans aralığı var. Diğer tarafta vivaldi tip antenler de iyi bir bant genişliği ve yönlü radyasyonları var. Özel tipte çember patchlı L-şekilli veya parabolik şeklinde ground sayfalı monopol mikroşerit antenler, mikrodalga görüntüleme sisteminde kullanılmak için sunulmuştur. Bu çalışmalarda ground sayfasının iyileştirmesini anten kazancı ve direktivitesinin performansını nasıl etkilediği ve optimize etmesini gösteriyor. Monopol mikroşerit antenler popüler ve fabrikasyon ve özellikleri ve küçük boyutu ve mikroşerit teknolojinin diğer avantajları kolaylığı nedeni ile.

Bizim çalışmalar için parabolik şeklinde yansıtıcı ground sayfalı monopol türü mikroşerit anten göz önüne alınmıştır.

Bu Tez bu uygulama için modifiye tasarım olarak, gerekli geniş bant üzerinden çalışabilen bir parabolik şeklinde yansıtıcı ground sayfalı yönlü monopol anten sunuyor. Bu çalışmada, ground sayfasının antenin istenen yönsel özellikleri elde etmek üzerinde etkisi gösterdiği ve artırıldı.

Bu tezin amacı, özellikle mikrodalga meme kanseri görüntüleme gibi yakın yüzey ve yakın alanda ölçüm uygulamalarında , kullanımı uygun yeni bir modifiye anten yapısı tasarlamaktır. Antenin Ground Sayfasi ekseni substrat diyagonalının yönü boyunca uzatılmış simetrik bir parabolik eğriden oluşur. Direktivite, ground sayfanın parabolünün eksenini substratın çaprazında yönlendirmek ile, daha sonra ground sayfasında parabolik yuvaları ekleyerek iyileştirilmiştir. Ground düzlem içinde parabolün eksenini, kare substrat diyagonalın yönü boyunca uzatmak ile ground sayfasının yeteneğine doğru ve simetrik bir yansıtıcı olarak artıyor. Ayrıca ground sayfasında yuva ekleyerek oluşturulan ikinci kenarlar kazanç ve direktivite artmasına neden olup ek bir reflektör gibi davranır.

Sunulan düzlemsel anten 50 Ω mikrostrip-beslemeli bir disk-monopoldan oluşur. Tercih edilen bant genişliğinde antenin kazanç ve büyüklüğü arasında bir trade-off korumak için, ε_r = 4.4 dielektrik sabiti olan 50 mm boyutlarında kare FR4 taban üzerinde tasarlanmıştır. Dielektrik ve iletken tabakaların kalınlıkları, sırasıyla, 1.6 milimetre ve 35 mikrometredir. Hem simülasyonları ve hem ölçümleri önerilen antenin Frekansa karşı stabil bir ışıma olduğunu onaylandırır. Antenin empedans bantı 4-9 GHz frekans aralığı kapsıyor. Ölçülen HPBW aynı frekans aralığında 54-22 derece arasındadır. Önceki monopoller ile kıyasladığında 4-9GHz bir frekans aralığında, 5-15 derece direktivite ve 1.1-3.1 dBi kazanç iyileştirildiği teyit edilir. Anten kazancı 8 GHz frekansında 10 dBi kaldırdı. Antenin ışıma yönü 5-9 GHz arasında, Phi = 130 ˚ ve Phi = 151˚ arasında değişiyor, Ve bu mesele frekansa karşı iyi bir ışın kararlılığını gösteriyor. HPBW azalma nedeni ile antenin ve neticeten radar sisteminin çözünürlük parametresi artıyor. Ornek olarak 8.5 GHz te HPBW 38 dereceden 23 dereceye azalıyor, HPBW 40 % iyileşmesini gosteriyor.

Ek bir çalışma olarak, mikroşerit teknolojisinde başka bir yeni kompakt yönlü monopol anten de sunulmuştur. Bu antenin boyutları oldukça geleneksel yönlü antenler ile karşılaştırıldığında küçülmüştür. Bu antenin kazancı istenilen frekanslarda 5 dBi kadar artırılmıştır. Antenin yansıtma katsayısı bant genişliği 5-9 GHz arasındaki frekansları kapsar. Küçültülmüş boyut ve antenin iyi yönlü karakteristiği, mikrodalga görüntüleme sistemleri ve radar uygulamalarında kullanmak için uygundur.

1. INTRODUCTION

Microwave imaging technology for breast cancer detection has attracted many interests nowadays. The physical basis for breast cancer detection with microwave imaging is the difference in dielectric properties of normal and malignant breast tissues. The motivation for developing a microwave imaging technique for detecting breast cancer is the lower numbers of missed-detections and false-positives which is due to the significant difference in the dielectric properties of normal and malignant breast at microwave frequencies. The estimated malignant-to-normal breast tissue contrast is between 2: 1 and 10: 1, depending on the density of the normal tissue. As another advantage, microwave imaging techniques result in a three-dimensional (3-D) volumetric map of the relevant tissue properties. Also Microwave breast cancer imaging is a noninvasive and indeed potentially low cost alternative. Because of all mentioned reasons, microwave breast imaging has the potential to overcome some of the restrictions of conventional breast cancer screening systems [1].

There is an extended body of literature on medical applications of microwave imaging. Two different methods of active microwave imaging techniques make use of contrasts in dielectric properties: topographic methods and backscatter methods. In microwave tomography the purpose is to recovery of the dielectric-properties profile of an object from measurements of the microwave energy transmitted through the object. But in the other side, as in the case of ground penetrating radar, backscatter methods use the measured reflected signals to infer the locations of significant microwave scatterers. Between normal breast tissue and malignant lesions, Scattering arises from significant contrasts in dielectric properties.

Recently another approach to breast cancer detection is proposed, which is called as confocal microwave imaging (CMI). The procedure of detection of breast tumor in CMI is comprises illuminating the breast with an ultra-wideband pulse from a number of physical antenna locations. In order to provide information that is used to determine the scattered location, the relative arrival times and amplitudes of the backscattered signal are analyzed, using related algorithms. In comparison with

microwave tomography, instead of attempting to completely reconstruct the dielectric-properties profile, the CMI approach seeks only to identify the location of strong scatterers in the breast [1, 2].

Briefly in Radar-based microwave breast imaging, the procedure of attempt is to illuminating the breast with an ultra-wideband pulse of microwaves and consequently detecting reflections. The reflected waves from the tissue are then processed to create images that identify and indicate the location of tumors in the breast. An important section of these systems is the antenna that is used to radiate and receive the ultra-wideband signal. Both in the terms of input impedance matching and radiation pattern over the desired bandwidth, the antenna must demonstrate good performance, in order to use in these applications.

1.1 Statement of the Problem

Directivity of the antenna is the most important characteristic of the antenna in order to achieve high resolution. The Half Power Beam Width (HPBW) of the antenna must be small enough in order to detect smaller details. In the other side, a compact antenna design is desirable in order to reduce the complexities of physical mounting the antenna and also to achieve a degree of conformity with the body [3, 4].

So the antenna design requirements for use in near field near surface measurement applications, such as radar-based microwave breast cancer imaging are as follows: radiation of ultra-wideband signal to transmit short pulses, size of the antenna on the order of a few centimeters to selectively illuminate and permit scanning, an optimum half power near-field beam width(HPBW) to avoid smearing of the scatterers that occurs if the field of view of each antenna is too broad, and finally a good impedance matching across the entire band, This ensures that most of the energy is transmitted. In order to decrease the HPBW of an antenna we have to increase the directivity of the antenna in a desired direction. Various different types of antennas are being considered by research groups involved in tissue-sensing applications using pulsed radar techniques; typical examples of such antennas include the Vivaldi, bowtie, slot line bowtie, horn, and microstrip antennas [5]. This Thesis also presents a printed monopole antenna with the optimum directional characteristics for use in microwave imaging.

1.2 Literature Review

Nowadays there are increasing demands for directional antennas, for the Ultra Wide Band (UWB) applications. Directional antennas are used to optimize Half Power Beam Width (HPBW), more clearly, to increase the radiation intensity in a desired direction by converging radiation pattern. Antenna's HPBW at radar systems is one of the main parameters determining the radar's resolution, in the other words, finer details can be resolved by using a narrower beam. As the other advantages of directive antennas, it is required to minimize the HPBW in order to cover the long distances [6]. Directional beam of an antenna is also desirable for Body-Worn Devices in order to use in Wireless Body Area Network (WBAN), to reduce the effects of human body to electromagnetic radiation [7]. Nevertheless, most of the wide band and UWB antennas like planar monopoles, which are in use, have almost Omni-Directional radiation pattern [8, 9, 10].

Application of interest is microwave breast cancer detection which exploits the contrasts in dielectric properties between healthy and malignant tissue. There are different types of directive antennas. Directivity can be achieved if the antenna is large in a desired direction, such as Horn or Vivaldi antennas [11]. Many efforts have been presented in order to design compact wideband directional antennas for microwave breast imaging which can usually be classified as one of three types (dipole, slot, or monopole) based on their physical features and radiation properties. In other types, antenna includes cavity or shielding plane behind itself, or uses the absorbing materials in order to obtain directivity. But using such approaches cause either increment in the antenna size or decrease in the antenna efficiency as well as complication in the production process [7, 12]. Some other directional antennas such as conventional slot antennas are also presented but as a disadvantage they have a limited operating frequency range [7, 13], while Vivaldi type antennas have a good bandwidth and directional radiation pattern [14]. Printed disc monopole antennas with an L-shaped or parabolic-shaped ground plane also are presented as a directional antennas [15, 16]. Compact bowtie antenna operating at 2-4 GHz for radar-based breast cancer detection [17], Wideband monopole antenna fed by a 50-ohm coplanar waveguide working at 3.4-9.6 GHz for microwave near-field imaging are also presented [18].

As the special type of microstrip directive antennas, Printed disc monopole antennas with an L-shaped or parabolic-shaped ground plane are introduced as a directional antenna for use in microwave imaging system [15, 16]. In these studies it has been shown how partial ground optimization influences the antenna's performance in optimizing the gain and directivity of the antenna. These kinds of directional antennas are somewhat analogous to the UWB type Omni-Directional monopole antennas, where it is shown the effect of ground plane on obtaining the desired directional characteristics of the antenna.

Given that monopole microstrip antennas are the most popular in MWA, and their ease of fabrication, and properties and small size and other advantages of microstrip technology, we selected the monopole type printed antenna with a parabolic-shaped ground as a reflector for our studies. This Thesis presents a new modified design of directional monopole antenna with a parabolic-shaped ground plane as a reflector that can operate over the necessary wide bandwidth for this application.

1.3 Objectives

Printed disc monopole antennas with an L-shaped or parabolic-shaped ground plane are introduced as a directional antenna for use in radar and microwave imaging system. In these studies it has been shown how partial ground optimization influences the antenna's performance, in maximizing the directivity. In this study the effect of the ground plane on obtaining the desired directional characteristics of the antenna is demonstrated and improved.

The aim of this thesis is to design a new modified antenna structure which is convenient especially in the use of near field near surface measurement applications, such as microwave breast cancer imaging. The proposed antenna is a modification of the previous type monopole antennas, which is more directive compared to previous types. Ground plane of the antenna consists of a symmetrical parabolic curve, which its axis extended along the direction of the substrate's diagonal. Directivity is improved by extending parabola's axis of ground plane in the direction of the substrate's diagonal and subsequently, inserting parabolic slots on the ground plane. Extending the axis of parabola in the ground plane along the direction of square substrate's diagonal maximizes the capability of symmetrical ground plane as a reflector. Also the second edge of the ground plane which is created by inserting the

slots, behaves as an additional reflector which cause to increase in the gain and directivity.

The presented planar antenna is composed of a disc-monopole fed by a 50Ω microstrip line. In order to maintain a trade-off between the gain in the favored bandwidth and the size of the antenna, it is designed on square FR4 substrate with dimension of 50mm, where dielectric constant is ε_r=4.4. Thicknesses of the dielectric (d) and conductor layers are 1.6mm and 35μm, respectively. Both simulations and measurements confirm that the proposed antenna has a stable radiation pattern versus frequency. Impedance bandwidth of the antenna covers the frequency range of 4-9 GHz. Improved directivity of 5-15 degrees and improved gain of 1.1-3.1 dBi in the frequency range of 4-9GHz compared to conventional monopole [16] are confirmed. Also in comparison with [15] improved gain of 1.2-5 dBi is obtained.

As an additional attempt, another novel compact directional monopole antenna in microstrip technology is also presented. Dimensions of this antenna are considerably miniaturized in comparison with conventional directional antennas. The ground plane and parasitic element are accurately designed in a way that make the surface currents of radiating elements to move toward the desired direction, which increase the radiation density in the preferred direction and also decrease the radiation intensity in the opposite sides. Gain of the antenna is increased over 5 dBi at the desired frequencies. Reflection coefficient bandwidth of the antenna covers the frequencies among 5-9 GHz. Miniaturized size and a good directional characteristic of the antenna make it possible to use it in the microwave imaging systems and radar applications.

2. FUNDAMENTAL PARAMETERS OF ANTENNAS

2.1 Purpose

In order to study the performance of an antenna, it is required to know about various parameters of the antenna. Radiation pattern, gain, directivity, reflection coefficient and other parameters of an antenna are necessary to be defined in order to have more study in the field of any particular type of an antenna. Parameter definitions are given in this chapter.

2.2 Radiation Pattern

An antenna radiation pattern or antenna pattern is defined as "a mathematical function or a graphical representation of the radiation properties of the antenna as a function of space coordinates" [19]. Radiation pattern of an antenna is determined in the far field region and it is also represented as a function of the directional coordinates. Radiation properties include power flux density, radiation intensity, field strength, directivity, phase or polarization. In the most cases radiation pattern is two or three dimensional spatial distribution of radiated energy as a function of the observer's position beside a surface of constant radius. A convenient set of coordinates is shown in Figure 2.1. The power pattern is usually plotted on a logarithmic scale or more commonly in decibels (dB). This scale is usually desirable because a logarithmic scale can accentuate in more details those parts of the pattern that have very low values, which later we will refer to as minor lobes.

In order to have the full picture of radiation pattern of an antenna we have to measure the E-plane and H-plane patterns. The E-plane contains the electric field (E-field) vector and the direction of maximum radiation. Whereas the magnetic field or H-plane lies at a right angle to the E-plane and contains the magnetic field (H-field) vector and direction of maximum radiation. Radiation pattern distribution depends on the application for which an antenna will be used. For example, in the case of radar

applications directional antennas are favored to use. Also in order to cover the long distances directional antennas can be used [6], [19].
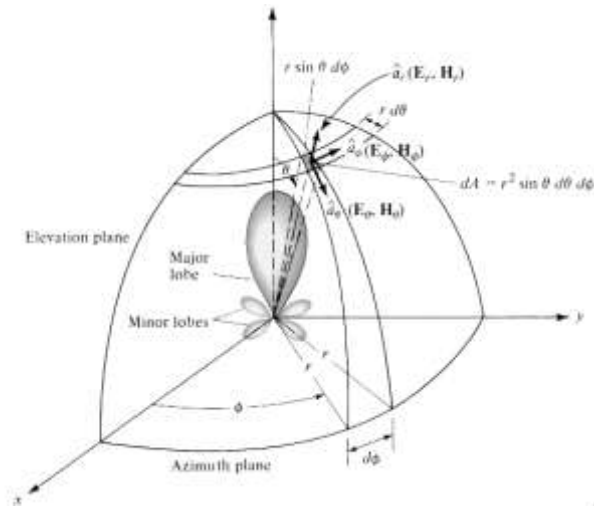
Figure 2.1 : Coordinate system for antenna analysis.

For an antenna, Field pattern in linear scale represents a plot of the magnitude of the electric or magnetic field as a function of the angular space. Power pattern in linear scale represents a plot of the square of the magnitude of the electric or magnetic field as a function of the angular space. Finally, Power pattern (in dB) represents the magnitude of the electric or magnetic field, in decibels, as a function of the angular space.

The two-dimensional normalized field pattern (linear scale), power pattern (plotted in linear scale), and power pattern (dB scale) of a 10-element linear antenna array of isotropic sources, with a spacing of d = 0.25λ between the elements, are shown in Figure 2.2.
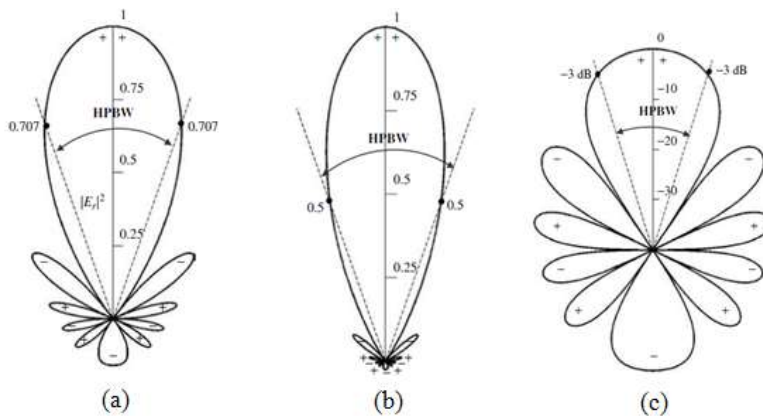
Figure 2.2 : Two-dimensional normalized (a) field pattern (linear scale), (b) power pattern(linear scale), and (c) power pattern(in dB) of a 10-element linear array with a spacing of d = 0.25λ.

8

In Figure 2.2 points where the pattern achieves its half-power, relative to the maximum value of the pattern, is in a. field pattern at 0.707 value of its maximum, as shown in Figure 2.2(a) b. power pattern (in a linear scale) at its 0.5 value of its maximum, as shown in Figure 2.2(b) c. power pattern (in dB) at −3 dB value of its maximum, as shown in Figure 2.2(c). All three patterns confirm the same angular separation between the two half-power points.

2.2.1 Radiation pattern lobes

A radiation lobe is a portion of the radiation pattern bounded by regions of relatively weak radiation intensity .Various parts of a radiation pattern are referred to as lobes, which is classified into major or main, minor, side, and back lobes. Figure 2.3 demonstrates a symmetrical three dimensional polar pattern with a number of radiation lobes. Some are of greater radiation intensity than others, but all are classified as lobes. Figure 2.4 illustrates a linear two-dimensional pattern [one plane of Figure 2.3] of the same Beam of the antenna.
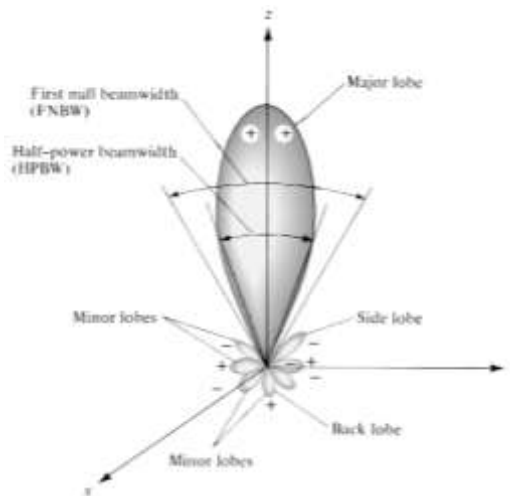
Figure 2.3 : Radiation lobes and beamwidths of an antenna pattern.
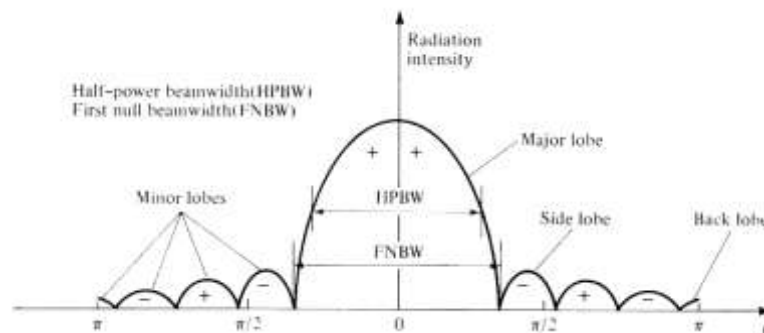
Figure 2.4 : Linear plot of power pattern and its associated lobes and beamwidths.

9

A major lobe (also called main beam) is defined as the radiation lobe containing the direction of maximum radiation. In Figure 2.3 the major lobe is poynting in the θ = 0 direction. A minor lobe is any lobe except a major lobe. In Figures 2.3(a) and (b) all the lobes with the exception of the major are the minor lobes. A side lobe is a radiation lobe in any direction other than the intended lobe. A back lobe is a radiation lobe whose axis makes an angle of approximately 180◦ with respect to the beam of an antenna. Minor lobes usually represent radiation in undesired directions, and they should be minimized. Side lobes are normally the largest of the minor lobes. The level of minor lobes is usually expressed as a ratio of the power density in the lobe in question to that of the major lobe. This ratio is often termed the side lobe ratio or side lobe level. Side lobe levels of −20 dB or smaller are usually not desirable in most applications.

2.2.2 Isotropic, directional, and omni-directional patterns

Directivity is defined as the ratio of radiation intensity in a given direction to the radiation intensity averaged over all directions. At the next sections we will present a complete concept of directivity. Figure 2.5 demonstrate a typical directional Horn antenna.

An isotropic antenna has an equal radiation in all directions. Although it is ideal and not physically realizable, it is often taken as a reference for expressing the directive properties of actual antennas. A directional antenna is one having the property of radiating or receiving electromagnetic waves more effectively in some directions than in others. This term is usually applied to an antenna whose maximum directivity is significantly greater than that of a half-wave dipole.
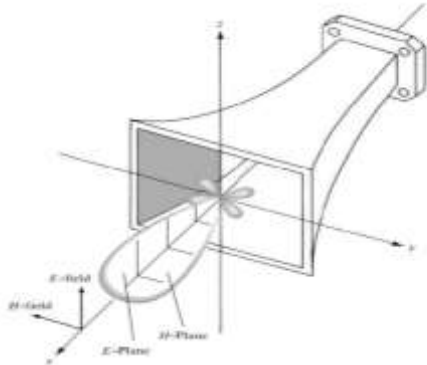
Figure 2.5 : L Principal E- and H-plane patterns for a pyramidal horn antenna.

2.3 Radiation Power Density

The quantity used to describe the power associated with an electromagnetic wave is the instantaneous Poynting vector defined as:

$$\dot{W} = \dot{E} \times \dot{H}$$

(2.1)

$\dot{W} =$ Instantaneous Poynting vector   (W/m2)

$\dot{E} =$ Instantaneous electric-field intensity   (V/m)

$\dot{H} =$ Instantaneous magnetic-field intensity   (A/m)

Note letters with the points are used to demonstrate the instantaneous fields and quantities, while normal letters are used to represent their complex counterparts. Since the Poynting vector is a power density, the total power crossing a closed surface can be obtained by integrating the normal component of the Poynting vector over the entire surface. In equation form:

$$\dot{P} = \oiint_s w.ds = \iint_s (w.n)da$$

(2.2)

$\dot{P} =$ instantaneous total power (W)

n = Unit vector normal to the surface

da = Infinitesimal area of the closed surface (m2)

For the applications of time-varying fields, it is desirable to find the average power density which is achieved by integrating the instantaneous Poynting vector over one period and dividing by the period. For time-harmonic variations of the form e^{jwt}, the complex fields E and H are defined, which are related to their instantaneous counterparts E and H by:

$$\dot{E}(x,y,z;t) = \mathrm{Re}\left[E(x,y,x)e^{jwt}\right]$$

(2.3)

$$\dot{H}(x,y,z;t) = \mathrm{Re}\left[H(x,y,x)e^{jwt}\right]$$

(2.4)

Using the definitions of (2-3) and (2-4) and the identity:

$$\text{Re}\left[Ee^{jwt}\right] = 1/2\left[Ee^{jwt} + E^* s^{-jwt}\right]$$

(2-1) can be written as:

$$\dot{W} = \dot{E} \times \dot{H} = \frac{\text{Re}\left[E \times H^{?*}\right] + \text{Re}\left[E \times He^{2jwt}\right]}{2} \tag{2.5}$$

The first term of (2-5) is not a function of time, and the time variations of the second are twice the given frequency. The time average Poynting vector (average power density) can be written as:

$$W_{av}(x,y,z) = \left[\dot{W}(x,y,x;t)\right]_{av} = \frac{\text{Re}\left[E \times H^*\right]}{2} \quad (\text{W/m}^2) \tag{2.6}$$

The ½ factor appears in (2-5) and (2-6) because the E and H fields represent peak values, and it should be omitted for RMS values. A close observation of (2-6) may raise a question. Based on the definition of (2-6), the average power radiated by an antenna is defined as:

$$P_{rad} = P_{av} = \oiint_s W_{rad}.ds = \oiint_s (W_{av}.n)da = 1/2\oiint_s \text{Re}(E \times H^*).ds \tag{2.7}$$

The observations are usually made on a large sphere of constant radius extending into the far field. In practice, absolute power patterns are usually not desired. However, the performance of the antenna is measured in terms of the gain (to be discussed in a subsequent section) and in terms of relative power patterns. Three dimensional patterns cannot be measured, but they can be constructed with a number of two-dimensional cuts.

Anisotropic radiator is an ideal source that radiates equally in all directions. Although it does not exist in practice, it provides a convenient isotropic reference with which to compare other antennas. Because of its symmetric radiation, its Poynting vector will not be a function of the spherical coordinate angles θ and φ. In addition, it will have only a radial component. Thus the total power radiated by it is given by:

$$p_{rad} = \iint_s W_0 . ds = \int_0^{2\pi} \int_0^{\pi} [a_r W_0(r)] . [a_r r^2 \sin\theta d\theta d\phi] = 4\pi r^2 W_0 \qquad \text{(2.8)}$$

And the power density by:

$$W_0 = a_r W_0 = a_r \left(\frac{P_{rad}}{4\pi r^2} \right) \qquad \text{(2.9)}$$

2.4 Radiation Intensity

The radiation intensity is a far-field parameter, is defined as the power radiated from an antenna per unit solid angle in a desired direction and it can be obtained by multiplying the radiation density by the square of the distance. In mathematical form it is expressed as:

$$U = r^2 W_{rad} \qquad \text{(2.10)}$$

where:

U   = radiation intensity (W/unit solid angle)

W_{rad} = radiation density (W/m^2)

The radiation intensity is also related to the far-zone electric field of an antenna, by:

$$U(\theta,\phi) = \frac{r^2}{2\eta} |E(r,\theta,\phi)|^2 \approx \frac{r^2}{2\eta} [|E_\theta(r,\theta,\phi)|^2 + |E_\phi(r,\theta,\phi)|^2] \approx$$
$$\frac{1}{2\eta} [|E_\theta^0(\theta,\phi)|^2 + |E_\phi^0(\theta,\phi)|^2] \qquad \text{(2.10a)}$$

where:

E(r, θ, ϕ) = far-zone electric-field intensity of the antenna

$$E(r, \theta, \phi) = E^0(\theta,\phi) \frac{e^{-jkr}}{r}$$

E_θ, E_ϕ = Far-zone electric-field components of the antenna

 η = intrinsic impedance of the medium

13

Thus the power pattern is also a measure of the radiation intensity. The total power is obtained by integrating the radiation intensity, as given by (2-10), over the entire solid angle of 4π. Thus:

$$P_{rad} = \oiint_{\Omega} U d\Omega = \int_0^{2\pi} \int_0^{\pi} U \sin\theta d\theta d\phi \qquad \textbf{(2.11)}$$

where:

d_Ω = element of solid angle = sinθ dθ dφ

For anisotropic source U will be independent of the angles θ and φ, as was the case for W_{rad}. Thus (2-11) can be written as:

$$P_{rad} = \oiint_{\Omega} U_0 d\Omega = U_0 \oiint_{\Omega} d\Omega = 4\pi U_0 \qquad \textbf{(2.12)}$$

Or the radiation intensity of an isotropic source as:

$$U_0 = \frac{P_{rad}}{4\pi} \qquad \textbf{(2.13)}$$

2.5 Beamwidth

The beamwidth of a pattern is defined as the angular separation between two identical points on opposite side of the pattern maximum. In an antenna pattern, one of the most widely used beamwidths is the Half-Power Beamwidth (HPBW). This is demonstrated in Figure 2.2. HPBW is defined as the angle between the two directions in which the radiation intensity is one-half value of the beam. Another important beamwidth is the angular separation between the first nulls of the pattern, and it is referred to as the First-Null Beamwidth (FNBW). Both the HPBW and FNBW are demonstrated for the pattern in Figure 2.6. The beamwidth of an antenna is a very important figure of merit and often is used as a trade-off between it and the side lobe level; that is, as the beamwidth decreases, the side lobe increases and vice versa. In addition, the beamwidth of the antenna is also used to describe the resolution capabilities of the antenna to distinguish between two adjacent radiating sources or radar targets. Resolution capability of an antenna to distinguish between two sources is equal to half the first-null beamwidth (FNBW/2), or the half power

beamwidth (HPBW). That is, two sources separated by angular distances equal or greater than FNBW/2 ≈ HPBW of an antenna with a uniform distribution can be resolved. If the separation is smaller, then the antenna will tend to smooth the angular separation distance.
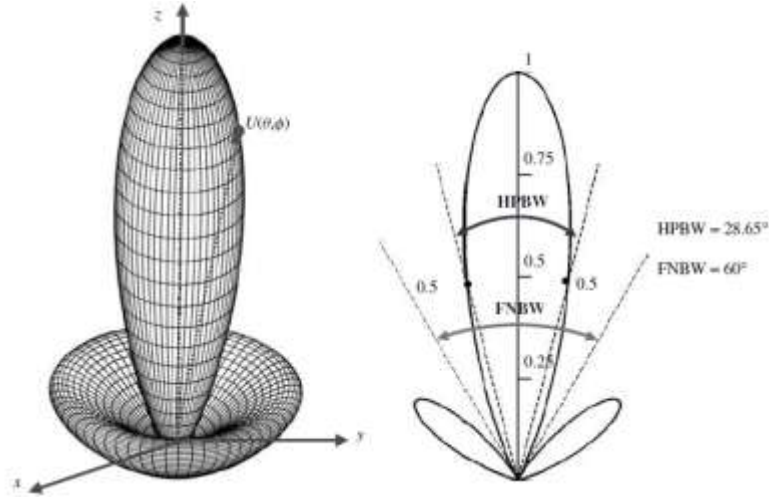
Figure 2.6 : Three (left) and two (right) dimensional power patterns (in linear scale) of $U(\theta) = \cos^2(\theta) \cos^2(3\theta)$.

2.6 Directivity

In a given direction from the antenna directivity is defined as the ratio of the radiation intensity to the radiation intensity averaged over all directions. The average radiation intensity is equal to the total power radiated by the antenna divided by 4π. More simply, the directivity of a nonisotropic source is equal to the ratio of its radiation intensity in a given direction over that of an isotropic source [20]. In mathematical form, using (2-13), it can be written as:

$$D = \frac{U}{U_0} = \frac{4\pi U}{P_{rad}}$$

(2.14)

If the direction is not specified, it implies the direction of maximum radiation intensity (maximum directivity) expressed as:

$$D_{max} = D_0 = \frac{U_{max}}{U_0} = \frac{4\pi U_{max}}{P_{rad}}$$

(2.14a)

D = directivity (dimensionless)

D_0 = maximum directivity (dimensionless)

15

U = radiation intensity (W/unit solid angle)

U_{max} = maximum radiation intensity (W/unit solid angle)

U_0 = radiation intensity of isotropic source (W/unit solid angle)

P_{rad} = total radiated power (W)

From (2-14) or (2-14a) for anisotropic source the directivity is unity since U, U_{max}, and U_0 are all equal to each other. For the case which antennas have orthogonal polarization components, the partial directivity of an antenna for a given polarization in a given direction is defined as that part of the radiation intensity corresponding to a given polarization divided by the total radiation intensity averaged over all directions. Then in a given direction the total directivity is the sum of the partial directivities for any two orthogonal polarizations. The total maximum directivity D_0 for the orthogonal θ and φ components of an antenna can be written as:

$$D_0 = D_\theta + D_\phi \tag{2.15}$$

While the partial directivities D_θ and D_ϕ are expressed as:

$$D_\theta = \frac{4\pi U_\theta}{(P_{rad})_\vartheta + (P_{rad})_\phi} \tag{2.15a}$$

$$D_\phi = \frac{4\pi U_\phi}{(P_{rad})_\vartheta + (P_{rad})_\phi} \tag{2.15b}$$

Where:

U_θ = radiation intensity in a given direction contained in θ field component

U_ϕ = radiation intensity in a given direction contained in φ field component

$(P_{rad})_\theta$ = radiated power in all directions contained in θ field component

$(P_{rad})_\phi$ = radiated power in all directions contained in φ field component

The directivity of an isotropic source is unity since its power is radiated equally well in all directions. For all other sources, the maximum directivity will always be greater than unity, and it is a relative figure of merit. In equation form, this is

indicated in (2-14a). The directivity can be smaller than unity; in fact it can be equal to zero. The values of directivity will be equal to or greater than zero and equal to or less than the maximum directivity ($0 \leq D \leq D_0$).

A more general expression for the directivity can be developed to include sources with radiation patterns that may be functions of both spherical coordinate angles θ and φ. So it may now be proper, since the basic definitions have been illustrated by simple examples, to formulate the more general expressions. Let the radiation intensity of an antenna be of the form:

$$U = B_0 F(\theta,\phi) \approx \frac{1}{2\eta}\left[\left|E_\theta^0(\theta,\phi)\right|^2 + \left|E_\phi^0(\theta,\phi)\right|^2\right] \tag{2.16}$$

where B_0 is a constant, and E_θ and E_φ are the antenna's far-zone electric-field components.

The maximum value of (2-16) is given by:

$$U_{max} = B_0 F(\theta,\phi)_{max} = B_0 F_{max}(\theta,\phi) \tag{2.16a}$$

The total radiated power is found using:

$$P_{rad} = \oiint_\Omega U(\theta,\phi)d\Omega = B_0 \int_0^{2\pi} \int_0^\pi F(\theta,\phi)\sin\theta d\theta d\phi \tag{2.17}$$

We now write the general expression for the directivity and maximum directivity using (2-14) and (2-14a), respectively, as:

$$D(\theta,\phi) = 4\pi \frac{F(\theta,\phi)}{\int_0^{2\pi} \int_0^\pi F(\theta,\phi)\sin\theta d\theta d\phi} \tag{2.18}$$

$$D_0 = 4\pi \frac{F(\theta,\phi)_{max}}{\int_0^{2\pi} \int_0^\pi F(\theta,\phi)\sin\theta d\theta d\phi} \tag{2.19}$$

Equation (2-19) can also be written as:

$$D_0 = \cfrac{4\pi}{\left[\displaystyle\int_0^{2\pi}\int_0^{\pi} F(\theta,\phi)\sin\theta d\theta d\phi \middle/ F(\theta,\phi)_{max} \right]} = \frac{4\pi}{\Omega_A}$$

(2.20)

where Ω_A is the beam solid angle, and it is given by:

$$\Omega_A = \frac{1}{F(\theta,\phi)_{max}} \int_0^{2\pi}\int_0^{\pi} F(\theta,\phi)\sin\theta d\theta d\phi = \int_0^{2\pi}\int_0^{\pi} F_n(\theta,\phi)\sin\theta d\theta d\phi$$

(2.21)

$$F_n(\theta,\phi) = \frac{F(\theta,\phi)}{F(\theta,\phi)_{max}}$$

(2.22)

The beam solid angle Ω_A is defined as the solid angle through which all the power of the antenna would flow if its radiation intensity is constant for all angles within Ω_A. Dividing by $F(\theta, \varphi)|_{max}$ merely normalizes the radiation intensity $F(\theta, \varphi)$, and it makes its maximum value unity.

2.7 Directional Patterns

It is proper to derive simpler expressions, Instead of using the exact expression of (2-20) even if they are approximate. For antennas with one narrow major lobe and very negligible minor lobes, the beam solid angle is approximately equal to the product of the half-power beamwidths in two perpendicular planes shown in Figure 2.7(a). For a rotationally symmetric pattern, the half-power beamwidths in any two perpendicular planes are the same, as illustrated in Figure 2.7(b).

With this approximation, (2-23) can be approximated by:

$$D_0 = \frac{4\pi}{\Omega_A} \approx \frac{4\pi}{\Theta_{1r}\Theta_{2r}}$$

(2.23)
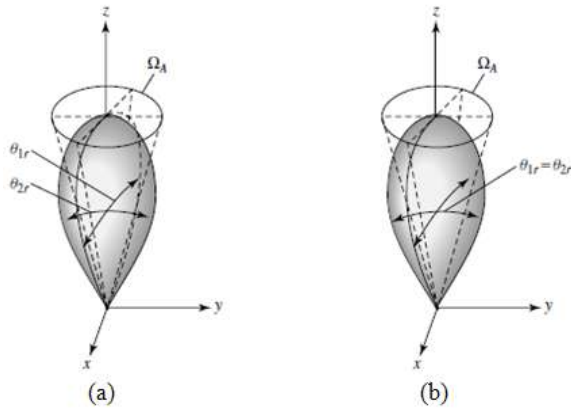
Figure 2.7 : Beam solid angles for nonsymmetrical (a) and symmetrical (b) radiation patterns.

The beam solid angle Ω_A has been approximated by:

$$\Omega_A = \Theta_{1r}\Theta_{2r}$$

(2.23a)

where:

Θ_{1r}= half-power beamwidth in one plane (rad)

Θ_{2r}= half-power beamwidth in a plane at a right angle to the other (rad)

If the beamwidths are known in degrees, (2-23) can be written as:

$$D_0 = \frac{4\pi(180/\pi)^2}{\Theta_{1d}\Theta_{2d}} \approx \frac{41253}{\Theta_{1d}\Theta_{2d}}$$

(2.24)

where:

Θ_{1d}= half-power beamwidth in one plane (degrees)

Θ_{2d}= half-power beamwidth in a plane at a right angle to the other (degrees)

For patterns with significant minor lobes, the values of maximum directivity obtained using (2-23) or (2-24), which neglect any minor lobes, will usually be too high.

Many times it is desirable to express the directivity in decibels (dB) instead of dimensionless quantities. The expressions for converting the dimensionless quantities of directivity and maximum directivity to decibels (dB) are:

$$D(dB) = 10\log_{10}[D(\dim ensionless)]$$

(2.25a)

$$D_0(dB) = 10\log_{10}[D_0(\mathrm{dim}ensionless)]$$

(2.25b)

It has also been proposed that the maximum directivity of an antenna can also be obtained approximately by using the formula:

$$\frac{1}{D_0} = \frac{1}{2}\left(\frac{1}{D_1} + \frac{1}{D_2}\right)$$

(2.26)

where:

$$D_1 \approx \frac{1}{\left[\dfrac{1}{2\ln 2}\displaystyle\int_0^{\Theta_{1r}/2}\sin\theta d\theta\right]} \approx \frac{16\ln 2}{\Theta_{1r}^{\,2}}$$

(2.26a)

$$D_2 \approx \frac{1}{\left[\dfrac{1}{2\ln 2}\displaystyle\int_0^{\Theta_{2r}/2}\sin\theta d\theta\right]} \approx \frac{16\ln 2}{\Theta_{2r}^{\,2}}$$

(2.26b)

Θ_{1r} and Θ_{2r} are the half-power beamwidths of the E- and H-planes, respectively. The formula of (2-26) will be referred to as the arithmetic mean of the maximum directivity. Using (2-26a) and (2-26b) we can write (2-26) as:

$$\frac{1}{D_0} \approx \frac{1}{2\ln 2}\left(\frac{\Theta_{1r}^2}{16} + \frac{\Theta_{2r}^2}{16}\right) = \frac{\Theta_{1r}^2 + \Theta_{2r}^2}{32\ln 2}$$

(2.27)

$$D_0 \approx \frac{32\ln 2}{\Theta_{1r}^2 + \Theta_{2r}^2}$$

(2.27a)

$$D_0 \approx \frac{72815}{\Theta_{1d}^2 + \Theta_{2d}^2}$$

(2.27b)

Where, Θ_{1d} and Θ_{2d} are the half power beam widths in degrees. Equation (2-a) is to be contrasted with (2-23) while (2-27b) should be compared with (2-24).

2.8 Antenna Efficiency

Using Figure 2.8 The total antenna efficiency e_0 is used to take into account losses at the input terminals and within the structure of the antenna. Such losses may be due, referring to Figure 2.8(b), to:

1. Reflections because of the mismatch between the transmission line and the antenna

2. $I^2 R$ losses (conduction and dielectric)
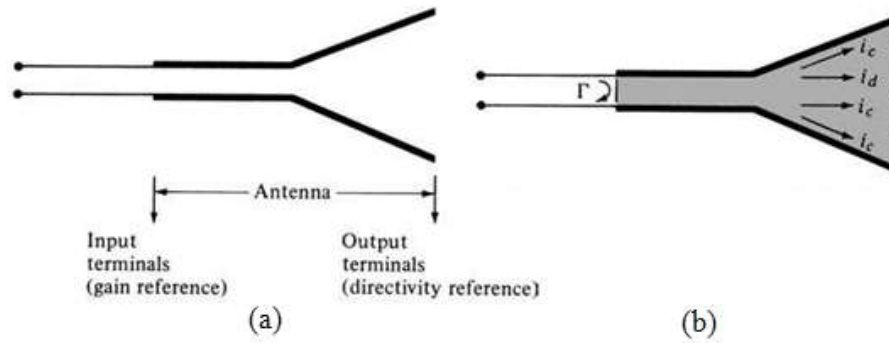
Figure 2.8 : (a) Reference terminals and (b) losses of an antenna.

In general, the overall efficiency can be written as:

$$e_0 = e_r e_c e_d \tag{2.28}$$

Where:

e_0 = total efficiency (dimensionless)

e_r = reflection (mismatch) efficiency $= \left(1 - |\Gamma|^2\right)$ (dimensionless)

e_c = conduction efficiency (dimensionless)

e_d = dielectric efficiency (dimensionless)

Γ = voltage reflection coefficient at the input terminals of the antenna

$\left[\Gamma = \left(Z_{in} - Z_0 / Z_{in} + Z_0\right)\right]$ Where Z_{in} = antenna input impedance

Z_0 = characteristic impedance of the transmission line]

VSWR = voltage standing wave ratio $= \dfrac{1+|\Gamma|}{1-|\Gamma|}$

Usually e_c and e_d are very difficult to compute, but they can be determined experimentally. Even by measurements they cannot be separated, and it is usually more convenient to write (2-28) as:

$$e_0 = e_r e_{cd} = e_{cd}\left(1-|\Gamma|^2\right)$$

(2.29)

Where $e_{cd} = e_c e_d$ = antenna radiation efficiency, which is used to relate the gain and directivity.

2.9 Gain

Gain of the antenna is a measure that takes into account the efficiency of the antenna as well as its directional capabilities. Gain of an antenna is defined as the ratio of the intensity, in a given direction, to the radiation intensity that would be obtained if the power accepted by the antenna were radiated isotropically. The radiation intensity corresponding to the isotropically radiated power is equal to the power accepted (input) by the antenna divided by 4π:

$$Gain = 4\pi \frac{radiation\ \mathrm{int}ensity}{total\ input\,(accepted\,)power} =$$
$$4\pi \frac{U(\theta,\phi)}{P_{in}}$$

(Dimensionless)

(2.30)

Also relative gain of an antenna is defined as the ratio of the power gain in a given direction to the power gain of a reference antenna in its referenced direction. Thus:

$$Gain = \frac{4\pi U(\theta,\phi)}{P_{in}(lossless\ isotropic\ soource)}$$

(Dimensionless)

(2.30a)

When the direction is not stated, the power gain is usually taken in the direction of maximum radiation. Considering the Figure 2.8(a), that the total radiated power (P_{rad}) is related to the total input power (P_{in}) by:

$$P_{rad} = e_{cd}P_{in} \tag{2.31}$$

where e_{cd} is the antenna radiation efficiency (dimensionless) which is defined before. Using (2-30) reduces (2-30a) to:

$$G(\theta,\phi) = e_{cd}\left[4\pi\frac{U(\theta,\phi)}{P_{rad}}\right] \tag{2.32}$$

which is related to the directivity of (2-16) and (2-21) by:

$$G(\theta,\phi) = e_{cd}D(\theta,\phi) \tag{2.33}$$

In a similar manner, the maximum value of the gain is related to the maximum directivity of (2-14a) and (2-20) by:

$$G_0 = G(\theta,\phi)_{max} = e_{cd}D(\theta,\phi)_{max} = e_{cd}D_0 \tag{2.33a}$$

and Consequently:

$$G_0(dB) = 10\log_{10}\left[e_{cd}D_0(\dim ensionless)\right] \tag{2.34}$$

2.10 Reflection Coefficient

The Reflection coefficient S11 indicates how well an antenna is matched to the input transmission line. It is a parameter that determines how well signal transition from the input transmission line to the free space is performed by the antenna. An antenna is said to be sufficiently matched if 10% or less of the incident signal is lost during this transition process. The frequency range over which the antenna reflection coefficient S_{11} is -10dB or less is said to be the impedance bandwidth of the antenna. Over this bandwidth it can be operated with minimum power reflection and maximum radiation.

3. MICROSTRIP ANTENNAS

3.1 Introduction

Firstly, the concept of the Microstrip antennas proposed by Deschamps in 1953. But, practical antennas were developed by Munson and Howell in the 1970s. Considering the advantages of MSAs the demand for smaller and low-profile microstrip antennas was increased with increasing requirements for personal and mobile communications. The simplest form of microstrip antenna consists of a radiating patch on one side of a dielectric substrate and a ground plane on the other side. The top and side views of a rectangular MSA (RMSA) are shown in Figure 3.1. However, other shapes, such as the square, circular, triangular, semicircular, sectoral, and annular ring shapes shown in Figure 3.2, are also used [21,22]. Radiation from the MSA can occur from the fringing fields between the periphery of the patch and the ground plane. The length L of the rectangular patch for the fundamental TM_{10} mode excitation is slightly smaller than $\lambda/2$, where λ is the wavelength in the dielectric medium, which in terms of free-space wavelength λ_0 is given as $\lambda/\sqrt{\varsigma_r}$ where, ε_e is the effective dielectric constant of a microstrip line of width W.
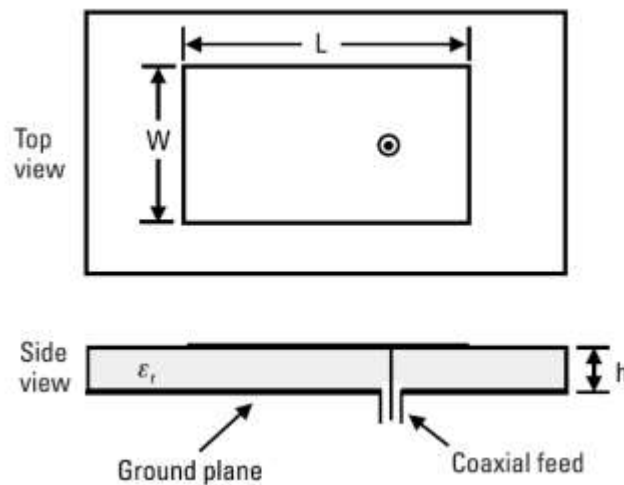
Figure 3.1 : MSA configuration.
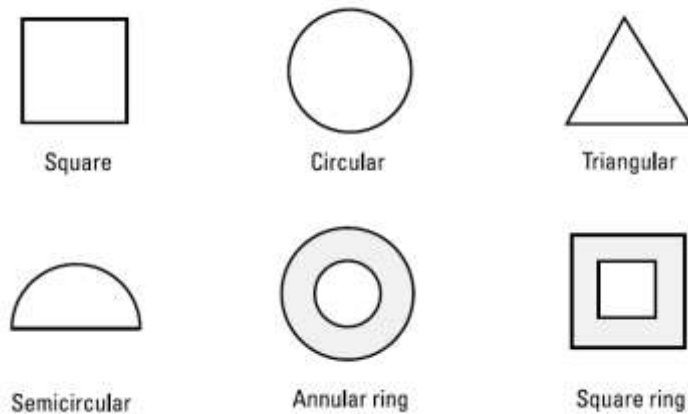
Figure 3.2 : Different shapes of microstrip patches.

3.2 Advantages

Microstrip antennas have several advantages compared to the conventional microwave antennas. The important and remarkable advantages of microstrip antennas are listed as follows:

- They are lightweight and have a small volume and low-profile configuration.

- They can be made conformal to the host surface.

- Their ease of mass production using printed-circuit technology leadsto a low fabrication cost.

- They are easier to integrate with other MICs on the same substrate.

- They allow both linear polarization and CP.

- They can be made compact for use in personal mobile communication.

- They allow for dual- and triple-frequency operations.

3.3 Disadvantages

Also microwave antennas have some disadvantages as compared to conventional microwave antennas. They are the following:

- Narrow BW

- Lower gain

- Low power-handling capability

MSAs have narrow BW, which is the major limiting factor for the widespread application of these antennas. Increasing the BW of MSAs has been the major thrust of research in this field.

3.4 Applications of MSAs

The advantages of MSAs make them suitable for numerous applications. The telemetry and communications antennas on missiles need to be thin and conformal and are often MSAs. Radar altimeters use small arrays of microstrip radiators. Also satellite communication and telephone are the other applications for microstrip antennas. Microstrip arrays have been used for satellite imaging systems. Patch antennas have been used on communication links between ships or buoys and satellites. Smart weapon systems use MSAs because of their thin profile. Pagers, the global system for mobile communication (GSM), and the global positioning system (GPS) are major users of MSAs.

3.5 Feeding Techniques

The MSA can be excited directly either by a coaxial probe or by a microstrip line. It can also be excited indirectly using electromagnetic coupling or aperture coupling and a coplanar waveguide feed, in which case there is no direct metallic contact between the feed line and the patch. Feeding technique influences the input impedance consequently is an important design parameter. The coaxial or probe feed arrangement is shown in Figure 3.1. The main advantage of this feed is that it can be placed at any desired location inside the patch to match with its input impedance. The disadvantages are that the hole has to be drilled in the substrate and that the connector protrudes outside the bottom ground plane, so that it is not completely planar. A patch excited by microstrip line feed is shown in Figure 3.3(a). This feed arrangement has the advantage that it can be etched on the same substrate, so the total structure remains planar. The drawback is the radiation from the feed line, which leads to an increase in the cross-polar level.

The indirect feed, discussed below, solves these problems. An electromagnetically coupled RMSA is shown in Figure 3.3(b). The advantages of this feed configuration include the elimination of spurious feed-network radiation; the choice between two

different dielectric media, one for the patch and the other for the feed line to optimize the individual performances; and an increase in the BW due to the increase in the overall substrate thickness of the MSA. Another method for indirectly exciting a patch employs aperture coupling. In the aperture-coupled MSA configuration, the field is coupled from the microstrip line feed to the radiating patch through an electrically small aperture or slot cut in the ground plane, as shown in Figure 3.3(c). The coupling aperture is usually centered under the patch, leading to lower cross-polarization due to symmetry of the configuration. The shape, size, and location of the aperture decide the amount of coupling from the feed line to the patch. The slot aperture can be either resonant or nonresonant [24,25].
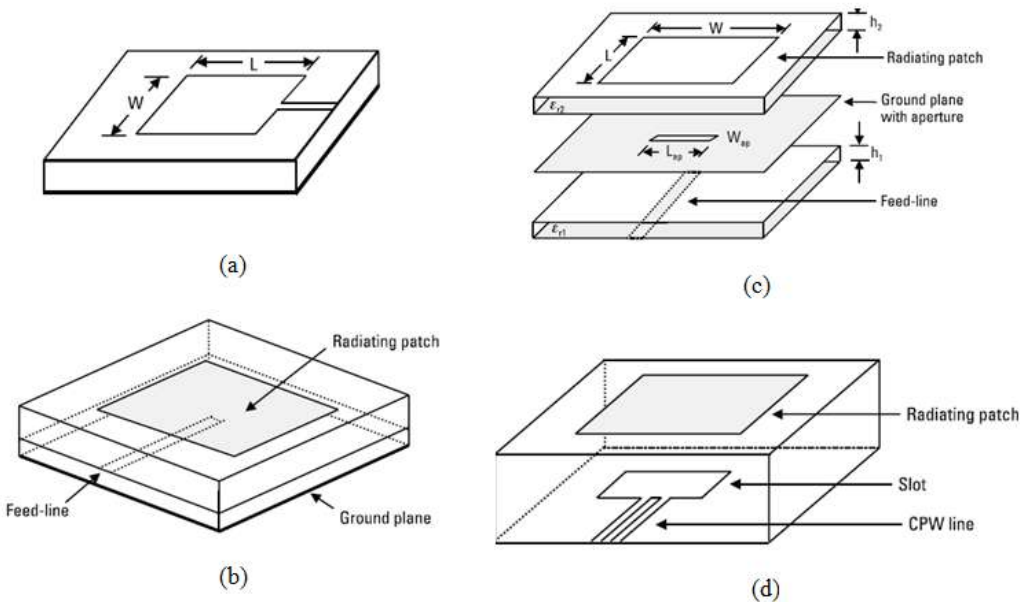
Figure 3.3 : Rectangular MSA fed by (a) microstrip line, (b) electromagnetic coupling, (c) aperture coupling, and (d) coplanar waveguide (CPW).

The resonant slot provides another resonance in addition to the patch resonance thereby increasing the BW at the expense of an increase in back radiation. This feeding method gives increased BW. The coplanar waveguide feed, shown in Figure 3.3(d), has also been used to excite the MSA. In this method, the coplanar waveguide is etched on the ground plane of the MSA. The line is excited by a coaxial feed and is terminated by a slot, whose length is chosen to be between 0.25 and 0.29 of the slot wavelength. The main disadvantage of this method is the high radiation from the rather longer slot, leading to the poor front-to back ratio.

3.6 Methods of Analysis

The analysis methods for MSAs is divided into two groups. In the first group, the methods are based on equivalent magnetic current distribution around the patch edges (similar to slot antennas). There are three popular analytical techniques:

- The transmission line model

- The cavity model

- The MNM

In the second group, the methods are based on the electric current distribution on the patch conductor and the ground plane (similar to dipole antennas, used in conjunction with full-wave simulation/numerical analysis methods). Some of the numerical methods for analyzing MSAs are listed as follows:

- The method of moments (MoM)

- The finite-element method (FEM)

- The spectral domain technique (SDT)

- The finite-difference time domain (FDTD) method

In this section some methods of analysis are explained.

3.6.1 MoM

In the MoM, the surface currents are used to model the microstrip patch, and volume polarization currents in the dielectric slab are used to model the fields in the dielectric slab. An integral equation is formulated for the unknown currents on the microstrip patches and the feed lines and their images in the ground plane. The integral equations are transformed into algebraic equations that can be easily solved using a computer.

3.6.2 FEM

The FEM, unlike the MoM, is suitable for volumetric configurations. In this method, the region of interest is divided into any number of finite surfaces or volume elements depending upon the planar or volumetric structures to be analyzed. These discretized units, generally referred to as finite elements, can be any well-defined

geometrical shapes such as triangular elements for planar configurations and tetrahedral and prismatic elements for three-dimensional configurations, which are suitable even for curved geometry. It involves the integration of certain basic functions over the entire conducting patch, which is divided into a number of subsections. The problem of solving wave equations with inhomogeneous boundary conditions is tackled by decomposing it into two boundary value problems, one with Laplace's equation with an inhomogeneous boundary and the other corresponding to an inhomogeneous wave equation with a homogeneous boundary condition.

3.6.3 SDT

In the SDT, a two-dimensional Fourier transform along the two orthogonal directions of the patch in the plane of substrate is employed. Boundary conditions are applied in Fourier transform plane. The current distribution on the conducting patch is expanded in terms of chosen basis functions, and the resulting matrix equation is solved to evaluate the electric current distribution on the conducting patch and the equivalent magnetic current distribution on the surrounding substrate surface. The various parameters of the antennas are then evaluated.

3.6.4 FDTD method

The FDTD method is well-suited for MSAs, as it can conveniently model numerous structural inhomogenities encountered in these configurations. It can also predict the response of the MSA over the wide BW with a single simulation. In this technique, spatial as well as time grid for the electric and magnetic fields are generated over which the solution is required. The spatial discretizations along three Cartesian coordinates are taken to be same. The E cell edges are aligned with the boundary of the configuration and H-fields are assumed to be located at the center of each E cell. Each cell contains information about material characteristics. The cells containing the sources are excited with a suitable excitation function, which propagates along the structure. The discretized time variations of the fields are determined at desired locations. Using a line integral of the electric field, the voltage across the two locations can be obtained. The current is computed by a loop integral of the magnetic field surrounding the conductor, where the Fourier transform yields a frequency response.

3.7 Review of Various Broadband Techniques for MSAs

Narrow BW is the most serious limitation of the microstrip antennas. The BW could be defined in terms of its VSWR or input impedance variation with frequency or in terms of radiation parameters. Therefore, the various definitions of the BW are described.

3.7.1 Definition of BW

The BW of the MSA is inversely proportional to its quality factor Q and is given by:

$$BW = \frac{VSWR - 1}{Q\sqrt{VSWR}}$$

(3.1)

where VSWR is defined in terms of the input reflection coefficient Γ as:

$$VSWR = \frac{1 + |\Gamma|}{1 - |\Gamma|}$$

(3.2)

The Γ is a measure of reflected signal at the feed-point of the antenna. It is defined in terms of input impedance Z_{in} of the antenna and the characteristic impedance Z_0 of the feed line as given below:

$$\Gamma = \frac{Z_{in} - Z_0}{Z_{in} + Z_0}$$

(3.3)

The BW is usually specified as frequency range over which VSWR is less than 2 (which corresponds to a reflection coefficient of 9.5 dB or 11% reflected power). Sometimes for stringent applications, the VSWR requirement is specified to be less than 1.5 (which corresponds to a reflection coefficient of 14 dB or 4% reflected power). Conversion of BW from one VSWR level to another can be accomplished by:

$$\frac{BW_1}{BW_2} = \frac{VSWR_1 - 1}{\sqrt{VSWR_1}} \times \frac{\sqrt{VSWR_2}}{VSWR_2 - 1}$$

(3.4)

Where, BW_1 and BW_2 correspond to $VSWR_1$ and $VSWR_2$, respectively. The variation of percentage BW for VSWR < 2 and efficiency η of a square MSA with normalized substrate thickness h/λ0 for two different values of ε_r (2.2 and 10) are given in Figure 3.4(a). Also, the variation of percentage BW with frequency for three commonly used values of η and ε_r = 2.32 is given in Figure 3.4(b). The BW of a

single-patch antenna increases with an increase in the substrate thickness and a decrease in the ε_r of the substrate.

(——) $\varepsilon_r = 2.2$, (- - -) $\varepsilon_r = 10$ and (b) variation of percentage BW with frequency for three values of h and $\varepsilon_r = 2.32$: (——) 0.318, (- - -) 0.159, (– – –) 0.079 cm.
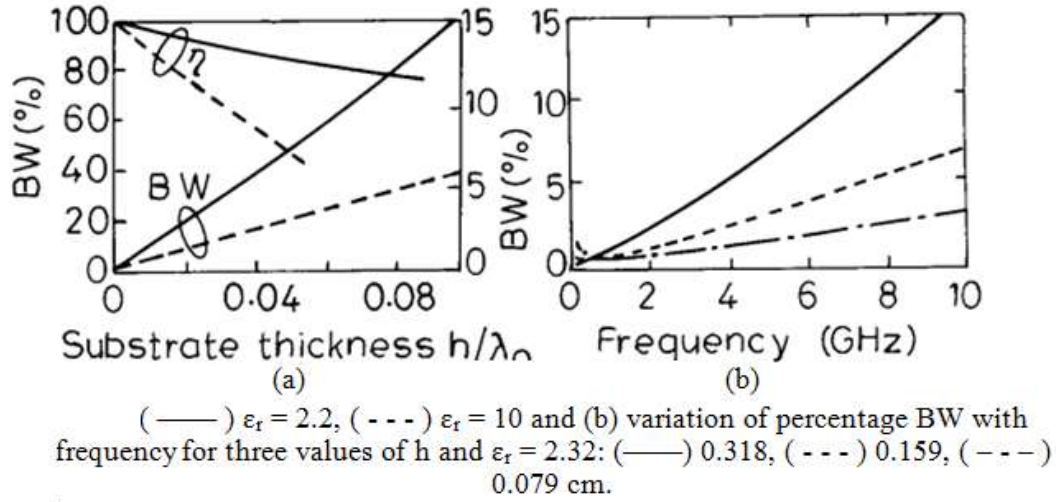
Figure 3.4 : (a) Variation of percentage BW and efficiency of a square MSA versus h/λ0.

for the coaxial feed and the excitation of surface waves, which reduces the efficiency h of the antenna as can be seen from Figure 3.4(a). The expressions for approximately calculating the percentage BW of the RMSA in terms of patch dimensions and substrate parameters is given by:

$$\%BW = \frac{Ah}{\lambda_0\sqrt{\xi_r}}\sqrt{\frac{W}{L}} \tag{3.5}$$

where

$$A = 180 \; for \; \frac{h}{\lambda_0\sqrt{\xi_r}} \leq 0.045 \tag{3.6}$$

$$A = 200 \; for \; 0.045 \leq \frac{h}{\lambda_0\sqrt{\xi_r}} \leq 0.075 \tag{3.7}$$

$$A = 180 \; for \; \frac{h}{\lambda_0\sqrt{\xi_r}} \geq 0.075 \tag{3.8}$$

where, W and L are the width and length of the RMSA. With an increase in W, BW increases. However, W should be taken less than λ to avoid excitation of higher order modes. Another simplified relation for quick calculation of BW for VSWR = 2 of the MSA operating at frequency f in gigahertz, with h expressed in centimeters, is given by:

32

$$BW \cong 50hf^2 \qquad\qquad\qquad\qquad \textbf{(3.9)}$$

The BW can also be defined in terms of the antenna's radiation parameters. It is defined as the frequency range over which radiation parameters such as the gain, half-power beamwidth (HPBW), and side lobe levels are within the specified minimum and maximum limits. This definition is more complete as it also takes care of the input impedance mismatch, which also contributes to change in the gain.

The expression for approximately calculating the directivity D of the RMSA is given by:

$$D \cong 0.2W + 6.6 + 10\log\left(1.6/\sqrt{\xi_r}\right) \quad dB \qquad\qquad \textbf{(3.10)}$$

3.7.2 Modified shape patches

The regular MSA configurations, such as rectangular and circular patches have been modified to rectangular ring and circular ring, respectively, to enhance the BW. The larger BW is because of a reduction in the quality factor Q of the patch resonator, which is due to less energy stored beneath the patch and higher radiation. When a U-shaped slot is cut inside the rectangular patch, it gives a BW of approximately 40% for VSWR <2. Similar results are obtained when a U-slot is cut inside a circular or a triangular MSA.

3.7.3 Planar multi resonator configurations

The planar stagger–tuned coupled multiple resonators yield wide BW in the same way as in the case of multistage tuned circuits. Several configurations are available yielding BW of 5–25% . Various parasitic patches like narrow strips, shorted quarter-wavelength rectangular patches, and rectangular resonator patches have been gap-coupled to the central-fed rectangular patch.

Three combinations of gap-coupled rectangular patches are shown in Figure 3.5. To reduce the criticality of the gap coupling, direct coupling as depicted in Figure 3.6 has been used to obtain broad BW. Both gap and direct (hybrid) coupling have been used with circular MSAs (CMSAs) and equilateral triangular MSAs (ETMSAs) to yield broad BW.
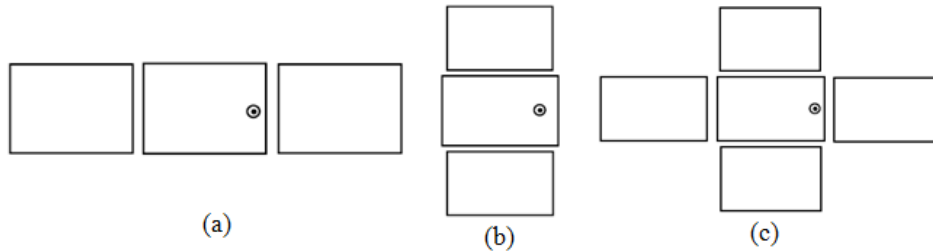
Figure 3.5 : Various gap-coupled multi resonator RMSA configurations: (a) three RMSAs gap - coupled along radiating edges, (b) three RMSAs gap - coupled along nonradiating edges, and (c) five gap-coupled RMSAs.

These planar multi resonator configurations yield broad BW but have the following disadvantages:

- The large size, which makes them unsuitable as an array element;

- The variation in the radiation pattern over the impedance BW.

A modification of the multi resonator patches—to avoid the abovementioned problems—entails using five or six narrow strips that are gap coupled along the width. This yielded wide BW with a relatively small variation in pattern over the BW.

3.7.4 Multilayer configurations

In the multilayer configuration, two or more patches on different layers of the dielectric substrate are stacked on each other. Based on the coupling mechanism, these configurations are categorized as electromagnetically coupled or aperture-coupled MSAs.
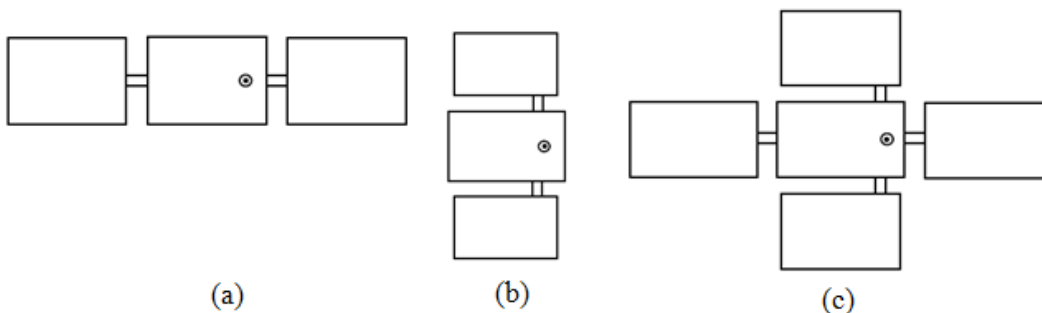

Figure 3.6 : Various direct-coupled multi resonators: (a) three RMSAs direct-coupled along radiating edges, (b) three RMSAs direct-coupled along nonradiating edges, and (c) five direct-coupled RMSAs.

3.7.4.1 Electromagnetically coupled MSAs

In the electromagnetically coupled MSA, one or more patches at the different dielectric layers are electromagnetically coupled to the feed line located at the bottom dielectric layer as shown in Figure 3.3(b). Alternatively, one of the patches is fed by a coaxial probe and the other patch is electromagnetically coupled. Either the bottom or top patch is fed with a coaxial probe as shown in Figure 3.7. The patches can be fabricated on different substrates, and accordingly the patch dimensions are to be optimized so that the resonance frequencies of the patches are close to each other to yield broad BW. These two layers may be separated by either air-gap or foam yielding BW of 15–30%.
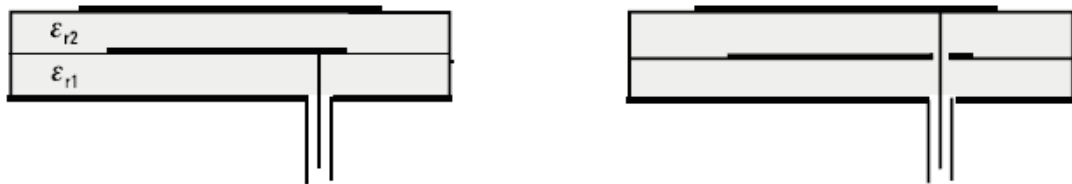
Figure 3.7 : An electromagnetically coupled MSA, in which the bottom patch is fed(left) And the top patch is fed(right).

3.7.4.2 Aperture-coupled MSAs

In the aperture-coupled MSA, the field is coupled from the microstrip feed line placed on the other side of the ground plane to the radiating patch through an electrically small aperture/slot in the ground plane, as shown in Figure 3.3(c). Two different dielectric substrates could be chosen, one for the patch and the other for the feed line to optimize the individual performances. The coupling to the patch from the feed line can be maximized by choosing the optimum shape of the aperture. Two patches of rectangular or circular shapes, which are stacked on each other in different dielectric layers, yield around 30% BW. A BW of nearly 70% has been obtained by stacking patches with resonant apertures. The multilayer broadband MSAs, unlike single-layer multi resonator configurations, show a very small degradation in radiation pattern over the complete VSWR BW. The drawback of these structures is the increased height, which is not desirable for conformal applications and increased back radiation for aperture-coupled MSAs.

3.7.5 Stacked multi resonator MSAs

The planar and stacked multi resonator techniques are combined to further increase the BW and gain. A probe-fed single rectangular or circular patch located on the bottom layer has been used to excite multiple rectangular or circular patches on the top layer, respectively. Besides increasing the BW, these configurations also provide an increase in gain.

3.7.6 Impedance-matching networks for broadband MSAs

The impedance-matching networks are used to increase the BW of the MSA. Some examples that provide about 10% BW are the rectangular MSA with a coplanar microstrip impedance-matching network and an electromagnetically coupled MSA with single-stub matching as shown in Figure 3.8.

3.7.7 Log-periodic MSA configurations

The concept of log-periodic antenna has been applied to MSA to obtain a multi-octave BW. In this configuration, the patch dimensions are increased logarithmically and the subsequent patches are fed at 180˚ out of phase with respect to the previous patch. The main disadvantage of this configuration is that the radiation pattern varies significantly over the impedance BW.
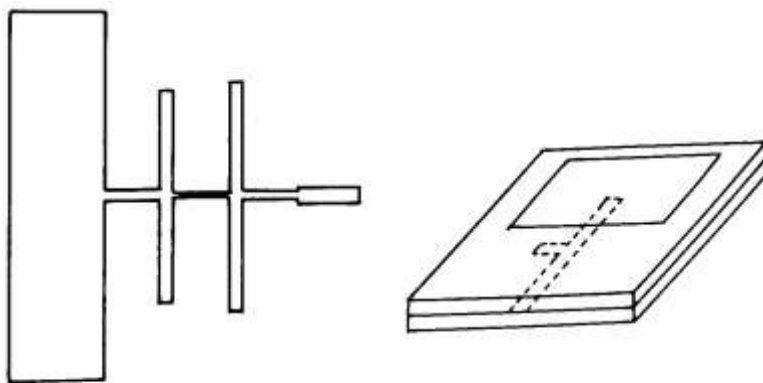
Figure 3.8 : Rectangular MSA with a coplanar microstrip impedance-matching network (left) and single-stub matched electromagnetically coupled MSA(right).

3.7.8 Ferrite substrate-based broadband MSAs

The multi resonant behavior of a patch on a ferrite substrate yields a broad BW of about three octaves by changing the magnetic field. Also, the dimensions of the patch are reduced because of the high dielectric constant of the ferrite substrate. However,

the efficiency of these antennas is poor because of lossy substrate and requires external magnetic fields, which makes it bulky. The methods for increasing the BW of MSA are continuously getting upgraded. The search for an ideal broadband MSA is still continuing. Perhaps a combination of various approaches would lead to an optimum broadband configuration.

3.8 Compact MSAs

Many techniques have been reported to reduce the size of microstrip antennas at a fixed operating frequency. In general, microstrip antennas are half-wavelength structures and are operated at the fundamental resonant mode TM_{01} or TM_{10}, with a resonant frequency given by (valid for a rectangular microstrip antenna with a thin microwave substrate):

$$f \cong \frac{c}{2L\sqrt{\xi_r}}$$ (3.11)

microwave substrate ($\varepsilon_r = 3.0$, h = 1.524 mm)   ceramic substrate ($\varepsilon_r = 28.2$, h = 4.75 mm)
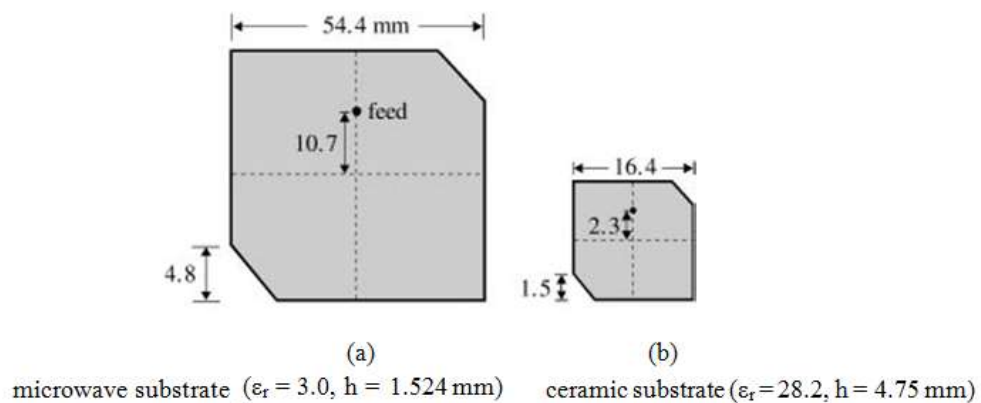
Figure 3.9 : Circularly polarized corner-truncated square microstrip antennas for GPS application at 1575 MHz.

Where, c is the speed of light, L is the patch length of the rectangular microstrip antenna, and ε_r is the relative permittivity of the grounded microwave substrate. From (3.1), it is found that the radiating patch of the microstrip antenna has a resonant length approximately proportional to $1/\sqrt{\zeta_r}$, and the use of a microwave substrate with a larger permittivity thus can result in a smaller physical antenna length at a fixed operating frequency. Figure 3.9 shows a comparison of the required dimensions for two circularly polarized corner-truncated square microstrip antennas with different substrates for global positioning system (GPS) application. The first design

uses a microwave substrate with relative permittivity $\varepsilon_r = 3.0$ and thickness h = 1.524 mm; the second design uses a high-permittivity or ceramic substrate with $\varepsilon r = 28.2$ and h = 4.75 mm. The relatively larger substrate thickness for the second design is needed to obtain the required circular polarization (CP) bandwidth for GPS application. From the patch areas of the two designs, it can be seen that the second design has a patch size about 10% of that of the first design. This reduction in antenna size can be expected from (1.1), from which the antenna's fundamental resonant frequency of the design with $\varepsilon_r = 28.2$ is expected to be only about 0.326 times that of the design with $\varepsilon_r = 3.0$ for a fixed patch size. This result suggests that an antenna size reduction as large as about 90% can be obtained if the design with $\varepsilon_r = 28.2$ is used instead of the case with $\varepsilon_r = 3.0$ for a fixed operating frequency. The use of an edge-shorted patch for size reduction is also well known [see the geometry in Figure 3.10(a)], and makes a microstrip antenna act as a quarter wavelength structure and thus can reduce the antenna's physical length by half at a fixed operating frequency. When a shorting plate (also called a partial shorting wall) [Figure 3.10(b)] or a shorting pin [Figure 3.10(c)] is used instead of a shorting wall, the antenna's fundamental resonant frequency can be further lowered and further size reduction can be obtained. In this case, the diameter of a shorting-pin-loaded circular microstrip patch or the linear dimension of a shorting-pin-loaded rectangular microstrip patch can be as small as one-third of that of the corresponding microstrip patch without a shorting pin at the same operating frequency. This suggests that an antenna size reduction of about 89% can be obtained[23, 24].
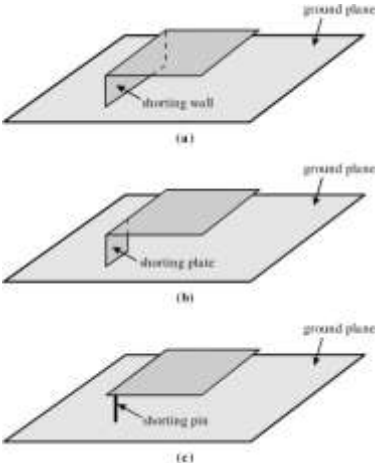

Figure 3.10 : Geometries of a rectangular patch antenna with (a) a shorting wall, (b) a shorting plate or partial shorting wall, and (c) a shorting pin.

38

Moreover, by applying the shorting-pin loading technique to an equilateral-triangular microstrip antenna, the size reduction can be made even greater, reaching as large as 94%. This is largely because an equilateral-triangular microstrip antenna operates at its fundamental resonant mode, whose null-voltage point is at two-thirds of the distance from the triangle tip to the bottom side of the triangle; when a shorting pin is loaded at the triangle tip, a larger shifting of the null-voltage point compared to the cases of shorted rectangular and circular microstrip antennas occurs, leading to a greatly lowered antenna fundamental resonant frequency.

Meandering the excited patch surface current paths in the antenna's radiating patch is also an effective method for achieving a lowered fundamental resonant frequency for the microstrip antenna. For the case of a rectangular radiating patch, the meandering can be achieved by inserting several narrow slits at the patch's nonradiating edges. It can be seen in Figure 3.11(a) that the excited patch's surface currents are effectively meandered, leading to a greatly lengthened current path for a fixed patch linear dimension. This behavior results in a greatly lowered antenna fundamental resonant frequency, and thus a large antenna size reduction at a fixed operating frequency can be obtained. Figure 3.11(b) shows similar design, cutting a pair of triangular notches at the patch's nonradiating edges to lengthen the excited patch surface current path.
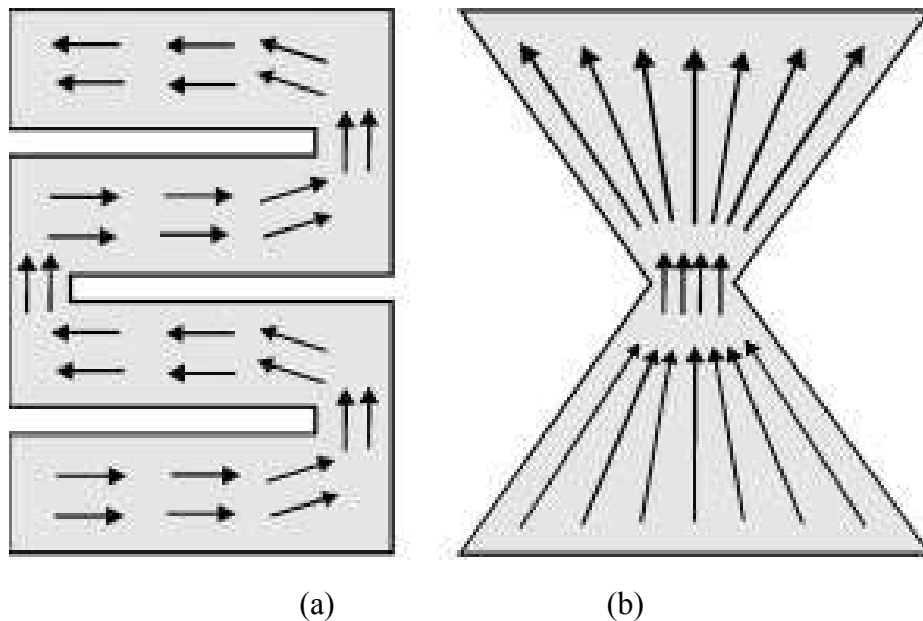

(a)   (b)

Figure 3.11 : Surface current distributions for meandered rectangular microstrip patches with (a) meandering slits and (b) a pair of triangular notches cut at the patch's nonradiating edges.

The resulting geometry is referred to as a bow-tie patch. Compared to a rectangular patch with the same linear dimension, a bow-tie patch will have a lower resonant frequency, and thus a size reduction can be obtained for bow-tie microstrip antennas at a given operating frequency.

The technique for lengthening the excited patch surface current path mentioned above is based on a coplanar or single-layer microstrip structure. Surface current lengthening for a fixed patch projection area can also be obtained by using an inverted U-shaped patch [Figure 3.12(a)], a folded patch [Figure 3.12(b)], or a double-folded patch [Figure 3.12(c)]. With these microstrip patches, the resonant frequency can be greatly lowered compared to a regular single-layer microstrip antenna with the same projection area.

Note that the resonant frequency is greatly lowered due to the bending of the patch surface current paths along the antenna's resonant or excitation direction, and that no lateral current components are generated, in contrast to the case of the meandering technique shown in Figure 3.11. Probably for this reason, it has been observed that compact microstrip antennas using the bending technique described here have good cross-polarization levels for frequencies within the operating bandwidth.

By embedding suitable slots in the radiating patch, compact operation of microstrip antennas can be obtained. Figure 3.13 shows some slotted patches suitable for the design of compact microstrip antennas. In Figure 3.13(a), the embedded slot is a cross slot, whose two orthogonal arms can be of unequal or equal lengths. This kind of slotted patch causes meandering of the patch surface current path in two orthogonal directions and is suitable for achieving compact circularly polarized radiation or compact dual-frequency operation with orthogonal polarizations. Similarly, designs with a pair of bent slots [Figure 3.13(b)], a group of four bent slots [Figure 3.13 (c)], four 90∘-spaced inserted slits [Figure 3.13(d)], a perforated square patch or a square-ring patch with a cross strip [Figure 3.13(e)], a circular slot [Figure 3.13 (f)], a square slot [Figure 3.13(g)], an offset circular slot [Figure 3.13(h)], and a perforated tip-truncated triangular patch [Figure 3.13 (i)] have been successfully applied to achieve compact circularly polarized or compact dual-frequency microstrip antennas.
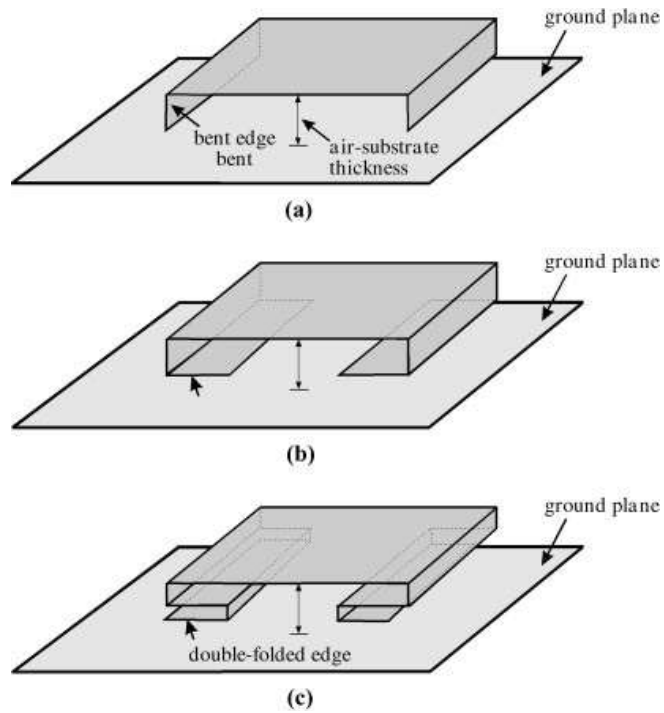
Figure 3.12 : Compact microstrip antennas with (a) an inverted U-shaped patch, (b) a folded patch, and (c) a double-folded patch for achieving lengthening of the excited patch surface current path at a fixed patch projection area.
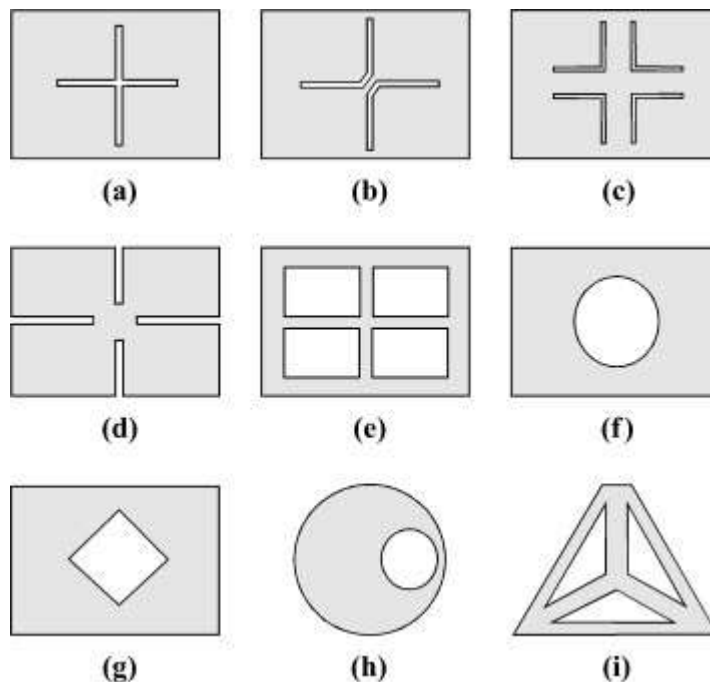

Figure 3.13 : Some reported slotted patches suitable for the design of compact microstrip antennas.
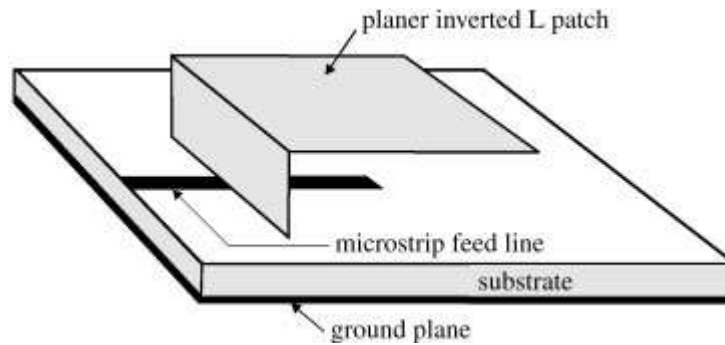
Figure 3.14 : Geometry of a microstrip-line-fed planar inverted-L patch antenna for compact operation.

The microstrip-line-fed planar inverted-L (PIL) patch antenna is a good candidate for compact operation. The antenna geometry is shown in Figure 3.14 When the antenna height is less than $0.1\lambda 0$ ($\lambda 0$ is the free-space wavelength of the center operating frequency), a PIL patch antenna can be used for broadside radiation with a resonant length of about $0.25\lambda 0$; that is, the PIL patch antenna is a quarter-wavelength structure, and has the same broadside radiation characteristics as conventional half wavelength microstrip antennas. This suggests that at a fixed operating frequency, the PIL patch antenna can have much reduced physical dimensions (by about 50%) compared to the conventional microstrip antenna.

Figure 3.15 shows another interesting compact design for a microstrip antenna. The antenna's ground plane is meandered by inserting several meandering slits at its edges. It has been experimentally observed that similar meandering effects to those with the design with a meandering patch shown in Figure 3.11(a) can be obtained [25]. Moreover, probably because the meandering slits in the antenna's ground plane can effectively reduce the quality factor of the microstrip structure, the obtained impedance bandwidth for a compact design with a meandered ground plane can be greater than that of the corresponding conventional microstrip antenna.
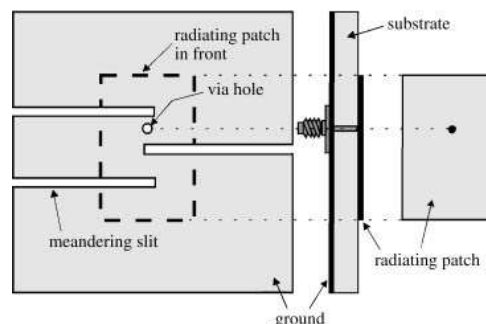

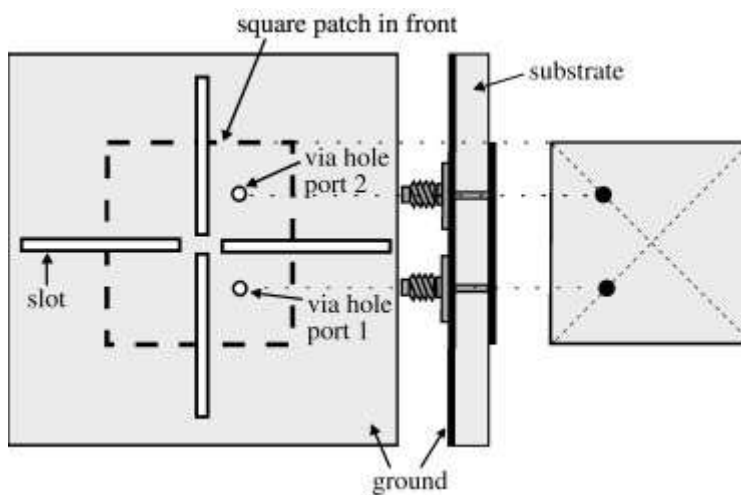**Figure 3.15** : Geometry of a probe-fed compact microstrip antenna with a meandered ground plane.

42

Figure 3.16 : Geometry of a probe-fed compact microstrip antenna with a slotted ground.

4. BROADBAND PLANAR MONOPOLE ANTENNAS

4.1 Introduction

An increase in the thickness of the dielectric and a decrease in the dielectric constant of the substrate increase the BW of the MSA. For a thick substrate with a low dielectric constant, a BW of 5% to 10% is obtained. Further increase in the substrate thickness decreases the efficiency of the antenna. Also, a long coaxial probe is required to feed the patch of the antenna suspended in air at a large height as shown in Figure 4.1(a). The large h increases the impedance bandwidth of the antenna. This large inductive input impedance can be taken care of by feeding the patch with a shorter probe of length p as shown in Figure 4.1(b). In this case, the patch is fed along the periphery and an additional perpendicular ground plane is required. If h is very large, the bottom ground plane would have a negligible effect and hence can be removed. This configuration becomes similar to that of a planar monopole antenna, as shown in Figure 4.1(c). The planar disc monopole antennas yield a very large-impedance BW, which can be explained in the following two ways [26,27]:
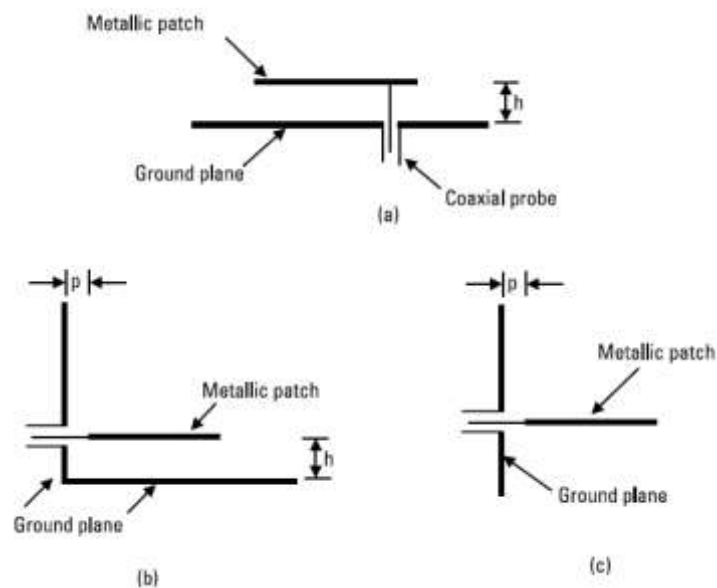

Figure 4.1 : (a) MSA suspended in air, (b) modified MSA with side feed, and (c) planar monopole antenna.

1. A monopole antenna generally consists of a thin vertical wire mounted over the ground plane, whose BW increases with an increase in its diameter. A planar monopole antenna can be equated to a cylindrical monopole antenna with a large effective diameter.

2. The planar monopole antenna can be viewed as a MSA on a very thick substrate with $\varepsilon_r = 1$, so a large BW is expected. In the radiating metallic patch, various higher order modes will get excited. The shape and size of these planar antennas can be optimized to bring several modes within the VSWR = 2 circle in the Smith chart, leading to very large-impedance BW.

4.2 Planar Rectangular and Square Monopole Antennas

A planar rectangular monopole antenna can be thought of as a variation of the RMSA, in which the horizontal ground plane is considered to be located at infinity. The following discussions bring out this analogy.

4.2.1 RMSA suspended in air with orthogonal ground plane

The side and the front views of a rectangular radiating patch with L = W = 12 cm made of a copper plate of thickness 0.1 cm with two orthogonal ground planes are shown in Figure 4.2(a, b). The patch is fed with a 50-Ω SMA connector of probe length p through a fixed ground plane and the orthogonal ground plane is moveable. For the moveable ground plane spacing h = 3 cm from the radiating patch and the probe length p = 0.4 cm, the measured input impedance and VSWR plots are shown in Figure 4.2 (c, d). Multiple loops occur due to the excitation of various higher order modes of RMSA. The value of p is increased to 1 cm to shift the impedance plot in the clockwise direction because the impedance plot shows less inductive shift due to the smaller value of the feed probe length p. The results are could be seen in Table 4.1. The measured BW for VSWR <2 is from 858 MHz to 988 MHz.

The formula for RMSA is used to calculate the resonance frequency of this antenna. Since the dielectric medium for all the cases under consideration is air, the effective dielectric constant ε_e is equal to 1. The theoretical resonance frequency for the fundamental mode can be calculated using:

$$f_0 = c/2L_e$$

(4.1)

Where:

L_e = effective resonant length;

c = velocity of light in free space.

For two orthogonal ground planes, $L_e = L + \Delta L + p$, because the extension of length ΔL due to the fringing fields is applicable only for one side, and on the other side, it is restricted to p due to the orthogonal ground plane. For a large width of the patch (W/h > 10) with $\varepsilon_r = 1$, ΔL is approximately equal to h.
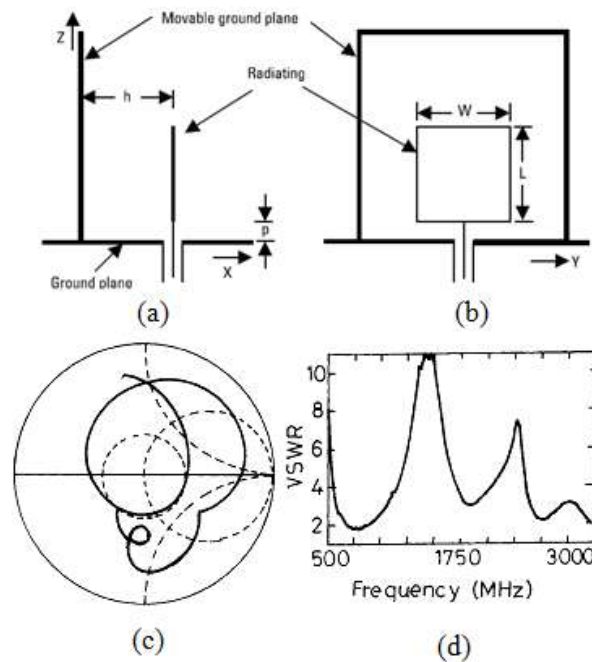
Figure 4.2 : (a) Side and (b) front views of modified RMSA with orthogonal ground planes. Measured (c) input impedance and (d) VSWR plots.

Table 4.1 : Resonance Frequency and Percentage BW of RMSA with L = W = 12 cm for Different Values of h, [a] Calculated using 4.1, [b] Calculated using 4.8.

Theoretical Frequency (MHz)	h (cm)	f_L(MHz)	f_H(MHz)	% BW
937[a]	3	858	988	14.1
789[a]	6	752	934	17.7
484[a],483[b]	18	515	1081	70.3
0[a],483[b]	∞	501	1154	81.2

The theoretical resonance frequency, calculated using (4.1) for p = 1.0 cm, is 937 MHz, which is close to the measured center frequency of 923 MHz.   Consequently, for different values of h with p = 1.0 cm, the measured lower and upper frequencies (f_L and f_H) corresponding to VSWR = 2 are shown in Table 4.1. With an increase in h from 3 cm to infinity (∞), band width of the antenna increases from 14.1% to 81.2%. By increase in h, lower resonance frequency decreases because of the increase in ΔL due to the large fringing fields. For smaller values of h, there is a reasonable agreement between the theoretical frequency obtained from (4.1) and the measured center frequency. As h increases, the theoretical frequency is close to the measured lower frequency corresponding to VSWR = 2. For two different values of h [18 cm (large) and ∞ (bottom ground plane removed)], the measured input impedance and VSWR plots are shown in Figure 4.3. As h increases from 18 cm to ∞ the measured lower frequency decreases from 515 MHz to 501 MHz. For these two values of h, Figure 4.3 Measured (a) input impedance and (b) VSWR plots of RMSA for two values of h:

(a)   (b)
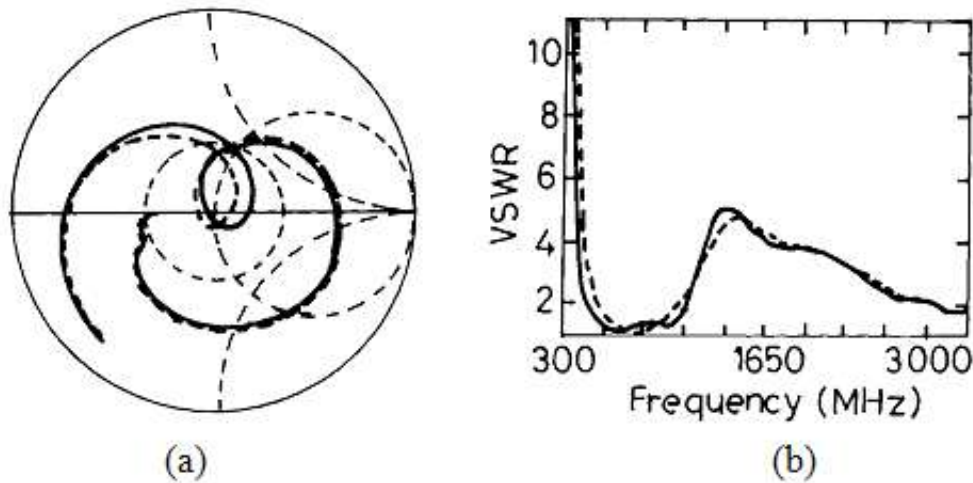
Figure 4.3 : Measured (a) input impedance and (b) VSWR plots of RMSA for two
values of h: (- - -) 18 cm and (——) ∞.

4.2.2 Calculation of the lower frequency of the planar monopole antennas

The lower frequency corresponding to VSWR = 2 for a monopole antenna can be calculated by equating its area to that of an equivalent cylindrical monopole antenna of same height L and equivalent radius r, as described below:

$$2\pi r L = WL \qquad\qquad \textbf{(4.2)}$$

48

which gives:

$$r = W/2\pi \tag{4.3}$$

The input impedance of a l /4 monopole antenna is half of that of the l /2 dipole antenna. Thus, the input impedance of an infinitesimally thin monopole antenna is $36.5 + j\ 21.25\ \Omega$, which is inductive. when using slightly smaller length of the monopole as given by:

$$L = 0.24\lambda f \tag{4.4}$$

The real input impedance is achieved. Where

$$F = (L/r)/(1 + L/r) = L/L + r \tag{4.5}$$

From (4.4) and (4.5), the wavelength l is obtained as:

$$\lambda = (L + r)/0.24 \tag{4.6}$$

Therefore, the lower frequency f_L is given by:

$$f_L = c/\lambda = (30 \times 0.24)/(L + r) = 7.2/(L + r) \quad GHz \tag{4.7}$$

Equation (4.7) does not account for the effect of the probe length p, which increases the total length of the antenna and consequently reduces the frequency. so, this equation could be written as:

$$f_L = 7.2/(L + r + p) \quad GHz \tag{4.8}$$

where, L, r, and p are in centimeters.

The theoretical frequency of 483 MHz for h = ∞ (monopole antenna) obtained using (4.8) is close to the measured f_L of 501 MHz. For h =18 cm, the theoretical frequencies obtained using the MSA and monopole concepts are very close to each other. Thus, an interesting transition in antenna characteristics (with respect to resonance frequency) is observed, as the ground plane spacing h is increased.

4.2.3 Effect of various parameters of planar rectangular monopole antennas

The large impedance bandwidth of these antennas depends mainly on the width W of the plate, the diameter d of the feeding probe, and the length of the probe p. The SMA connector is generally used above 1 GHz for feeding the antenna, and hence, d is kept fixed at 0.12 cm. When the height L of the monopole antenna increases (or decreases), the lower edge frequency decreases (or increases), which is quite obvious. Initially, the effect of p is described by keeping L = W = 4.5 cm. The input impedance and VSWR plots for two values of p are shown in Figure 4.4(a, b).

(a)

(b)

p [(———) 0.05 cm and (- - -) 0.2 cm]

(c)

(d)
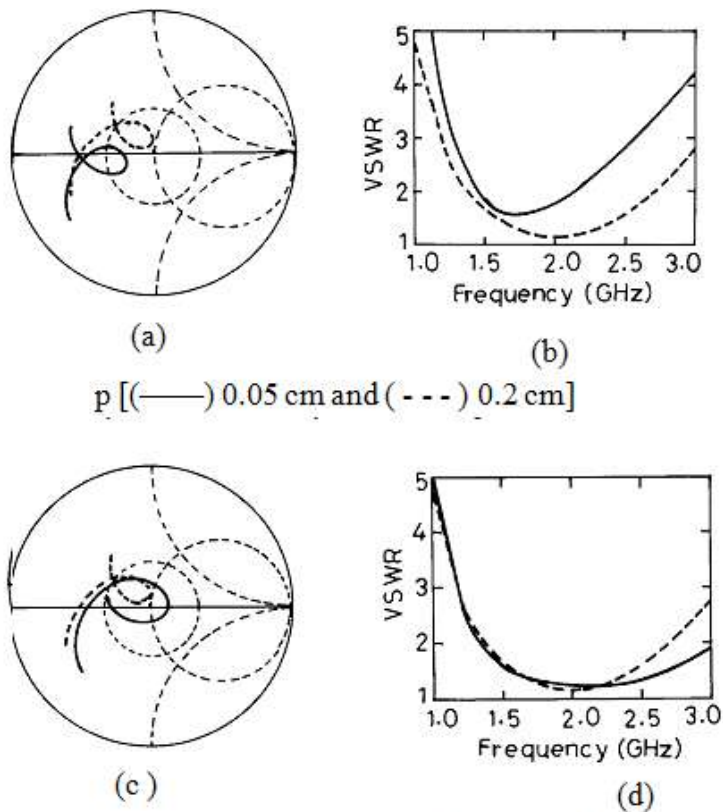
L = 4.5 cm and p = 0.2 cm for two values of W [(- - -) 4.5 cm and (———) 3.5 cm]

Figure 4.4 : (a) Input impedance and (b) VSWR plots of RM antenna for different values of p, L and W.

As, p is increased from 0.05 cm to 0.2 cm, the input impedance plot shifts up in the clockwise direction. When p increases, the probe inductance increases and therefore the input impedance becomes more inductive. A broad BW of 1,335 MHz (68%) is achieved for p = 0.2 cm, in comparison with the BW of 668 MHz (40%) for p = 0.05 cm.

The input impedance and VSWR plots also for the two different values of W (4.5 cm and 3.5 cm) with L = 4.5 cm and p = 0.2 cm are shown in Figure 4.4(c, d). With a decrease in W, the size of the loop in the impedance plot increases and the plot shifts toward the right in the Smith chart. As W decreases from 4.5 cm to 3.5 cm, the BW increases from 1,335 MHz to 1,715 MHz due to an increase in loop size.

4.2.5 Various planar RMs with equal areas

The effects of various parameters on the BW of the monopole antenna are studied, the dimensions L and W of RM are chosen such that their surface areas are equal, so that a comparison of performances of these planar monopole antennas may be made. The SM is fed in the middle of the one side by a SMA connector as shown in Figure 4.5(a), whereas RM is fed in two different ways. The size of the ground plane is chosen to be 30 cm * 30 cm with p = 0.1 cm in this measuements. The RMs with feeds in the middle of the smaller and larger dimensions are coined RMAs and RMBs, respectively. The dimensions and VSWR BW of these configurations are listed in Table 4.2. The theoretical lower frequency f_L for VSWR = 2 obtained using (4.8), is also tabulated. The percentage error is calculated using:

$$\%error = \frac{f_L - f_m}{f_m} \times 100 \qquad (4.9)$$

The theoretical frequencies predicted by (9.8) are within $\pm 6.6\%$ of the measured values. The f_L of RMB is higher than that of the RMA, because the height of the RMB is smaller than that of the RMA. In (4.9) f_m is the lower measured frequency.
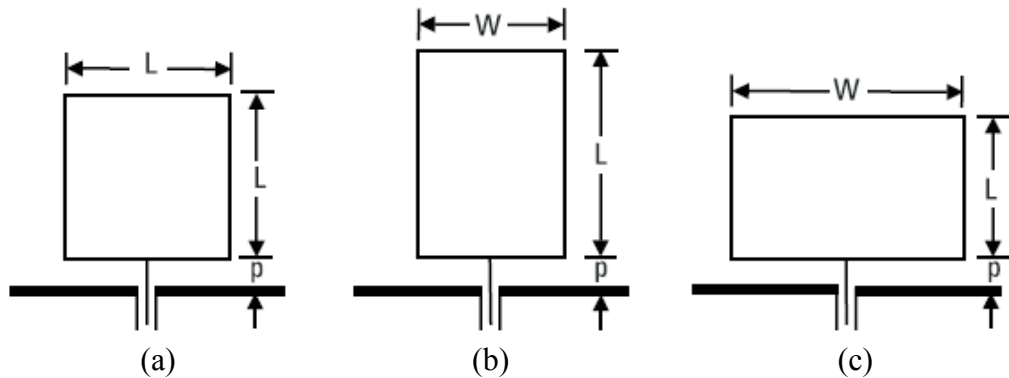

Figure 4.5 : (a) Square monopole antenna. RM antennas with feed in the middle of (b) smaller W and (c) larger W.

Table 4.2 : Comparison of square, rectangular, triangular, and hexagonal
monopole antennas.

Configuration	L*W (cm*cm)	Measured f_m Range for VSWR<2 (GHz)	f_L(GHz)	Measured BW Ratio	Percentage Error in Frequency
SM	4.5*4.5	1.27 to 2.81	1.354	1:2.2	+6.6
RMA	4.6*4.2	1.38 to 2.75	1.341	1:2.0	-2.8
RMB	4.2*4.6	1.40 to 2.02	1.431	1:1.4	+2.2
TMB	5.9*6.8	1.07 to 1.11	1.101	1:1.04	+2.9
HMA	4.8*5.6	1.37 to 2.68	1.282	1:1.9	-6.5
HMB	5.6*4.8	1.20 to 3.92	1.147	1:3.2	-4.4

The measured VSWR plots of SM, RMA, and RMB are given in Figure 4.6. The
VSWR values fluctuate from as high as 8 to as low as 1.05 in the frequency range of
1–13 GHz. Optimizing the dimensions of the patches and length of the probe,
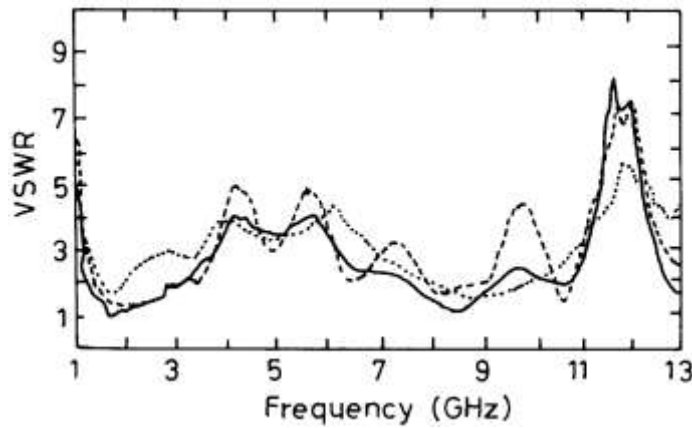optimize the frequency and bandwidth of the antenna.

Figure 4.6 : Measured VSWR plots for three monopole antennas: (——) SM, (- - -)
RMA, and (…) RMB.

4.3 Planar Circular Monopole Antennas

A planar circular monopole (CM) antenna is another type of monopole antennas
which yields very broad band width. A CM of radius a is shown in Figure 4.7. The
radius a is taken equal to 2.5 cm, so that its surface area is approximately equal to
that of the other monopole antennas given in Table 4.2. As in the earlier cases, the
size of the ground plane is kept same as 30 cm * 30 cm. For the CM, the values L
and r of the equivalent cylindrical monopole antenna are given by:

$$L = 2a$$

(4.10)

$$r = a/4 \qquad\qquad \textbf{(4.11)}$$
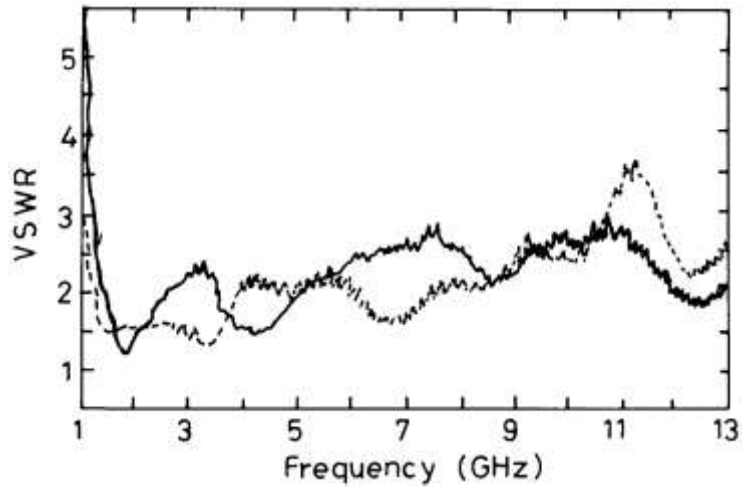

Figure 4.7 : Measured VSWR plots of two-feed configurations of hexagonal monopole antennas: (———) HMA and (- - -) HMB.
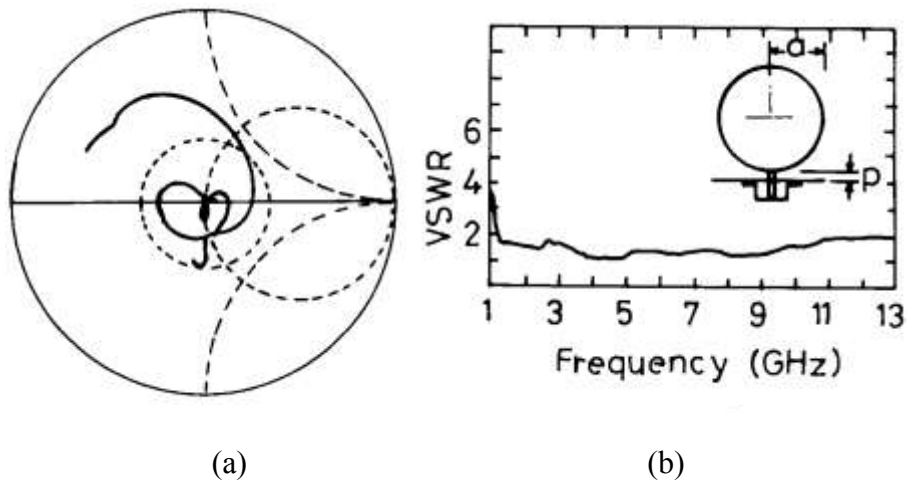

| (a) | (b) |

Figure 4.8: Measured (a) input impedance and (b) VSWR plots of CM antenna.

For p = 0.1 cm, the measured input impedance and VSWR plots are shown in Figure 4.8. The BW for VSWR <2 is from 1.17 GHz to 12 GHz, which corresponds to a BW ratio of 1:10.2. The BW of the CM is larger than all the monopole antennas described earlier. This could be interpreted in terms of various higher order modes of the circular patch. Unlike the various modes of rectangular resonator, modes of the circular resonator (characterized by the roots of the derivative of the Bessel function) are closely spaced. The BW associated with the various modes is very large because the disc is in the air; accordingly, the change in the input impedance from one mode to another mode is very small. This can also be noted from the impedance plot shown

in Figure 4.8 (a), which has multiple loops corresponding to the various modes. Since these loops are within the VSWR = 2 circle, a large BW is obtained.

5. DIRECTIONAL MICROSTRIP ANTENNAS

5.1 Introduction

Directional antennas can focus electromagnetic energy in one direction and enhance coverage range for a given power level. They also minimize co-channel interference and reduce noise level in a contention based access scheme, thereby reducing the collision probability. Further, they provide longer range and/or more stable links due to increased signal strength and reduced multipath components. Increased spatial reuse and longer ranges translate into higher network capacity (more simultaneous transmissions and fewer hops), and longer ranges also provide richer connectivity. On the receiving side, directional antennas enable a node to selectively receive signals only from a certain desired direction [28,29]. Figure 5.1 illustrates the increased spatial reuse capability provided with the use of directional antennas when nodes C and D, and X and Y want to simultaneously communicate. If Omni-directional antennas are in use as in Figure 5.1(a), only one pair of nodes can communicate as nodes D and X are within the radio range of each other. Although we are confining our discussion here to nodes C, D, X and Y, note that all the nodes within the radio range of these nodes (nodes A, B, E and F) are also affected when employing Omni-directional antennas. In the case of Figure 5.1(a), if we assume that nodes C and D initiated their communication first, all neighbors of C and D, including node X, will stay silent for the duration of their transmission. However, when directional antennas are in place, both the node pairs C-D and X-Y can simultaneously carry out their communication as depicted in Figure 5.1(b). Consequently, the capacity of the network can be considerably increased and the overall interference decreased, as transmissions are now directed towards the intended receiver, thus allowing multiple transmissions in the same neighborhood (which is not possible with Omni-directional antennas) to occur in parallel using the same channel. Table 5.1 briefly compares omni-directional and directional antennas under five self-explaining criteria.
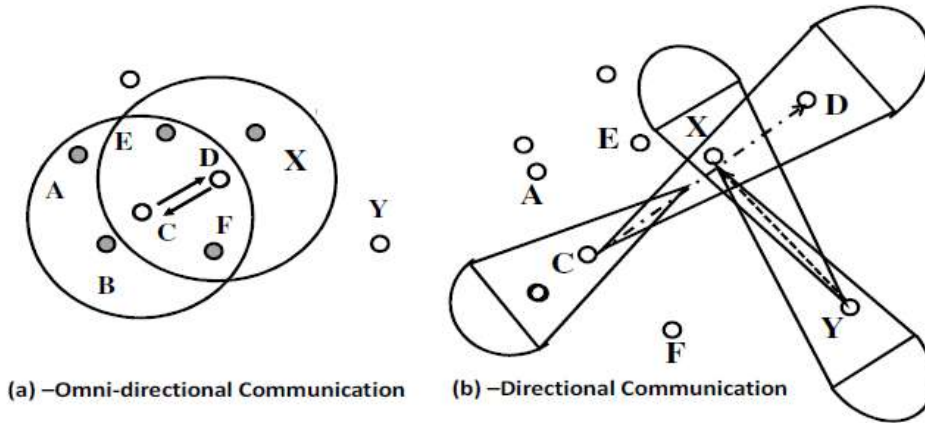
Figure 5.1: Communication using omni-directional antennas and directional antennas.

Table 5.1 : Comparison of omni and directional antennas.

Characteristics	Omni	Directional
Spatial reuse	Low	High
Network connectivity	Low	High
Interference	High	Low
Coverage range for the same amount of transmitting power	Low	High
Cost and complexity	Low	High

Directivity can be achieved if the antenna is large in a desired direction, such as Horn or Vivaldi antennas. In other types, antenna includes cavity or shielding plane behind itself, or uses the absorbing materials in order to obtain directivity. On the other hand, such approaches cause either increment in the antenna size or decrease in the antenna efficiency as well as complication in the production process. Compact bowtie antenna operating at 2-4 GHz for radar-based breast cancer detection, Wideband monopole antenna fed by a 50-ohm coplanar waveguide working at 3.4-9.6 GHz for microwave near-field imaging are also presented. Some other directional antennas such as conventional slot antennas have limited operating frequency range, while Vivaldi type antennas have a good bandwidth and directional radiation pattern. Wide band printed monopole antenna with a parabolic-shaped or L-shaped ground plane as a reflector is also presented as a directive antenna in order to use in the application of radar- based imaging system. Application of interest is microwave imaging, which requires an optimized size and wide band impedance bandwidth, also

a directive radiation pattern. In the follow we will study some directive antenna structures.

5.2 Wideband Directional Slot Antenna

The geometry of the proposed slot antenna is demonstrated in Figure 5.2. This antenna consists of a standard RT/duroid 5880 (εr =2.2) with a thickness of 1.58 mm and also a quarter-wavelength slot on the edge of the ground plane and fed by an L shape microstrip line. The overall size of the antenna is fixed at L-ground and W-ground, the length and width of the slot are L-slot and W-slot respectively. L-offset is the distance from the 100 ohms feed line to the edge of the ground plane and L-stub is the length of the shorting stub. The impedance of the feed line delivered to the slot is 100 ohms which is different from the 50 ohms input impedance [13].
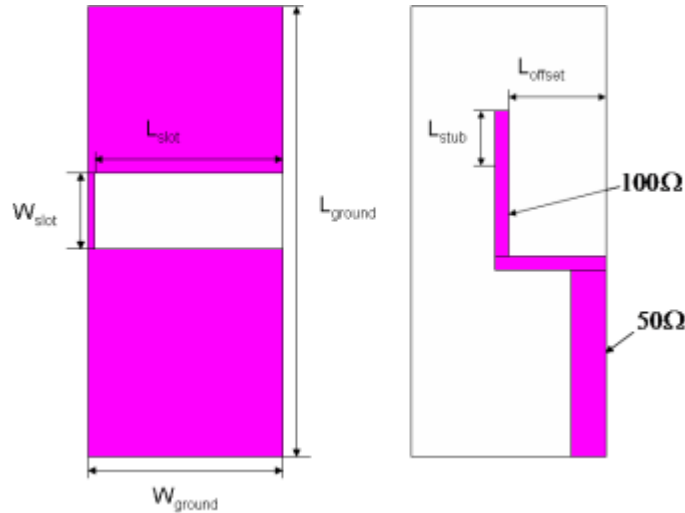

Figure 5.2: Geometry of the slot antenna (left) top view (right) bottom view.

According to parametric study an optimized structure was designed and fabricated. All the major parameters are given in table 5.2.

Table 5.2 : Design parameters of the slot.

Antenna Parameters	Column C
Length of ground (L_{ground})	41mm
Width of ground(W_{ground})	18mm
Length of slot (L_{slot})	17mm
Width length of slot (W_{slot})	7mm
Offset distance (L_{offset})	8mm
Length of stub (L_{stub})	2mm

Measured and simulated reflection coefficients of the antenna are given figure 5.3. Reflection coefficient frequency band is from 4.5GHz to 8.5GHz with S11 less than -10dB. The antenna is printed on the substrate and also the simulation did not take the SMA connector into account, so the simulated results are some different with the measurements.
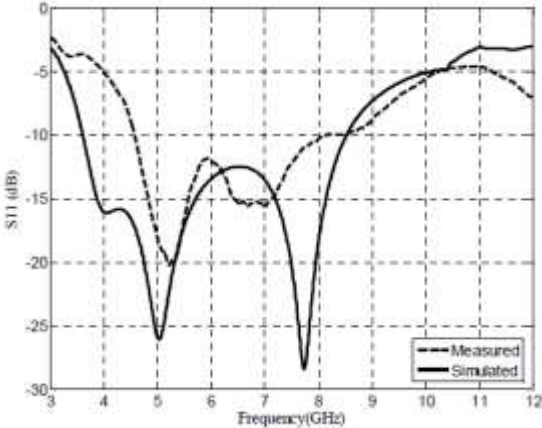

Figure 5.3 : The simulated and measured reflection coefficient of the slot antenna.

Then, a reflector is placed behind the slot at a distance of 10mm to keep the overall size of the antenna compact. Considering the diffraction at the edge of reflector the size of it is chosen to be 60mm×60mm which is comparable with the wavelength at 5GHz. Comparison between the reflection coefficient of the antenna with and without reflector is represented in figure 5.4. Almost the same impedance bandwidth is obtained with a large reflector at 10mm away behind the slot when no reflector is added.
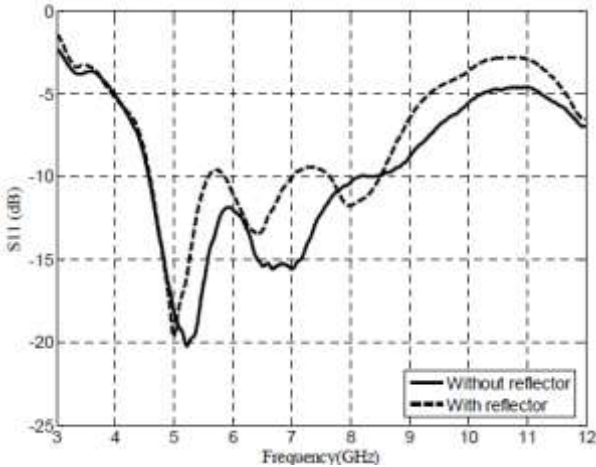

Figure 5.4 : The measured reflection coefficient of the slot with and without reflector.

The effect of the reflector on the radiation patterns is investigated and the results are shown in figures 5.5a and 5.5b. As expected the reflector makes the antenna radiating towards one direction through the frequency range. Small differences between the measured and simulated results are observed. This may due to the finite size of reflector was used in the measurement which is different from the simulation.
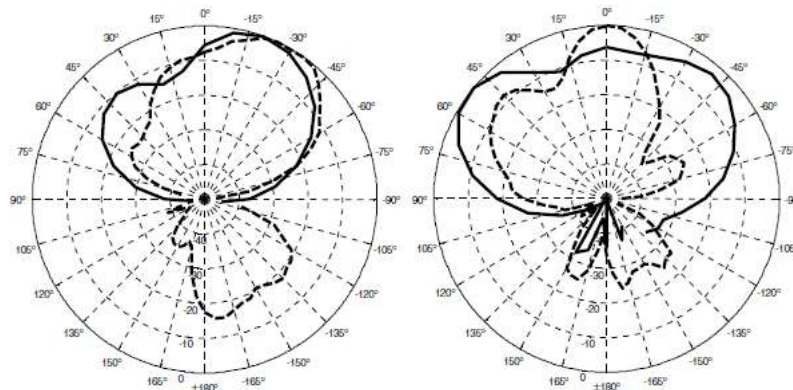

Figure 5.5 : The simulated (solid line) and measured (dash line) E-plane radiation pattern (dB) of the slot with reflector (a) f = 6GHz, (b) f = 8GHz.

5.3 Directional Planar UWB Antenna With an L-shaped Ground Plane

The antennas were designed to be fabricated on a low cost FR4 substrate. The thickness of the dielectric and the conductor layers are 1.6 mm and 35 μm, respectively. The relative permittivity of the dielectric in the whole analysis are 4.5. In Figure 5.6 geometry of the printed directional antenna with an L-shaped ground plane is shown [15].
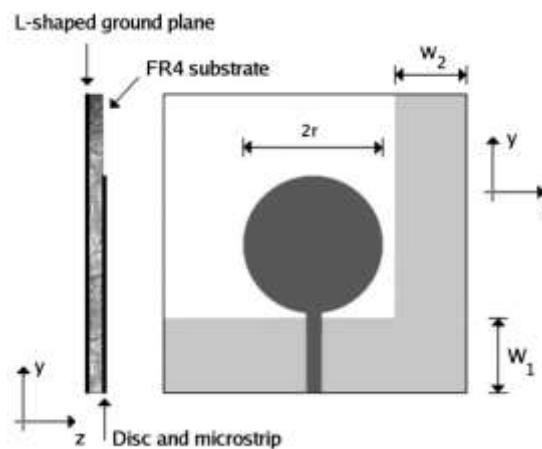

Figure 5.6 : Schematic view of the printed disc monopole with L- shaped ground plane. On the left (right) a side (front) view of the designed antenna is shown.

59

The substrate is a square dielectric FR4 board with dimensions 5 cm × 5 cm. On one side of the board we have a 50-Ohm microstrip feeding line (width 3 mm), and a disc with radius r centered in the middle of the board. On the other side of the substrate we have an L-shaped ground plane. The part of the conductor plane with the long side parallel to x-axis (width W1) forms the microstrip line, whereas the conductor strip with the long side parallel to y-axis (width W2) acts as a reflector, and this is the key element which is introduced to improve directionality. The final goal of the work is to get a planar antenna with low reflection coefficient, near constant group delay and radiation patterns, and increased directivity in the band between 6 and 8 GHz. Massive numerical simulation using the CST Microwave Studio package were performed, which utilizes the finite integration technique for electromagnetic computation, in order to find a good tradeoff between these requirements. The radius of the disc and the width of the two strips that compose the ground plane were varied and the optimum sets of geometric parameters: r = 9.1 mm, W1 = 1.49 cm, and W2 = 1.39 cm are obtained. Two prototypes with the same optimum geometric parameters have been fabricated. In Figure 5.6 a photograph of the two antennas are shown. On the left it is possible to see the side of the board with the L-shaped ground plane, whereas on the right we have the other side with the disc and the microstrip line. The fabricated prototypes have been fully characterized through measurements in anechoic chamber. Simulations predict a 10-dB bandwidth extending from 5.76 to over 10 GHz, with a good uniformity of the response in the band of interest between 6 and 8 GHz.
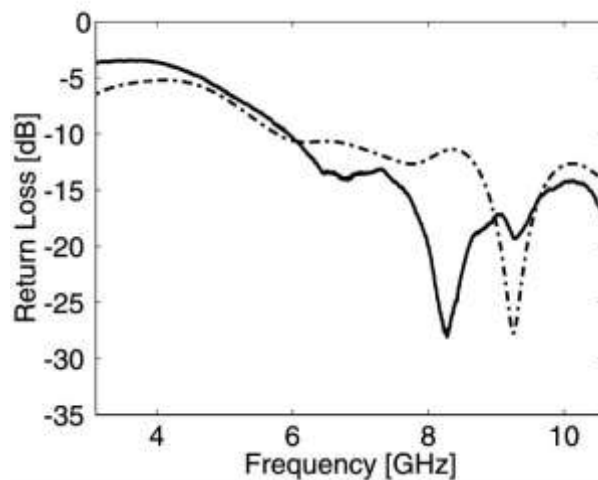

Figure 5.7 : Measured (solid line) and simulated (dash-dotted line) reflection coefficient curves in the full UWB window.

The radiation patterns of the proposed antenna have been calculated through CST Microwave Studio simulations and the radiative properties of the fabricated prototypes have been fully characterized in anechoic chamber.
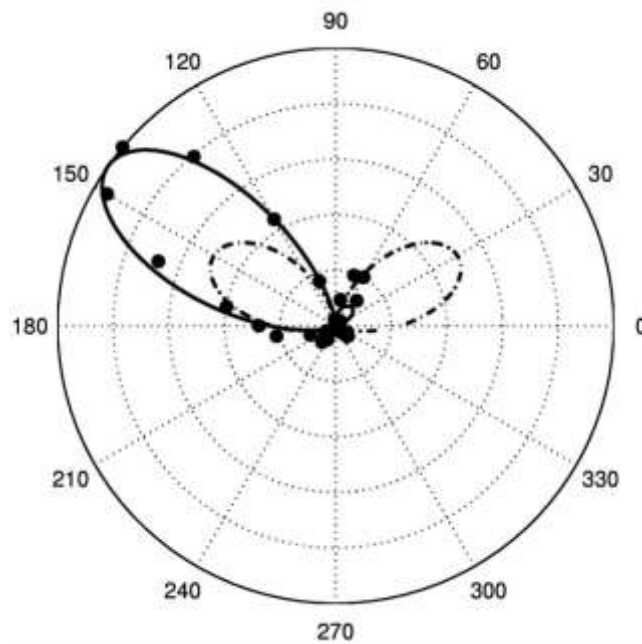

Figure 5.8: Radiation pattern of the disc monopole with L - shaped ground plane (solid line) and of the conventional disc monopole (dash-dotted line) in the x - y plane at 6 GHz. Black circles represent measurements on a prototype in anechoic chamber. results are reported in linear scale.
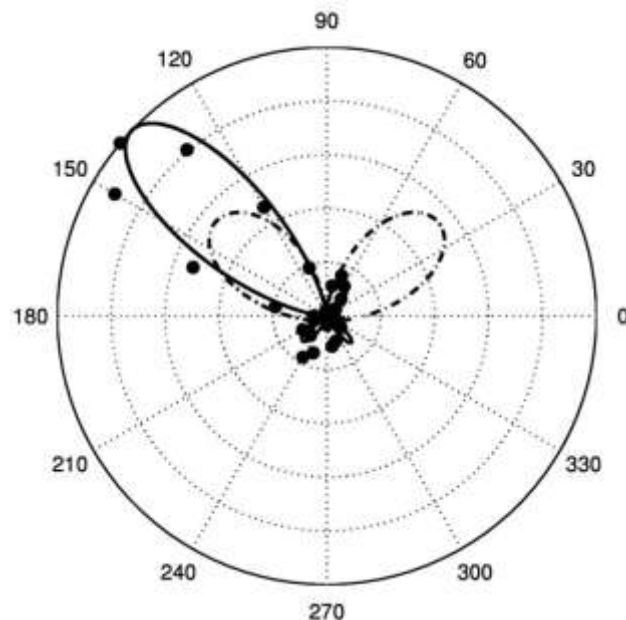

Figure 5.9 : Radiation pattern of the disc monopole with L- shaped ground plane (solid line) and of the conventional disc monopole (dash-dotted line) in the x - y plane at 7 GHz. Black circles represent measurements on a prototype in anechoic chamber. results are reported in linear scale.

5.4 Directional Monopole Antenna With a Parabolic-Shaped Ground Plane

The UWB antenna presented here is designed for fabrication on FR4 substrate with εr=4.4, thickness of 1.6mm and 35μm metallization thickness. Geometries of the antenna in various technologies are demonstrated in Figure 5.10 including the top and bottom metal layers[16].
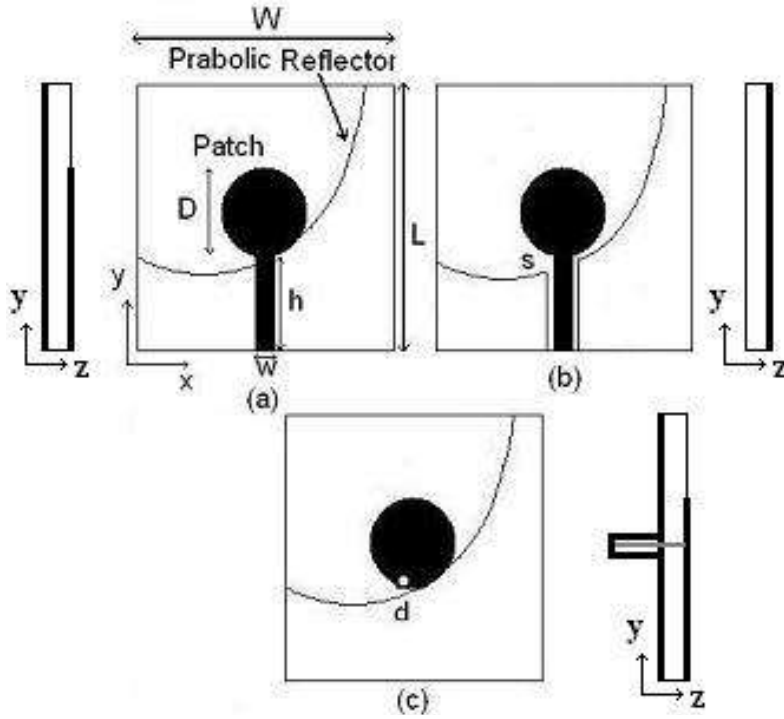

Figure 5.10 : Dark top and transparent ground-plane and side views of the proposed directional planar UWB antennas in microstrip technology (a), coplanar technology (b), and microstrip with coaxial feed (c).

The top layer in Figure 5.10a consists of a centered circular patch element with 50 Ω microstrip feed. The parameters D, w and h are the diameter of the patch, and the width and length of the feed line, respectively. The transparently shown metallization on the bottom of the substrate is recognized as a parabolic reflector of which the patch is located in the focal point based on:

$$y - y_0 = \frac{1}{4f}(x - x_0)^2$$

(5.1)

where x_0 and y_0 are the displacements in the Cartesian coordinate system, and f is the focal length, which is assumed to be one half of the patch diameter. Figure 5.10b and Figure 5.10c illustrate the respective antenna structures in coplanar waveguide

technology as well as with a coaxial feed. The parameters in Figure 5.10b is the gap between the ground reflector and the patch for 50 Ω input matching. The parameter d in Figure 5.9c is the diameter of the via hole through the substrate, which is equal to the inner diameter of the coaxial feed line at the bottom of the substrate. The design of the UWB antennas is centered at 8 GHz with more than 120 percent bandwidth. The fundamental design goals are a low reflection coefficient, enhanced radiation pattern in the desired direction as well as good group delay performance. The diameter of the disc is calculated as D=18 mm for 8GHz center frequency. Figure 5.11 shows the input reflection coefficient of the directional microstrip antenna as obtained from CST Microwave Studio and Ansoft HFSS. The width of the input line is w=3mm for a characteristic impedance of 50Ω. In order to find a good trade-off between all desired properties, the width and the length of the substrate were varied and finally identified as W=50mm and L=46mm. The predicted reflection coefficient is better than 9.5dB between 3.1GHz and 12.6GHz.
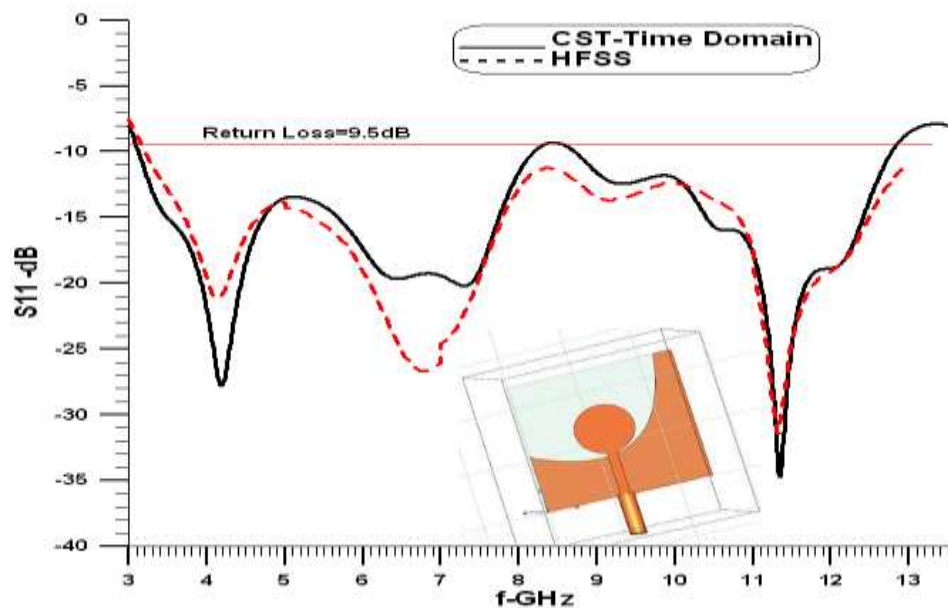

Figure 5.11 : Reflection coefficient of the antenna.

The radiation patterns have been computed with both simulation packages at various frequencies. The largest differences between the two results are observed at 11 GHz, and these patterns are shown in Figure 5.12 as an example and representative of largest variation of radiation patterns obtained for the antenna to follow.
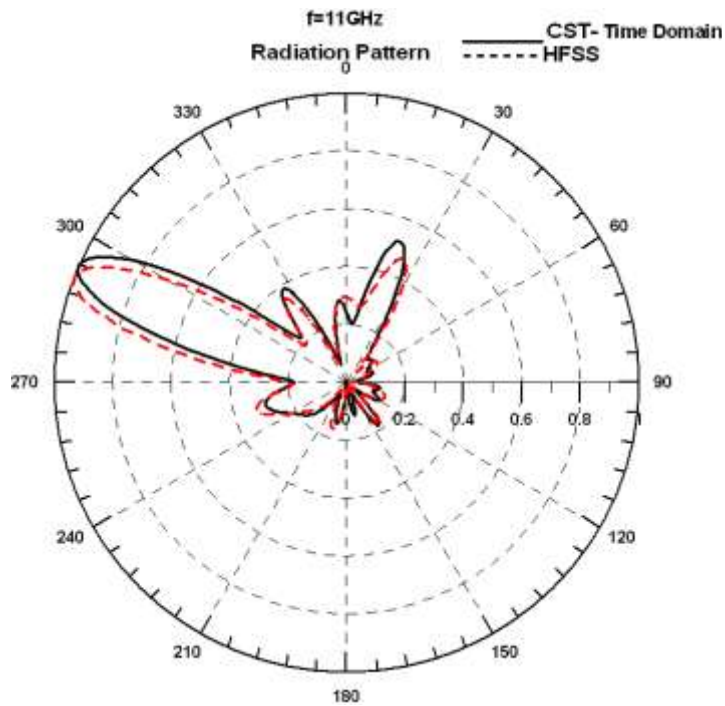
Figure 5.12: Radiation pattern of the antenna at the freauency of 11 GHz.

Figure 5.13 shows that the direction of the beam moves between 348 and 285 degrees between 3GHz and 12.6GHz. In addition, the half-power beamwidth of the main lobe varies between 75 and 25 degrees.
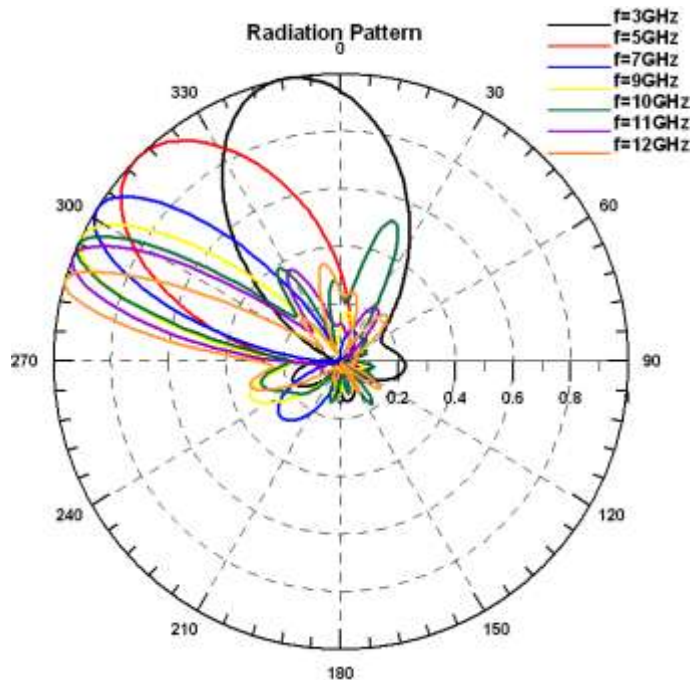

Figure 5.13: Radiation pattern of the antenna at the differrent frequencies.

The maximum gain versus frequency is shown in Figure 5.14 and is around 8 dB at mid-band frequency..
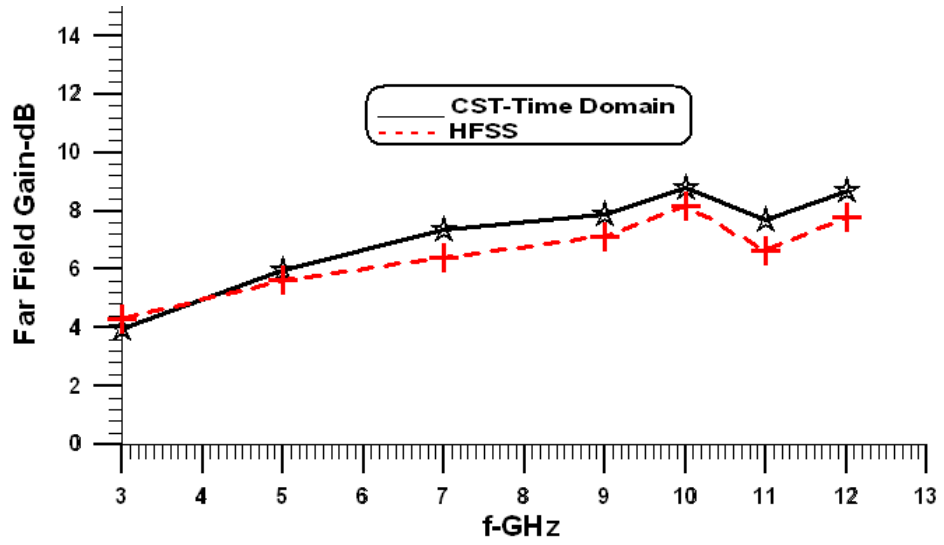

Figure 5.14 : Simulated gain of the antenna.

6. DIRECTIONAL WIDE BAND PRINTED MONOPOLE ANTENNA FOR USE IN MICROWAVE BREAST CANCER IMAGING

6.1 Introduction

Currently there are increasing demands for directional and high gain antennas, especially for the Ultra Wide Band (UWB) applications. Radars and microwave breast cancer imaging systems are the main examples where the directive antenna systems are required. Application of interest is microwave breast cancer detection which exploits the contrasts in dielectric properties between healthy and malignant tissue. Directional antennas are used to optimize Half Power Beam Width (HPBW), more clearly, to increase the radiation intensity in a favored direction by converging radiation pattern. In radars, antenna's HPBW is one of the main parameters determining the radar's resolution; finer details can be resolved by using a narrower beam. Many efforts have been addressed to design compact wideband antennas for microwave breast imaging. These antennas can usually be classified as one of three types (dipole, slot, or monopole) based on their physical features and radiative properties. A key component of Radar-Based Microwave breast cancer imaging systems is the antenna that is used to radiate and receive the ultra-wideband pulses [30]. So the antenna design requirements are as follows:

- Radiate an ultra-wideband signal to transmit short pulses.

- Size on the order of it few centimeters to selectively illuminate and permit scanning.

- An Optimum half power near-field beam width to avoid smearing of the scatterers that occurs if the field of view of each antenna is too broad.

- Good impedance matching across the entire band width. This ensures that most of the energy is transmitted.

The directional monopole antennas with a parabolic-shaped or L-shaped ground plane, (chapter 5), have a good directional characteristics, bandwidth and also a proper size, in order to use in microwave imaging system. In this chapter, a new

modified directional monopole antenna with a parabolic-shaped ground plane is presented. At the following, another novel compact directional monopole antenna in microstrip technology is also presented. Miniaturized size and an acceptable directional characteristic of this antenna make it possible to use it in the microwave imaging systems and radar applications.

6.2 Directional Monopole Antenna With a Parabolic-Shaped Ground Plane

6.2.1 Design and characteristics of the antenna

The purpose of this design is to propose an antenna which has the impedance bandwidth between 4 and 9GHz, with a highly directional radiation pattern throughout the desired bandwidth, for use in near field near surface imaging applications. Geometry of the proposed antenna is illustrated in Figure 6.1, including the top and bottom metal layers. In order to maintain a trade-off between the gain in the favored bandwidth and the size of the antenna, it is designed on square FR4 substrate with dimension of 50mm, where dielectric constant is ε_r=4.4. Thicknesses of the dielectric (d) and conductor layers are 1.6mm and 35μm, respectively. The top layer in Figure 6.1 consists of a circular patch element with 50Ω microstrip feed.
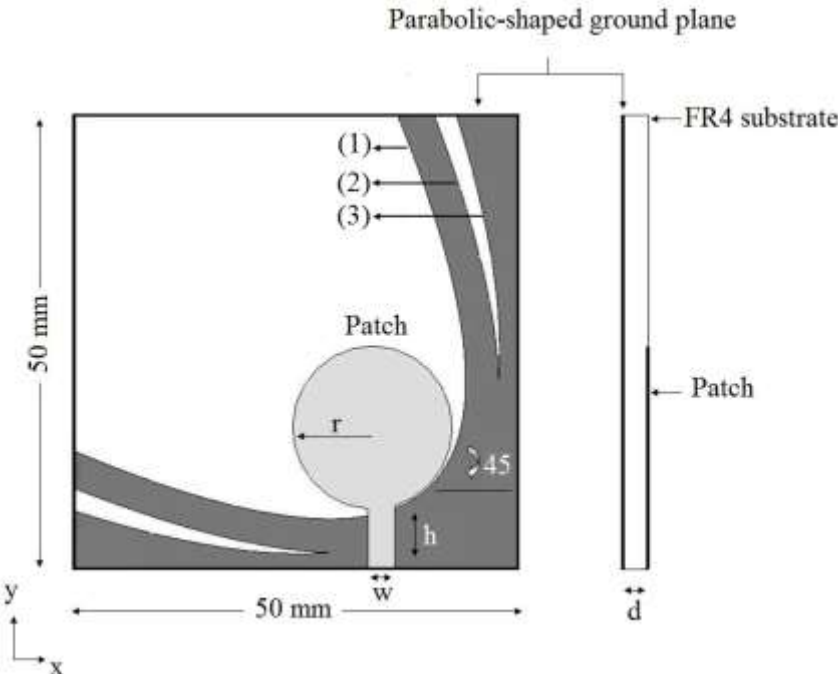

Figure 6.1 : Top and side views of the antenna.

The Parameters r, w and h are the radius of the patch, and the width and length of the feed line, respectively. In the other side of the substrate there is a parabolic-shaped

ground plane. The oil-colored part of Figure 6.1 on the bottom of the substrate acts as a parabolic reflector. A prominent feature of this antenna is the carefully designed ground plane that improves the directivity. Main edge of the reflector, which is shown by (1) in Figure 6.1, is inserted based on equation (6.1):

$$y - y_1 = \frac{(x - x_1)^2}{4f_1}$$

(6.1)

Where, x_1 and y_1 are measured with regard to the coordinate system which is shown in Figure 6.1 The factor $1/(4f_1)$ appearing in equation (6.1) is defined as the concavity factor of the curve, where f_1 is the length between the focal point and vertex point of the parabola which is known as the focal length. Parabolic curve which is based on Equation (6.1) is rotated 45° in order to extend the axis of the parabola merely in the direction of the substrate's diagonal. Also the vertex point of the parabola is considered to the nearest place of the substrate's diagonal. In order to making optimum trade-off between the reflection coefficient and directivity through the bandwidth of 4-9 GHz, the optimal values of x_1 and y_1 are determined as 40.4mm and 9.3mm, respectively. Radius r is chosen as 9mm according to obtain the desired reflection coefficient bandwidth. Center point of circular patch is inserted in 33.6 mm and 15.5 mm respectively in x and y directions. Width of the microstrip feed is selected 3mm to obtain 50 Ohm impedance, while the center of w is inserted at 34.6mm in the x direction. Consequently, length of the feed line h is chosen 6.9mm. Focal length of f_1 is recognized as 5.4mm, to obtain the optimum concavity for curve (1) according to the location of the circular patch, that is to say, locating patch exactly on the focus of the curve (1).

Furthermore, in order to improve the reflection of radiation pattern from the ground plane, two parabolic slots are inserted at the corners of the ground plane. These slots are formed by subtracting the area between the curves (2) and (3) from the ground plane.

$$y - y_2 = \frac{(x - x_2)^2}{4f_2}$$

(6.2)

$$y - y_3 = \frac{(x - x_3)^2}{4f_3}$$

(6.3)

All the parameters in equations (6.2) and (6.3) are defined as the same as in equation (6.1). Both vertex points of the curves (2) and (3) are inserted at the same point. Both

parabolic curves, based on equations (6.2) and (6.3), are rotated 45° to locate the axis of the parabolas in the direction of the substrate's diagonal. Focal lengths of f_2 and f_3 must be chosen longer than f_1, due to the reduced concavity of curves (2) and (3) compared to the curve (1). Therefore, the optimum quantities of $x_{2,3}$ and $y_{2,3}$ are determined as 42.4mm and 7.3mm, respectively. In order to obtain the optimum concavity for curve (3) to improve the directivity, focal length of f_3 is recognized as 8mm. Also focal length of f_2 is determined as 6.4mm, to optimize the dimensions of the slots.

A prototype with the mentioned optimum parameters has been fabricated. In Figure 6.2 the photo of the antenna is shown. On the left, the side of the antenna with the parabolic-shaped ground plane is observable, while on the right we have the other side with the circular patch and the microstrip line.
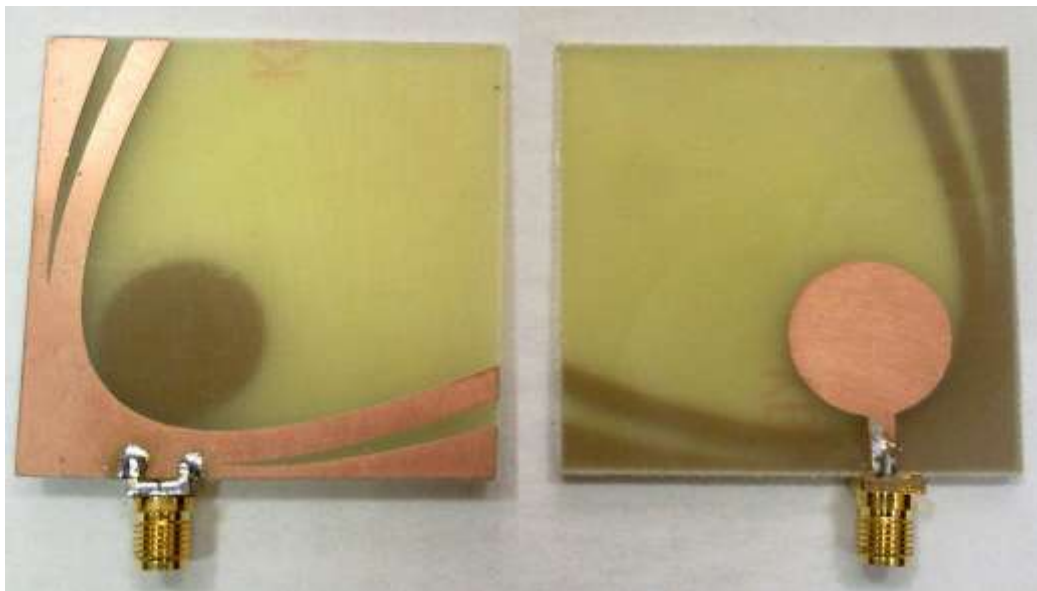

Figure 6.2 : A photograph of fabricated antenna.

6.2.2 Parametric study of the antenna

Ground plane of the antenna consists of a symmetrical parabolic curve, which its axis extended along the direction of the substrate's diagonal. Distribution of the surface fields is shown in Figure 6.3 , which demonstrates that the ground plane, expressed by equation (6.1), reflects the radiation through its surface, symmetrically. This extended reflector around the circular patch has the advantage of optimum converging of the radiation pattern. Effects of this design on the gain and directivity

are shown in Figure 6. 7. Compared to the antenna presented in [16], gain of the antenna is remarkably raised, among 1 - 2dB between 4 and 9GHz.
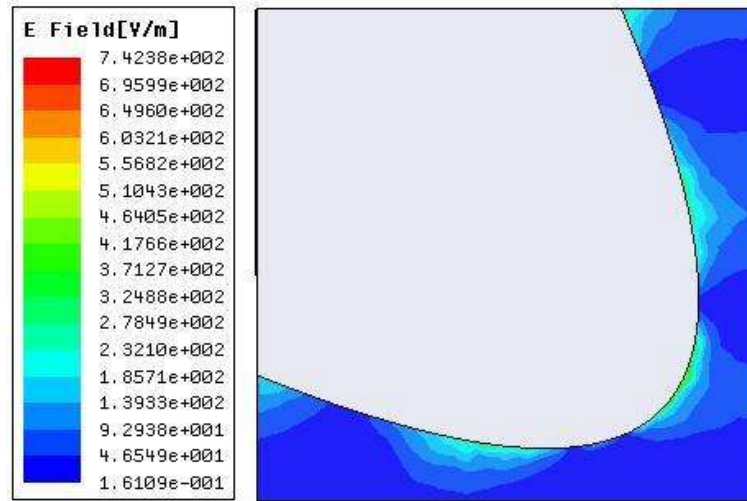

Figure 6.3 : Electrical field distribution around the ground plane at 6 GHz.

The ground plane acts as a reflector with its own original design. The second edge of the ground plane which is created by inserting the slots, behaves as an additional reflector which cause to increase in the gain and directivity. The effect of inserting parabolic slots on the surface fields of the ground plane is demonstrated in Figure 6.4. Other reflection occurs at the second parabolic edge which is in return raises the reflectance of the ground plane. Along with, optimizing the slots causes the reflector to improve the directivity. Besides, inserting the circular patch on the focal point of the reflector, another crucial design consideration is the size of the reflector's width through different parts of the ground plane.
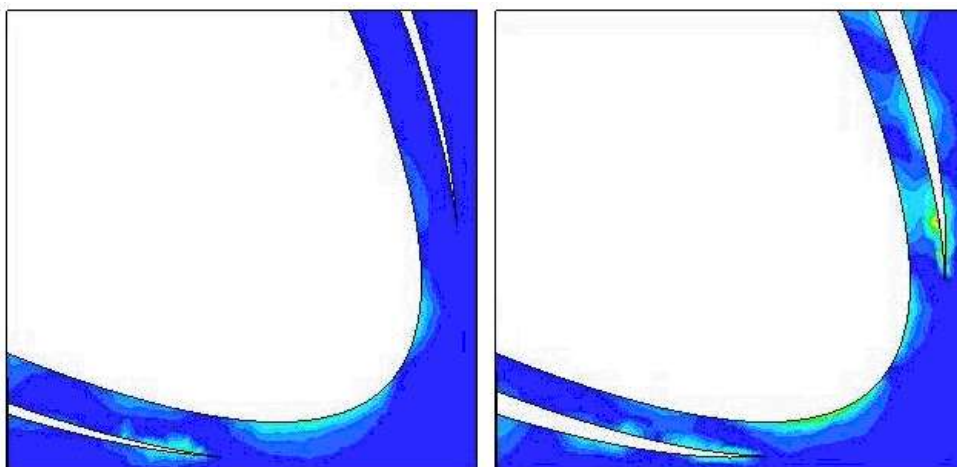

Figure 6.4 : Electrical field distribution around the ground plane at freq. of 8.5 GHz, f_2=7 mm (left) and f_2=6.4 mm, optimum (right).

Amount of the reflected radiation is depends on the proportion of the reflector's width to the wavelength. Focal length f_2 is used to optimize the reflector's width directly, and f_3 is not used due to the fact that f_1 and f_3 are already optimized according the concavities of curve (1) and (3), where the ground plane reflections occur both from. Figure 6.4 shows the distribution of the surface fields at the frequency of 8.5GHz for two values of f_2=7mm, and f_2=6.4mm (optimum), for constant values of f_3.

Surface Currents on the ground plane of the antenna for both the antenna with optimum slots ($f_2 = 6.4$) and without slots are shown in figure 6.5 and figure 6.6.
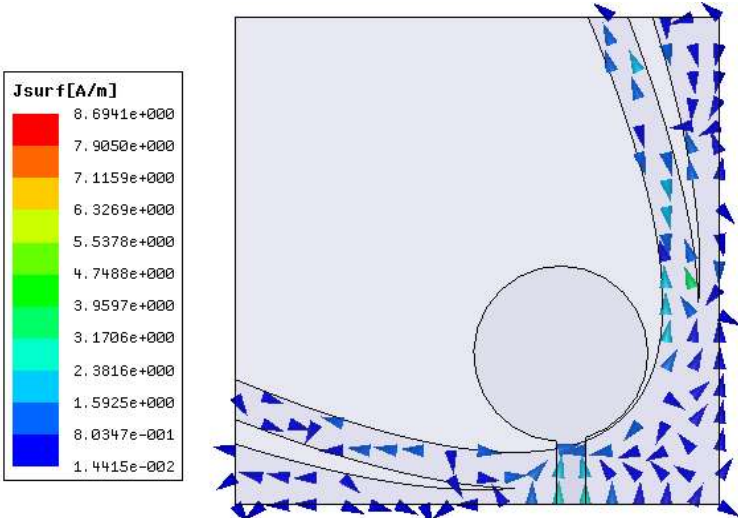

Figure 6.5 : Distribution of surface currents around the ground plane at the freq. of 8 GHz, f2=7 mm (with slots).
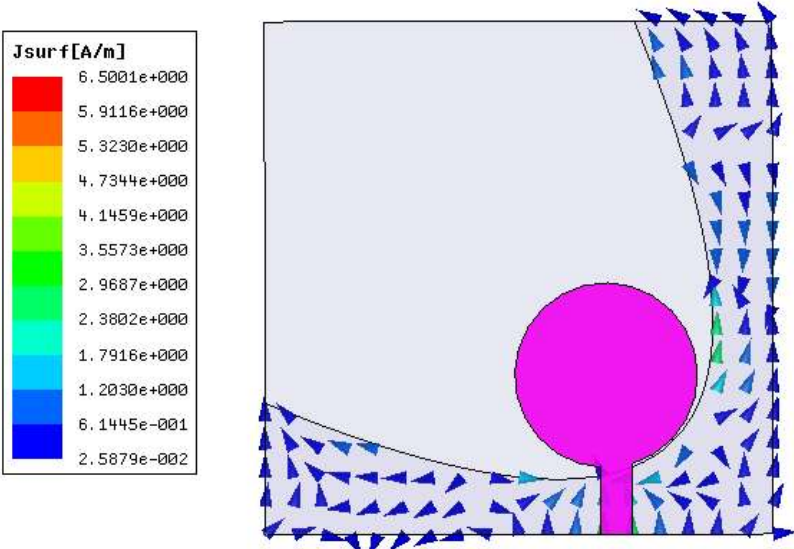

Figure 6.6 : Distribution of surface currents around the ground plane at the freq. of 8 GHz, (without slots).

As a result, Figure 6.7 shows that effect of the varying amounts of f_2 to the gain of the antenna for different frequencies. Therefore, we can use different values for f_2 depending on the frequency of application.
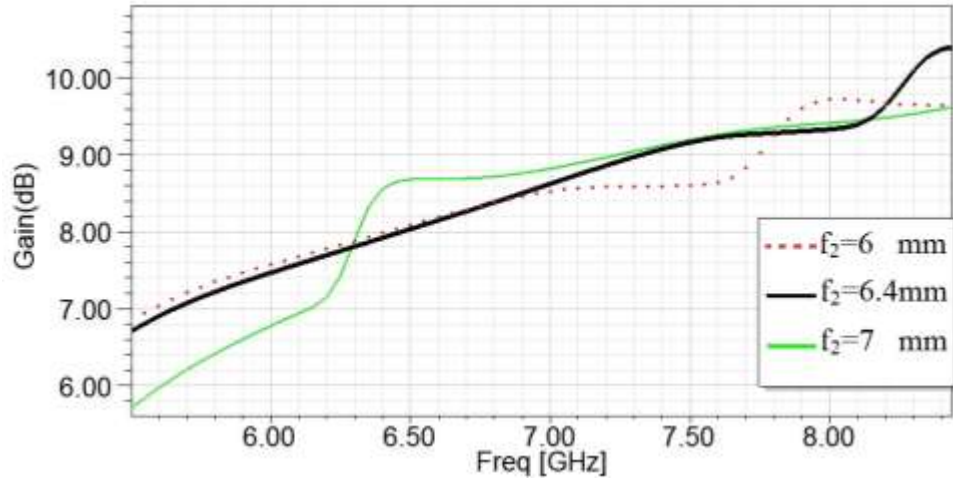

Figure 6.7 : Simulated gain at theta=90 degrees and phi=131 degrees for f_2=6, 6.4 and 7.

Considering Fig6.7 for an application with center frequency of 6.5GHz, f_2=7mm will give the optimum solution. In this antenna, for the frequencies between 4 and 9GHz, f_2=6.4mm is identified as an optimum value. The effect of varying amount of f_2 on the reflection coefficient is also shown in Figure 6.8; f_2=6.4mm is also determined to obtain the desired impedance bandwidth.
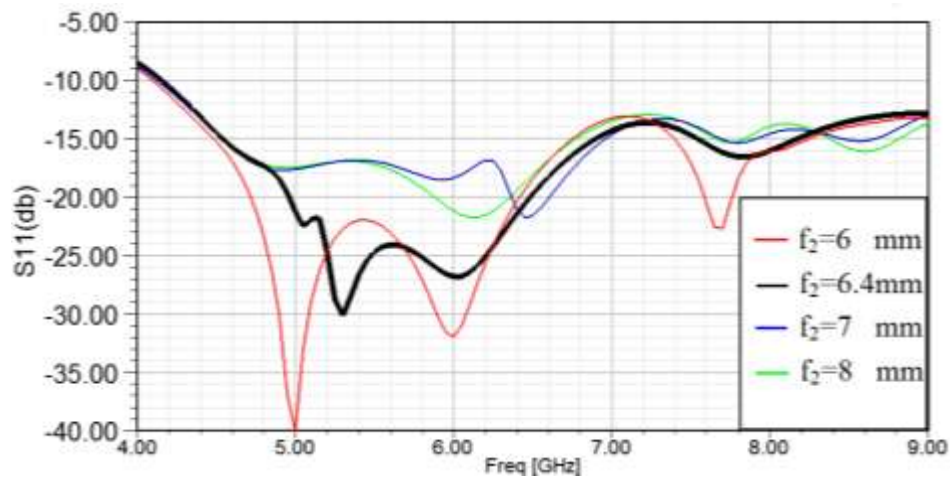

**Figure 6.8** : Simulated reflection coefficient for f_2=6, 6.4, 7 and 8.

6.2.3 Measurements and results

Compared to the antenna demonstrated in [16], gain of the antenna is improved among 1-2dB, between 4 and 9 GHz, without slots; consequently, inserting the slots

also improves the gain curve between 0.1 and 1.1 dBi. Results are shown in Figure 6 .9a, between 5.5 and 9GHz at Theta=90° and Phi=131°. Considering Figure 6.9a, at the frequency of 8.5GHz, the gain is raised from 7.6dBi to 10.4dBi with the slots compared to [16]. Also related radiation pattern in the frequency of 8.5GHz is shown in Figure 6.9 b. Simulated HPBW of the antenna for this frequency is 26° with slots, while HPBW is 31° without slots and also for the antenna designed in [16] is 38°. Between the frequencies of 4 and 9GHz, HPBW changes among 56° and 25°, respectively.
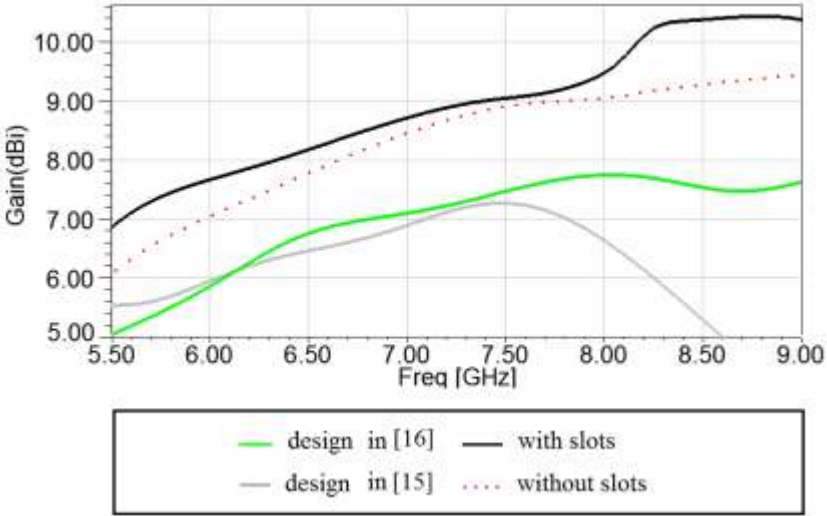
(a)
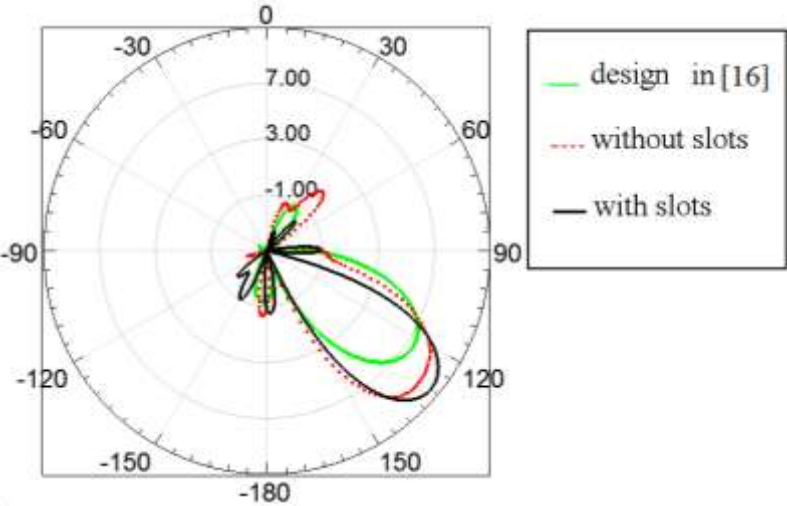
(b)

Figure 6.9: (a) Simulated gain of the antenna compared to [15] and [16] (b) simulated radiation pattern (logarithmic scale) of the antenna compared to [16] at the frequency of 8.5 GHz.

Also radiation pattern of the antenna in linear scale is demonstrated in figure 6.10 in comparison with the previous design in [16]
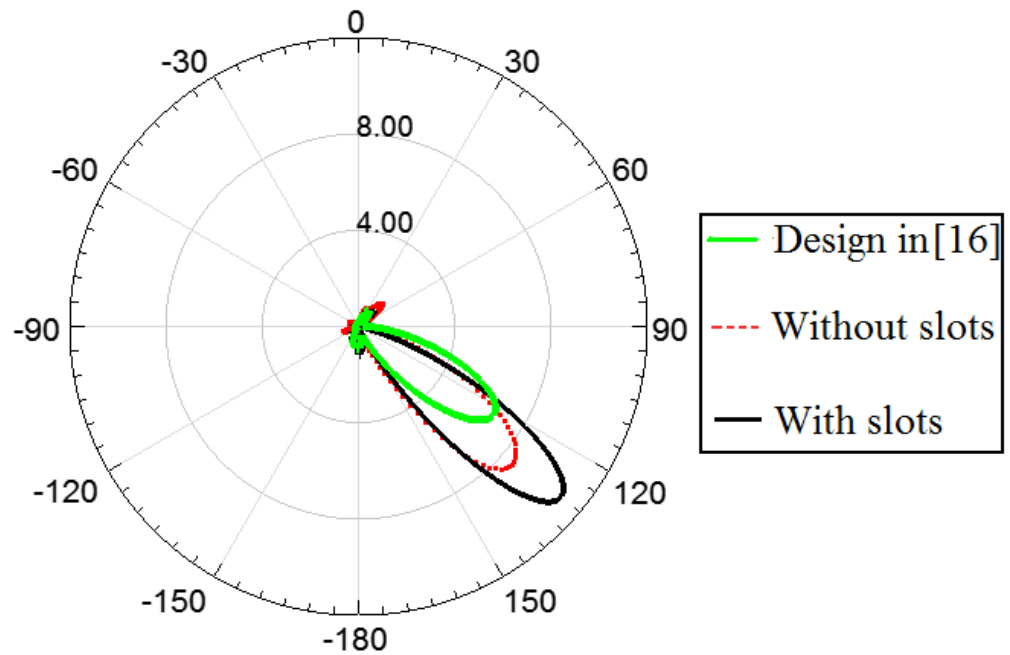

Figure 6.10 : Simulated radiation pattern (linear scale) of the antenna compared to [16] at the frequency of 8.5 GHz.

Direction of radiation pattern of the antenna moves between Phi=131° and Phi=152° among 5-9 GHz (Figure 6.11), that confirms a good stability of the antenna's beam versus frequency.
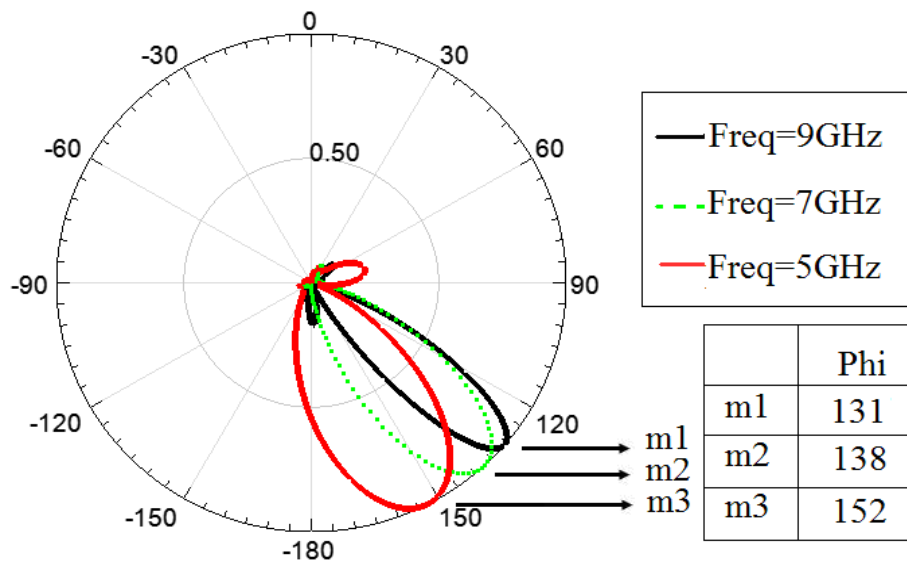

Figure 6.11 : Radiation pattern of the antenna (in linear scale). m1, m2 and m3 are the direction of maximum gain at the frequencies of 9, 7 and 5 GHz, respectively.

75

All simulations were done by HFSS v.11 and then compared to the measurements, which were done using Agilent N5230A network analyzer in the anechoic chamber with dimensions 6X7X3.3m and working frequencies 80MHz to 20GHz.   Good agreement is observed between the simulations and measurements. Figure 6.12 shows the simulated and measured beam of the antenna in two frequencies.
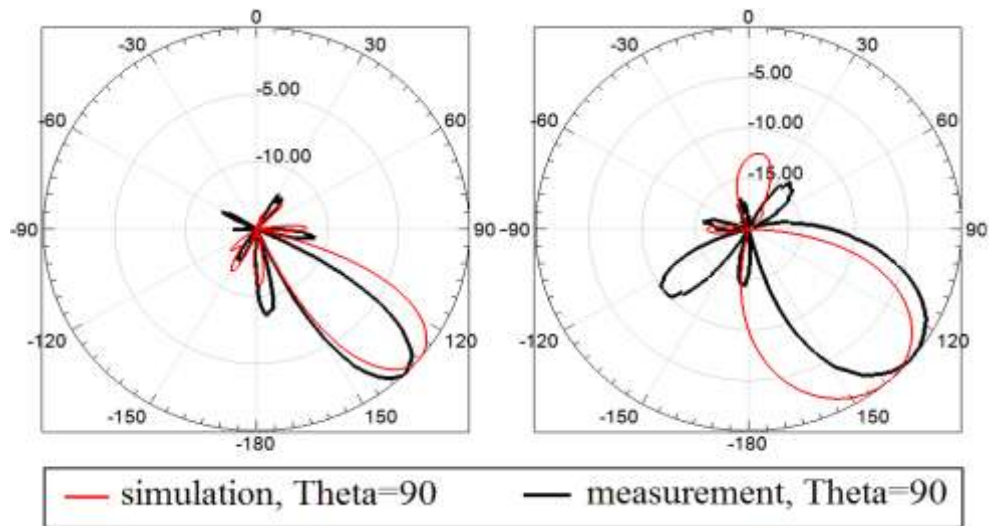

Figure 6.12 : Simulated and measured beam of the antenna at frequency= 8.5 GHz (left) and frequency=6 GHz (right) in logarithmic scale.

At the frequency of 6GHz, measured HPBW is 41˚ and simulated HPBW is 44˚, also for the frequency of 8.5GHz HPBW is obtained 23˚ compared to the simulated HPBW which is 26˚. There are 10˚ and 5˚ tilts between simulated and measured patterns at the frequencies of 6 and 8.5 GHz, respectively. Gain of the antenna also is shown in Figure 6.13, which shows a good agreement between the simulated and measured gain at Theta=90˚ and Phi =131˚.
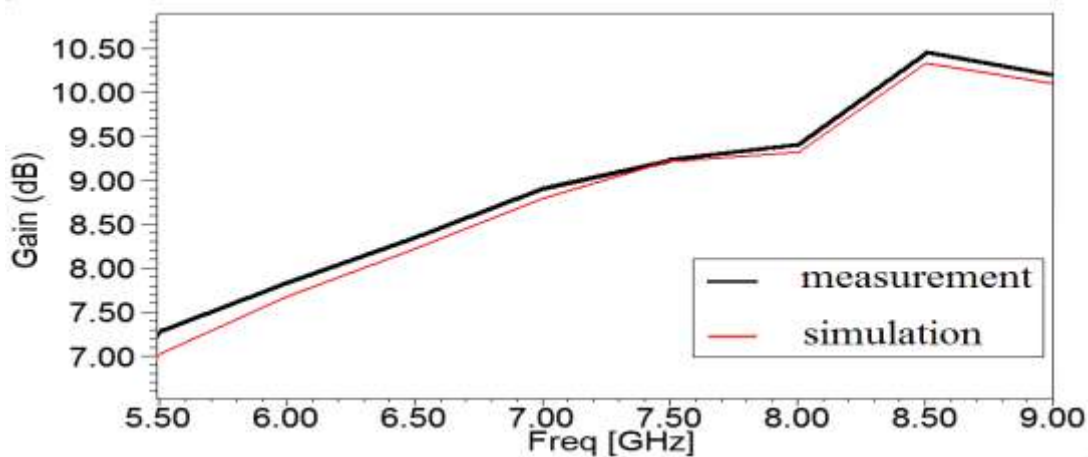

Figure 6.13 : Simulated and measured gain of the antenna.

Finally, simulated and measured reflection coefficient is shown in Fig 6. 14; which confirms the good characteristic of the antenna in the favored bandwidth. There are some differences in the reflection coefficient between the simulated and measured antenna which is because of some default in fabrication and measurement process but as it could be seen, between the frequencies of 4 and 9 GHz, antenna has a reflection coefficient under -10dB.
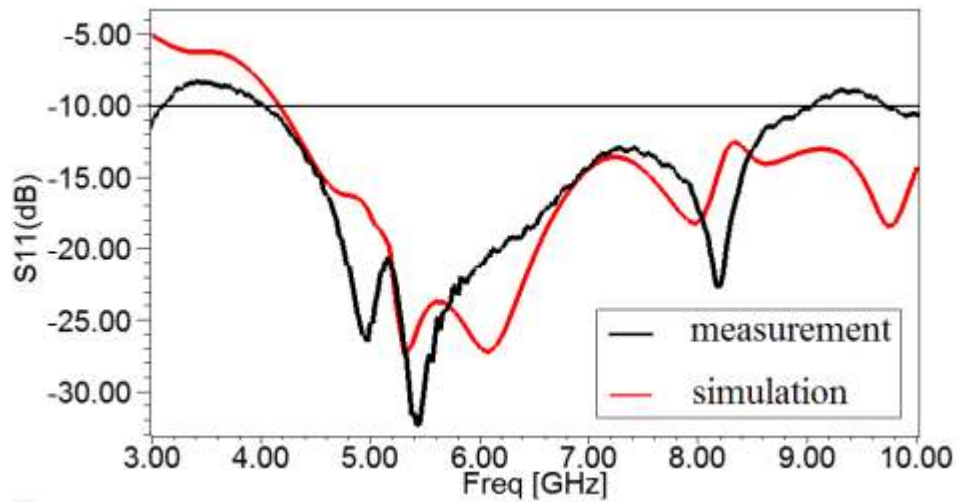
Figure 6.14 : Simulated and measured reflection coefficient.

6.2.4 Modification in the size of the antenna

As it was studied in the previous sections, size of the antenna is very important in order to use in the application of Radar-Based microwave breast cancer imaging. In this design size of the antenna is considered to be improved where the optimum trade-off is also maintained between the size, reflection coefficient and gain of the antenna. In this section just simulated design of the antenna is presented.

Figure 6.15 : Top view of the antenna.

This Presented directional antenna is also designed in more compact size of 40 * 40 mm. the structure of antenna is shown Figure 6.15. Aim of this attempt is to maintain a trade-off between the size and gain of the antenna, especially with more compact size.
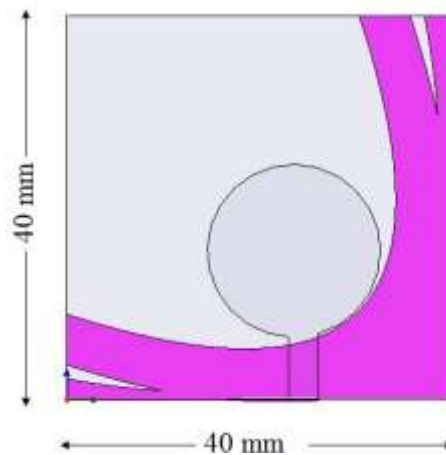
The purpose of this design is to optimize the size of antenna which has the optimum directional characteristics between the bandwidth of interest, for use in near field near surface imaging application. Geometry of the proposed antenna is illustrated in Figure 6.15. As in the case of the previous model, in order to maintain a trade-off between the gain in the favored bandwidth and the size of the antenna, it is designed on square FR4 substrate with dimension of 40mm, where dielectric constant is ε_r=4.4. Thicknesses of the dielectric (d) and conductor layers are 1.6mm and 35μm, respectively. The top layer in Fig6.12 consists of a circular patch element with 50Ω microstrip feed. The Parameters r and h are determined same as the previous design. but width of the feed line (w) is determined as 24.6 mm. The optimal values of x_1 and y_1 are determined as 30.4mm and 9.3mm, respectively. The optimum quantities of $x_{2,3}$ and $y_{2,3}$ are determined as 32.4mm and 7.3mm, respectively. The optimal values for f_1, f_2 and f_3 are determined as 5.5, 6.5 and 9, respectively. As in the case of the previous design, in this compact design, the small reflector also converges the radiation through its surface, especially in a symmetrical form. This can be seen clearly in the figure 6.16 at the frequency of 7 GHz. In this figure the electrical field distribution around the ground plane is demonstrated.
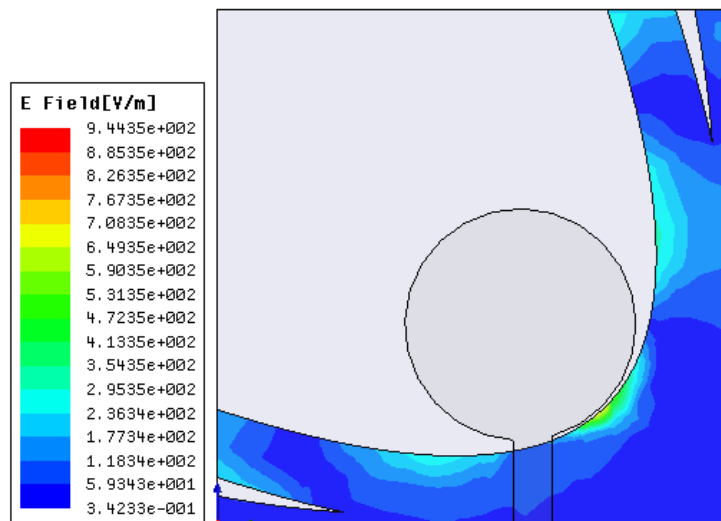

Figure 6.16 : Electrical field distribution around the ground plane at 7 GHz.

Also electrical field distribution around the ground plane for two amounts of f_2 (6.5 and 5.5) are demonstrated in figure 6.17 and compared with each other.
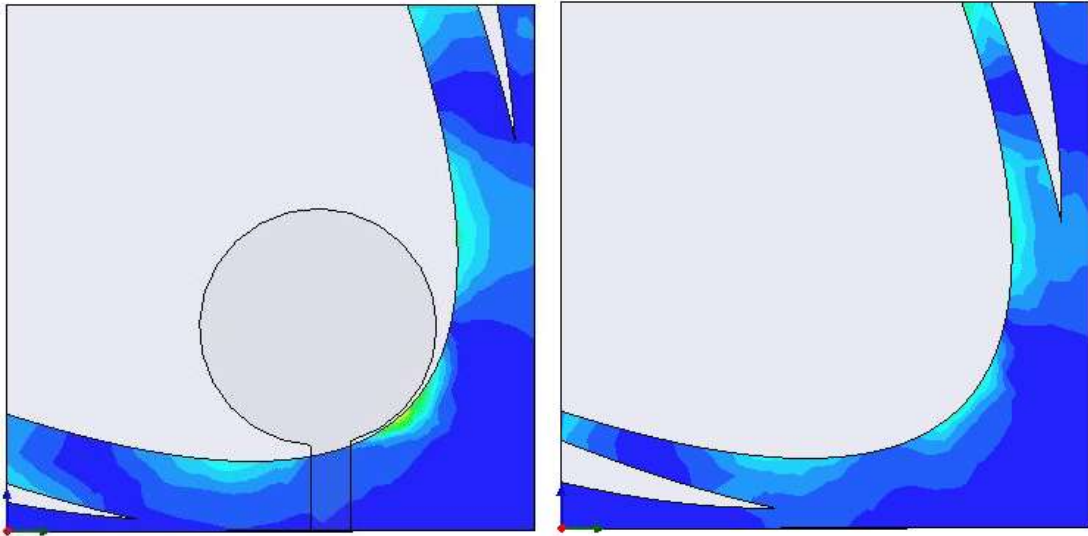
Figure 6.17 : Electrical field distribution around the ground plane at 7 GHz for two different amounts of f_2 (left f_2 =6.5 optimum).

Reflection coefficient of the antenna is under -9.5 dB between the frequency of 4 and 10 GHz (figure 6.18) . In comparison with the previous design, gain of the antenna just has a low decrease, where the size of the antenna is improved. Gain of the antenna is demonstrated in the fig. 6.19.

Figure 6.18 : Simulated reflection coefficient of the antenna.

Also gain of the antenna is still around the gain presented by [16] while in this case the size of the antenna is considered to be improved.
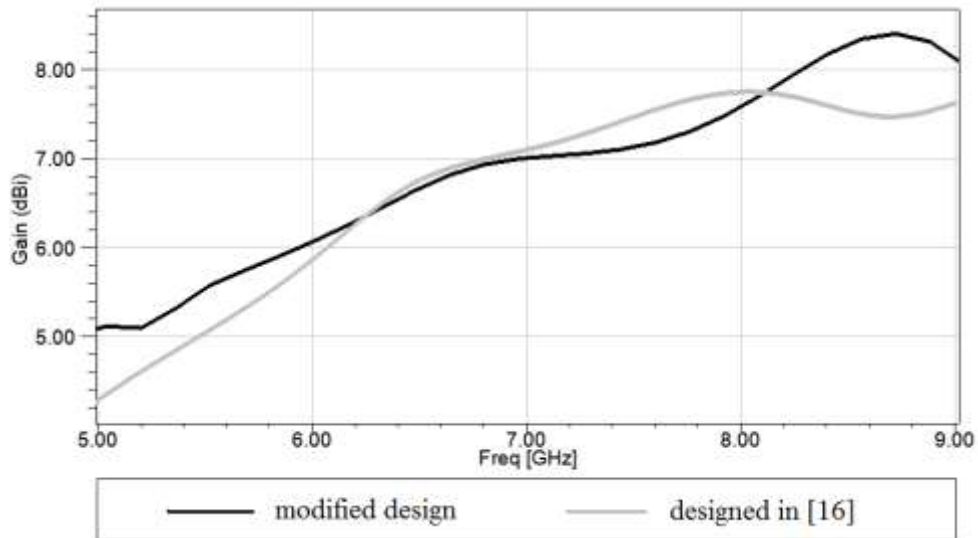
Figure 6.19 : Simulated gain of the antenna.

As it can be seen in the figure 6.19 the gain of the antenna is around the obtained gain in [16], where the size of the antenna i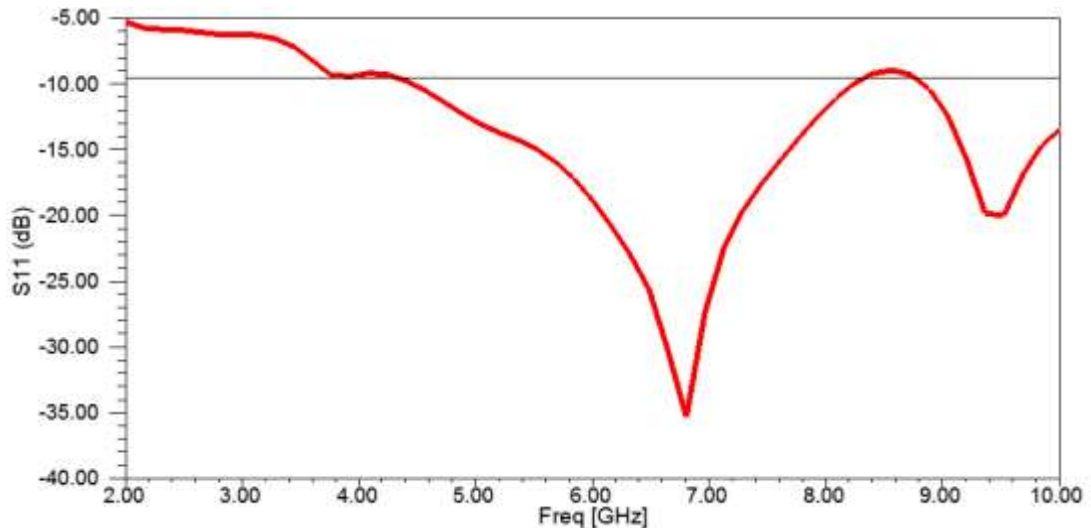s considered to be improved. Also radiation pattern of the antenna is presented in the figure 6.20 at different frequencies, which confirms the directional characteristic and also stability of the radiation pattern of the antenna.
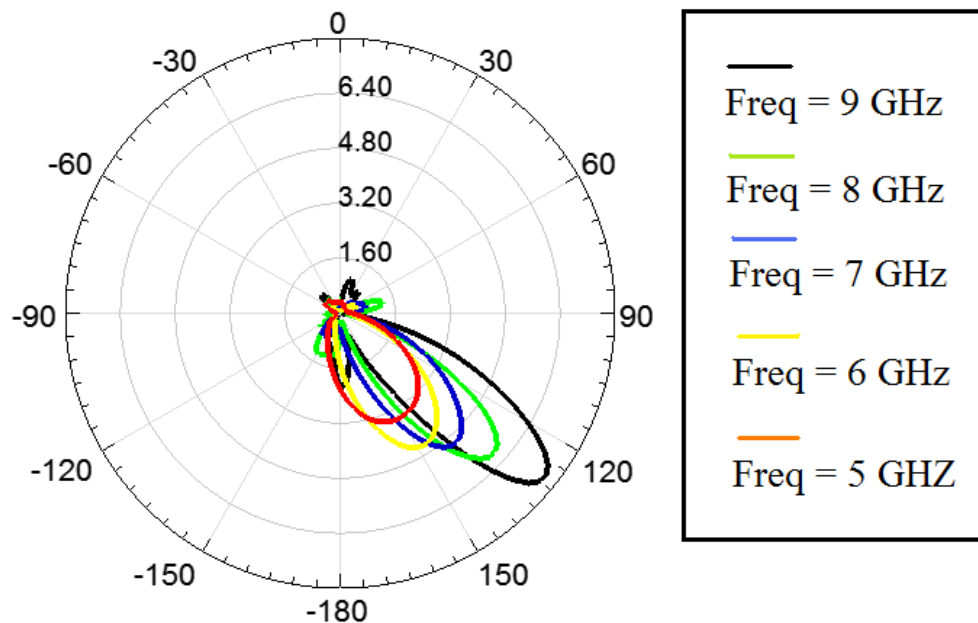
Figure 6.20 : Simulated radiation pattern of the antenna at different frequencies between the bandwidth.

This structure could be considered if the size of antenna is more important in comparison with the gain and half power beam with of the antenna. But the main purpose of this chapter of the thesis was to present a more directive and modified

antenna with a new design for use in the applications of microwave imaging, where high resolution is required. The favored antenna is designed and presented in section 6.2 and consequently the results are shown in the next sections. The measured result also compared with the simulations and confirmed the good characteristics of the antenna. But as the alternative in advantages of modified design of the antenna in the last section a modified size of the antenna is also presented where more compact size is needed. For the main antenna with the improved gain and directivity, for example, at 8.5 GHz, measured HPBW of the antenna is decreased from 38 degrees to 23 degrees, which confirms a 39 % decrease in HPBW of the antenna which is considerable in order to increase the resolution of a radar system.

6.3 A Novel Compact Monopole Antenna

6.3.1 Characteristics of the antenna

The final aim of the work is to get a planar antenna with a very compact size and a wide reflection coefficient bandwidth as well as a directive radiation patterns between the frequencies of 5 and 9 GHz. Fig. 6.21 shows the geometry of the proposed compact antenna, which consists of a semicircular patch with its coupling-fed complement as a parasitic element and an optimized deformed ground plane.
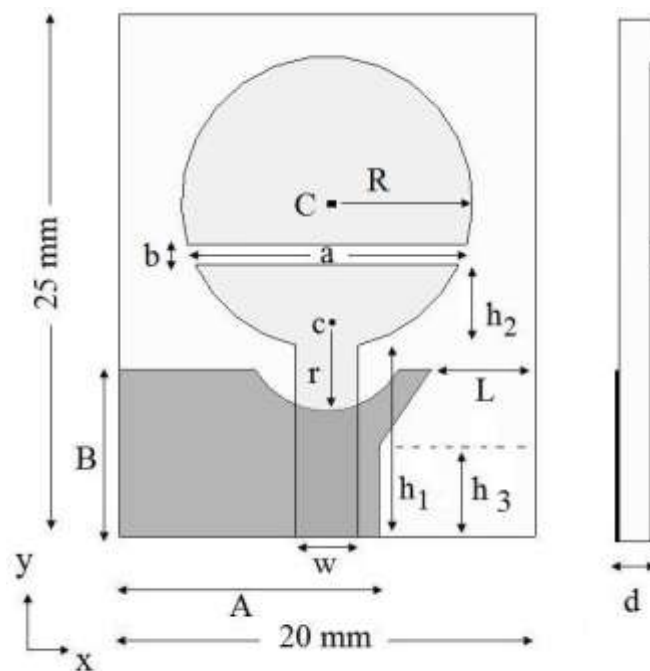

Figure 6.21 : Geometry of the antenna-top view (left) and side view (right).

In order to maintain an optimum impedance matching through the bandwidth, as well as an optimized size, the antenna is designed on a rectangular FR4 substrate with dimension of 20 and 25 mm, where dielectric constant is ε_r=4.4. Thicknesses of the dielectric (d) and conductor layers are 1.6 mm and 35 μm, respectively. Top metal layer of the antenna consists of two segments.

As it can be seen in Fig. 6.22, both elements at the top of the substrate, are the complementary segments of a broken circle, where the center point of the circle (C) is inserted at x = 10 mm and y = 16 mm. Where, x and y are measured with regard to the coordinate system which is shown in Fig. 6.22. Also radius (R) of the circle is chosen as 7 mm in order to obtain the desired bandwidth. Where the piece at the bottom of the break is fed directly by a 50 Ω microstrip line with the dimensions of w = 3mm and h_1 = 9.15 mm. Width of the microstrip line is chosen 3 mm to obtain 50 Ω impedance matching. While the center of w, is inserted at 10 mm in the x direction. The other complementary piece at the top of the break is fed by coupling from the main patch. Dimensions of the break on the circle, is optimized in order to achieve the favored reflection coefficient bandwidth. It also optimizes the directional characteristic of the antenna. Optimized dimensions of a = 13.4 mm and b = 1 mm is determined for the break on the circle. It causes to turn in the surface currents of the patch surface which improves the impedance matching. To accomplish an optimum impedance matching the break is inserted at h_2 = 3.86 mm from the bottom of the circle.

At the other side of the substrate we have a deformed ground plane which is demonstrated by an oil-colored part in Fig. 6.21. The ground plane is a prominent feature of this antenna which is carefully designed to improve the directivity. It can be considered same as a rectangular shape whose right side is cut and optimized. The length of the ground plane along the y direction (B) is determined as 8 mm to obtain the desired bandwidth. The right side of the ground is cut to remove the radiation in undesired direction. The optimized dimension for A to maintain a tradeoff between the radiation and reflection coefficient is determined as 12.5 mm. The cut segment of the ground plane consists of two rectangular and trapezoid shapes. By determining the length A equal to 12.5 mm the length of the rectangle and the bottom length of the trapezoid is determined as 8.5 mm. also the optimized size of the width of the rectangle (h_3) is determined as 4.36 mm. consequently the length L and the width of

the trapezoid is chosen as 5mm and 3.64 mm, respectively. In order to improve the impedance matching, another semicircular break is inserted on the bottom metal layer. Where, the center (c) of the circle is inserted at 10mm along the both x and y directions. And radius (r) of the circle is obtained as 4mm.

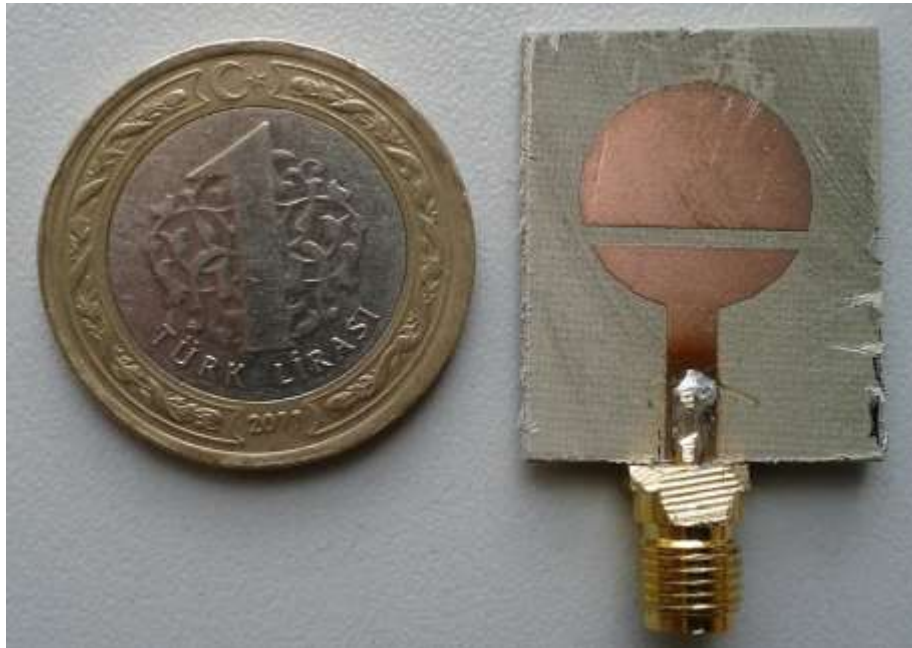A prototype with the discussed optimum parameters has been fabricated and demonstrated in Fig. 6.22.

Figure 6.22 : Photo of the antenna.

6.3.2 Parametric study of the antenna

Wideband monopole antenna with a very compact size is presented. In order to maintain an optimum impedance matching through the bandwidth, as well as an optimized size, the antenna is designed on a rectangular FR4 substrate with dimension of 20 and 25 mm. Using a simple semicircle patch at the top of the substrate, has the advantage of continuity in the connection point between the microstrip-fed line and the patch, which may be a significant factor for increasing the bandwidth especially at the higher frequencies. Considering the favored bandwidth of 5-9 GHz, in the application of interest, the radius of the circle is obtained 7 mm. Ground plane of the antenna consists of an optimized rectangle which has two rectangular and trapezoidal cuts on its surface. Without deforming the ground plane, the antenna has an omnidirectional radiation pattern. This issue is demonstrated in

Fig. 6.23. Radiation pattern of the antenna with this deformed ground plane is demonstrated and compared with the symmetrical rectangular ground plane.
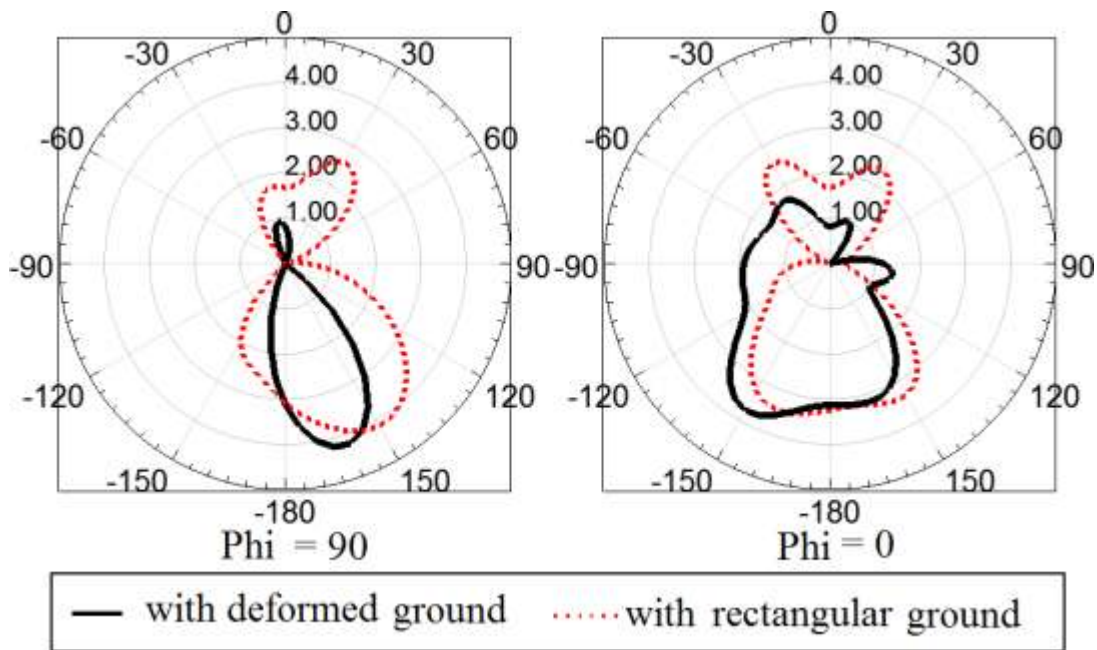

Figure 6.23 : Radiation pattern of the antenna with and without optimization at the frequency of 7.7 GHz and Theta= 135 degrees.

As it can be seen, radiation diversity is increased in the left and bottom sides of the antenna, and decreased in the right and top sides of the antenna. The idea behind this issue lies in the fact that, by using this asymmetric and deformed ground plane and cutting the right side of the ground, it is possible to remove the electrical fields caused by surface currents of that region of the ground plane. Furthermore, the surface currents of semicircular patch and the parasitic elements turn in the opposite side and increase the radiation in the opposite side of the antenna. More clearly, the ground plane is accurately designed in a way that makes the surface currents of the radiating elements to move toward the desired direction, which increases the radiation density in the preferred direction and also decreases the radiation intensity in the opposite sides.

Current distribution on the patch and ground plane is shown in the Fig. 6.24. It's clear that by optimal cutting the one side of the ground plane, surface currents on the patch and parasitic elements, move toward the opposite side, consequently diversity of the radiation around the antenna increased in the opposite side. This attempt also considerably affects the reflection coefficient of the antenna.
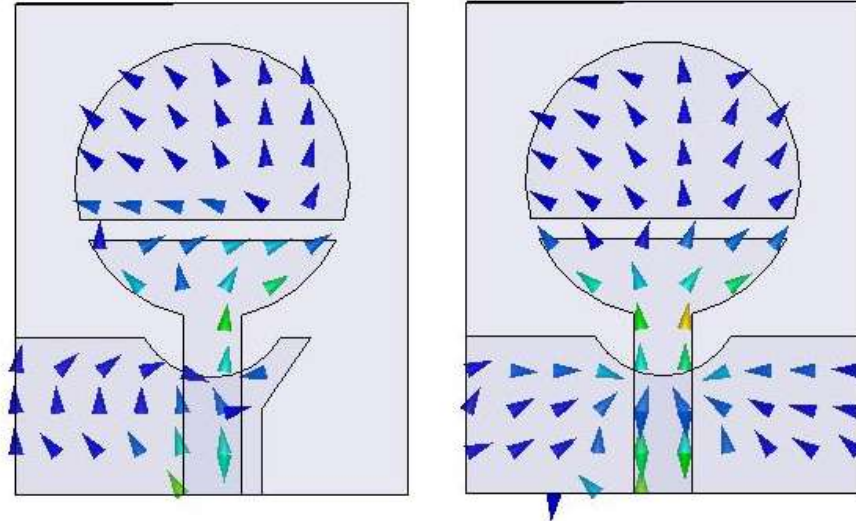
Figure 6.24 : Photo of the antenna distribution of surface currents with and without ground optimization at the frequency of 7.5 GHz.

The small semicircular cut on the ground plane also improves the impedance matching of the antenna, whose parameters are determined, earlier. Effect of this semicircular break on the top of the ground plane is considerable. So, in order to find a good tradeoff between the mentioned requirements, especially to maintain a good reflection coefficient bandwidth, a thin semicircular edge is still maintained at the broken side of the ground plane.

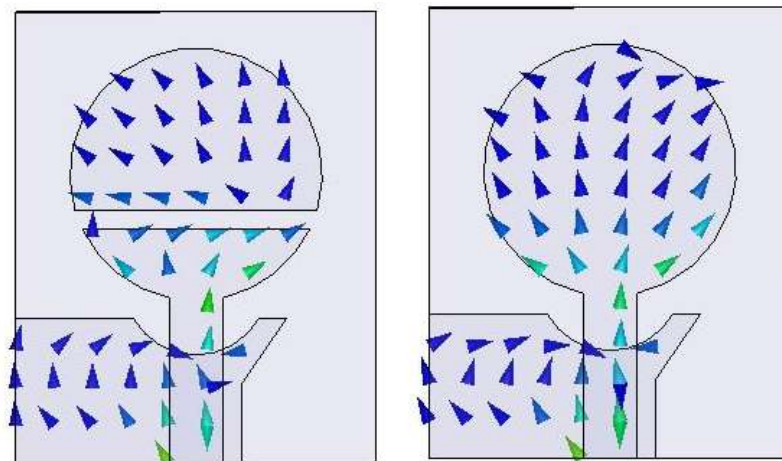**Figure 6.25** : Distribution of surface currents with and without break at the frequency of 7.5GHz.

In order to improve both the gain and reflection coefficient of the antenna a rectangular break is inserted on the circular patch, which divides the circle into two complementary segments composed of one main patch element and another parasitic element. The effect of this break is shown in Fig. 6.25 which demonstrates that the

surface currents further move toward the favored direction, which improves the directivity of the antenna.

In the Fig. 6.26, reflection coefficient of the antenna in the without break and without break is demonstrated. It is clear that the obtained and determined parameters in section II can be considered as the optimum amounts for the dimensions of the break on the circle.
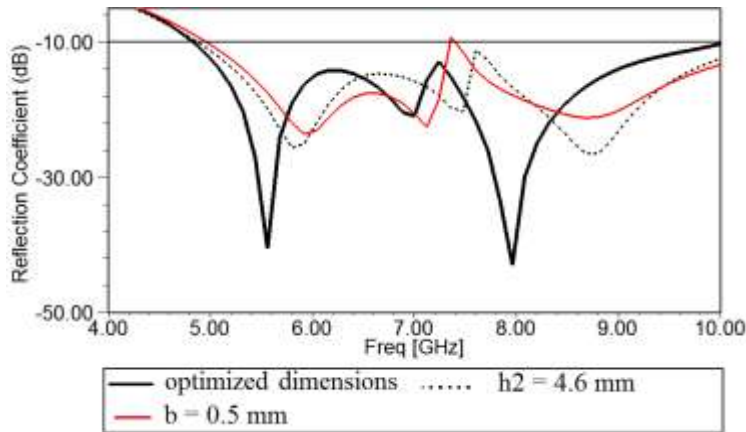
Figure 6.26 : Photo of the antenna reflection coefficient of the antenna with and without optimized dimensions of slots.

6.3.3 Measurement and simulation results

Simulations were done in HFSS v.11 and then compared to the measurements. Great SMA connector somewhat affects the characteristics of the antenna. This issue especially can be observed from Fig. 6.29, where the difference between the simulated and measured reflection coefficient can be seen. Fig. 6.27 shows the simulated beam of the antenna at the frequency of 7.5 GHz and Phi = 135 degrees, simulated HPBW is determined as 75 degrees.
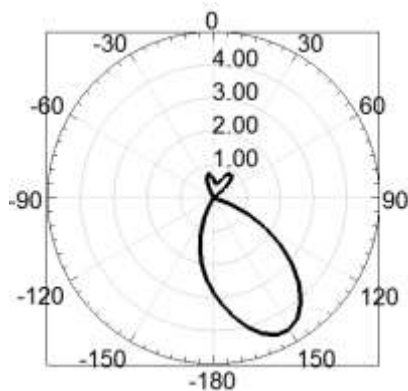
Figure 6.27 : Photo of the antenna radiation pattern of the antenna at the frequency of 7.5 GHz.

86

Gain of the antenna also is shown in Fig. 6.28, which shows a good agreement between the simulated and measured gain at Theta = 145 degrees and Phi = 145 degrees.
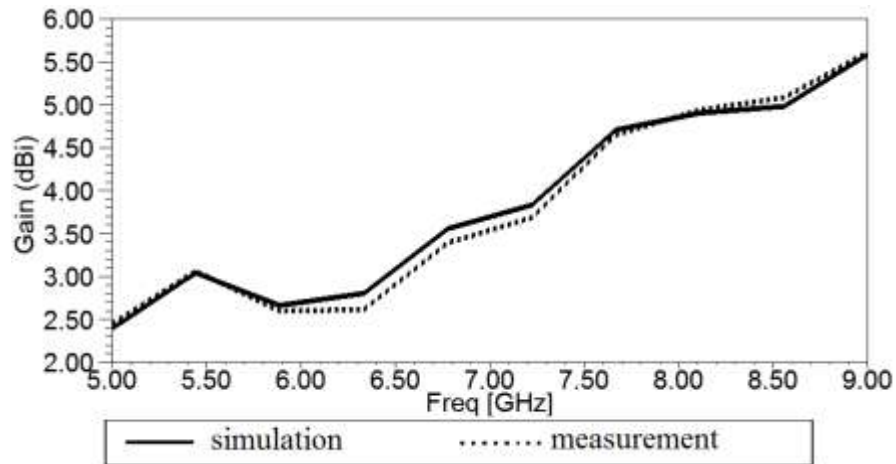
Figure 6.28 : Simulated and measured gain of the antenna.

Measured and simulated reflection coefficient of the antenna between the frequencies of 5 and 9 GHz is demonstrated In Fig. 29. Good agreement is observed between the simulation and measurements which confirms the good characteristics of the antenna in order to use in the favored frequencies of breast cancer imaging system.

Figure 6.29 : Simulated and measured reflection coefficient of the antenna.

7. CONCLUSIONS

Size, directivity and a good reflection coefficient are the most important characteristics of the antenna design requirements fo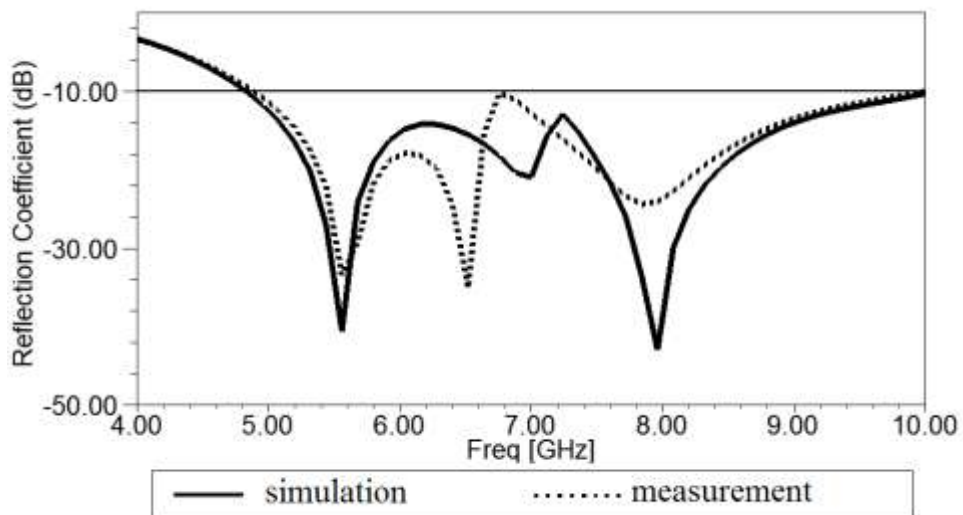r use in near field near surface measurement applications such as the microwave breast cancer imaging system. The directional monopole antennas with a parabolic-shaped or L-shaped ground plane have good directional characteristics, bandwidth and also a proper size, in order to use in microwave imaging system. In this Thesis, a new modified design of directional wide band monopole antenna with parabolic-shaped ground plane as a reflector, has been presented and studied. Two remarkable operations used to improve the directivity and gain. Firstly, parabola's axis mounted along the direction of the substrate's diagonal in order to increase the capability of the ground plane to optimal converge the radiation, axis of parabola in the ground plane is rotated 45 degrees (in comparison with the previous antenna) to extend throughout the direction of the substrate's diagonal. Consequently, vertex of the parabola is placed at the optimum point in the corner of the substrate. Consequently by inserting corrective slots the gain of the antenna is further improved. Also parametric design of the antenna allows constructing the antenna with the different dimensions of the slots for desired frequencies. Also in the other design a compact and small size of the antenna is presented. Aim of the second design is to improve the size of the antenna while maintaining a good trade-off between the size and gain of the antenna. Measurements confirm that reflection coefficient is under -10dB throughout 4-9 GHz. Furthermore, measured HPBW is between 54˚- 22˚ among 4-9 GHz. Improved HPBW of 5-15 degrees is obtained throughout the bandwidth. Gain of the antenna improved between 1.1-3.1dBi throughout the bandwidth compared to the antenna presented in [16], also in comparison with the antenna presented in [15] gain is improved between 1.2 and 5 dBi. At 8.5 GHz, measured HPBW of the antenna is decreased from 38 degrees to 23 degrees (mentioned in the result section), which confirms a 39 % decrease in HPBW of the antenna (simulated HPBW is 26 = 33 % improvement). That is very important in order to increase the resolution of a radar system. At the following, another novel compact directional monopole antenna in microstrip

technology was also presented. Reflection Coefficient bandwidth of this new antenna covers the frequency range of 5-9 GHz, and an acceptable directional characteristic is obtained. Measured and simulated gain of the antenna confirmed 5dBi reached gain at the desired frequencies of bandwidth. Miniaturized size and an acceptable directional characteristic of this antenna make it possible to use it in the microwave imaging systems and radar applications.

REFERENCES

[1] **E. C. Fear, X. Li, S. C. Hagness, and M. A. Stuchly.** (2002). Confocal microwave imaging for breast cancer detection: Localization of tumors in three dimensions, IEEE Trans. Biomed. Eng., vol. 49, no. 8, pp. 812–822, Aug.

[2] **D. J. Kurrant, E. C. Fear, D. T.Westwick.** (2008). Tumor Response Estimation in Radar-Based Microwave Breast Cancer Detection. IEEE Transactions on Biomedical Engineering, Vol. 55, No. 12, December 2008

[3] **R. Nilavalan, I. J. Craddock, A. Preece, J. Leendertz and R. Benjamin** (2007). Wideband Microstrip Patch Antenna Design for Breast Cancer Tumour. Detection. Microwaves, Antennas & Propagation, IET. Vol. 1, Issue: 2 On Page(s): 277 – 281.

[4] **C. J. Shannon, M. Okoniewski and E. C. Fear** (2003). A Dielectric Filled Ultra-Wideband Antenna for Breast Cancer Detection. Antennas and Propagation Society International Symposium, IEEE. Volume: 1, On Page(s): 218 - 221 vol.1.

[5] **J. Bourqui, M. Okoniewski and E. C. Fear** (2007). Balanced Antipodal Vivaldi Antenna For Breast Cancer Detection. Antennas and Propagation, 2007. EuCAP 2007. The Second European Conference on. On Page(s): 1 – 5. 11-16 Nov.

[6] **W.L. Stutzman and G.A. Thiele.** (1998). Antenna Theory and Design. John Wiley & Sons, 2nd ed.

[7] **M. Klemm, I. Z. Kovcs, G. F. Pederson and G. Troster.** (2005). Novel Small-Size Directional Antenna for UWB WBAN/WPAN Application. IEEE Transactions on Antennas and Propagation, Vol, 53,No. 12, December.

[8] **K. C. L. Chan, Y. Huang and X. Zhu.** (2005). A planar elliptical monopole antenna for UWB applications. IEEE/ACES International Conference on Wireless Communications and Applied Computational Electromagnetics, pp. 182-185, April.

[9] **J. X. Liang, C. C. Chian, X. D. Chen and C. G..** (2005). study of a printed circular disk monopole antenna for UWB systems. IEEE Tran. Antennas and Propagation, Vol.53, pp. 3500-3504,

[10] **X. Chen, J. Liang, P. Li, L. Guo, C. C. Chiau and C. G. Parini.** (2005). Planar UWB monopole antennas. Microwave Conference Proceedings Asia-Pacific Conference Proceedings, Vol. 1, pp. 4, December.

[11] **X. Qing and Z. N. Chen.** (2004). Antipodal Vivaldi antenna for UWB applications. presented at the EUROEM 2004 Conf., Magdeburg, Germany, Jul. 12-16.

[12] **A. G. YarovoyAbrahart, R. J., and See, L.** (2004). Antenna development for UWB impulse radio. presented at the Eur.Microwave Week, Amsterdam, The Netherlands, Oct.

[13] **Y. Lu, Y. Huang and H. T. Chattha.** (2009). Size reduction of a wideband slot antenna. Antennas and Propagation, 2009. EuCAP 2009. 3rd European Conference on, pp. 1455-1458, 23-27 march.

[14] **M. John, M. J. Ammann, P. McEvoy.** (2008). UWB Vivaldi antenna based on a spline geometry with frequency band-notch. Antennas and Propagations Society International Symposium, pp. 1-4, July.

[15] **A. locatelli, D. Modotto, F.M. pigazzo, S. Boscolo, E. Autizi, C. DeAngelis, A.-D. Capobianco and M. Midrio.** (2007). Highly Directional Planar Ultra wide band antennas for radar application. Proc. 37th European Microwave Conf., pp. 1421-1424, Oct.

[16] **M. Mokhtaari and J. Bornemann.** (2008). Directional Ultra-wideband antennas in Planar Technologies. Proceedings of the 38th European Microwave Conference, 2008, pp. 885-888.

[17] **X. Yun, E. C. Fear, R. H. Johnston.** (2005). Compact antenna for radar-based breast cancer detection. IEEE Trans. on Antennas and Propagation, ol. 53, no. 8, Aug. 2005, pp. 2374-2380.

[18] **H. M. Jafari, M. J. Deen, S. Hranilovic, N. K. Nikolova** (2007). A study of ultrawideband antennas for near-field imaging. IEEE Trans. On Antennas and Propagation, vol. 55, no. 4, Apr. 2007, pp. 1184-1188.

[19] **C. A. Balanis.n.** (2005). Antenna Theory Analysis and Design, 3rd edition, Wiley-Interscience.

[20] **N. A. McDonald.** (1978).Approximate Relationship Between Directivity and Beamwidth for Broadside Collinear Arrays, IEEE Trans. Antennas Propagat., Vol. AP-26, No. 2, pp. 340–341, March 1978.

[21] **G. Kumar, K. P. Ray** (2003). Broadband Microstrip Antennas. Artech House antennas and propagation library. Ó 2003 ARTECH HOUSE, INC. 685 Canton Street Norwood, MA 02062.

[22] **K. L. Wong.** (2008). Compact and Broadband Microstrip Antennas. Copyrightc 2002 John Wiley & Sons, Inc.

[23] **R. Waterhouse.** (1995): Small microstrip patch antenna, Electron. Lett. 31, 604–605, April 13, 1995.

[24] **S. Dey and R. Mittra** (1996) : Compact microstrip patch antenna, Microwave Opt. Technol. Lett. 13, 12–14, Sept. 1996.

[25] **J. S. Kuo and K. L. Wong.** (2001), A compact microstrip antenna with meandering slots in the ground plane, Microwave Opt. Technol. Lett. 29, 95–97, April 20, 2001

[26] **Agarwall, N. P., G. Kumar, and K. P. Ray.** (1998): Wide-Band Planar Monopole Antennas, IEEE Trans. Antennas Propagation, Vol. 46, No. 2, 1998, pp. 294–295.

[27] **Ray, K. P., et al** (2001): Broadband Planar Rectangular Monopole Antennas, Microwave Optical Tech. Letters, Vol. 28, No. 1, 2001, pp. 55–59.

[28] **J. Liberti and T. Rappaport.** (1999). Smart Antennas for Wireless communications: IS-95 and Third Generation CDMA Applications. Prentice Hall, Upper Saddle River, NJ.

[29] **Dharma Agrawal, Dharma Prakash Agrawal.** (2011). AD HOC AND SENSOR NETWORKS - Theory and Applications (2nd Edition) © World Scientific Publishing Co. Pte. Ltd.

[30] **E. C. Fear, S. C. Hagness, P. M. Meaney, M. Okoniewski, and M. A. Stuchly.** (2002):Enhancing Breast Tumor Detection with Near-Field Imaging, IEEE Microw. Magazine, vol. 3, no. 1, pp. 48–56, (2002).

CURRICULUM VITAE

Name Surname:	Javad Jangi Golezani
Place and Date of Birth:	Iran- Salmas-07/02/1983
Address:	Iran- Urmia
E-Mail:	Golezani@itu.edu.tr jangi.javad@gmail.com
B.Sc.:	Electronic and Communication Engineering

Professional Experience and Rewards:

List of Publications and Patents:

PUBLICATIONS/PRESENTATIONS ON THE THESIS

▪ Javad Jangi Golezani, Mehmet Abbak and Ibrahim Akduman: A Novel Compact Wideband Directional Monopole Antenna for Use in Radar Applications; 15th International Symposium of Antenna Technology and Applied ElectroMagnetics, 25-28 June 2012, Toulouse, France.

▪ Javad Jangi Golezani, Mehmet Abbak and Ibrahim Akduman: A Printed Wideband Miniature Antenna for Microwave Imaging Applications; 15th International Symposium of Antenna Technology and Applied ElectroMagnetics, 25-28 June 2012, Toulouse, France.